This dissertation has been
microfilmed exactly as received 68-13,321

HALL, William Davis, 1941-

POLARIZABILITY MEASUREMENTS OF THE ALKALI ATOMS SODIUM, POTASSIUM, RUBIDIUM AND CESIUM.

The University of Michigan, Ph.D., 1968
Physics, molecular

University Microfilms, Inc., Ann Arbor, Michigan

POLARIZABILITY MEASUREMENTS OF THE ALKALI ATOMS SODIUM, POTASSIUM, RUBIDIUM AND CESIUM

by

William Davis Hall

A dissertation submitted in partial fulfillment
of the requirements for the degree of
Doctor of Philosophy in the
University of Michigan
1968

Doctoral Committee:

Associate Professor Jens C. Zorn, Chairman
Professor David M. Dennison
Professor Peter A. Franken
Associate Professor Oliver E. Overseth, Jr.
Professor T. Michael Sanders, Jr.
Associate Professor George C. Summerfield

ACKNOWLEDGMENTS

I wish first to thank Professor Jens C. Zorn, who suggested this problem and provided the necessary assistance and guidance required to complete this investigation.

The assistance of my committee is gratefully acknowledged.

I would like to express my indebtedness to Professor Raymond F. Mosher of the University of Michigan Electrical Engineering staff for his assistance in calibrating the Fluke high voltage power supply.

I would like to thank Dr. Alan Gallagher for his discussion on the interpretation of the present polarizability measurements with respect to recent alkali lifetime measurements.

I would also like to thank Mr. J. T. Dickinson for his work on the velocity selector and Messrs. L. H. Shaefer and R. F. Hoeberling for their valuable assistance in the laboratory.

The partial support of this research by the United States Atomic Energy Commission and the financial aid received from the Walter Lewis and University Physics Fellowship is gratefully acknowledged.

Finally, I wish to thank my wife, Molly, without whose constant support and encouragement this work could not have been completed.

TABLE OF CONTENTS

	Page
LIST OF TABLES	vii
LIST OF FIGURES	ix
ABSTRACT	xi
CHAPTER ONE: INTRODUCTION	1
A. Method of Calculation of Atomic Polarizabilities	2
A.1 Perturbation Method	2
A.2 Sternheimer Perturbation Method	6
A.3 Coulomb Approximation	7
A.4 Variational Method	9
B. Polarizabilities as Related to Atomic Properties	9
B.1 Optical Dispersion	10
B.2 Lifetimes, Einstein Spontaneous Emission Coefficients and Oscillator Strengths	11
B.3 van der Waals Forces	12
C. Atomic Beam Deflection Measurements of Alkali Polarizabilities	14
CHAPTER TWO: PRINCIPLES OF THE EXPERIMENT	16
A. Polarizability	16
B. Non-Velocity Selected Small Shift Theory	17
C. Velocity Selected Small Shift Theory	19
D. Velocity Selected Large Shift Theory	20
E. Velocity Profile Measurements and Effects of Residual Gas Scattering	20

F. Polarizability Measurements and the Effects of Residual Gas Scattering..... 22

CHAPTER THREE: DESCRIPTION OF THE EXPERIMENTAL APPARATUS..... 24

A. Vacuum System..... 24

B. Pressure Measurements..... 29

C. Alkali Oven..... 31

D. Temperature Measurement..... 33

E. Collimator..... 34

F. Deflecting Field and High Voltage Power Supply..... 34

G. Velocity Selector..... 40

H. Detector..... 46

I. Telescope..... 47

J. Leak..... 47

K. Scattering Gas..... 47

L. Alkali Metal Purity..... 48

CHAPTER FOUR: EXPERIMENTAL PROCEDURE..... 49

A. Alignment Procedure..... 49

B. Small Shift Analysis..... 53

C. Large Shift Analysis..... 56

D. Velocity Profile Measurements..... 56

E. Scattering Cross Section Determination... 57

F. Polarizability Measurements versus Argon Scattering Gas Pressures..... 59

CHAPTER FIVE: EXPERIMENTAL RESULTS OF ALKALI POLARIZABILITY AND SCATTERING MEASUREMENTS 60

A. Small Shift Polarizability Results for Na, K, Rb, and Cs..... 61

B. Statistical Analysis..... 61

C. Large Shift Polarizability Measurements for the alkali metals Na, K, Rb, and Cs.. 73

D. Velocity Profile Measurements..... 78

E. Scattering Velocity Profile Measurements. 82

F. Polarizability Measurements Versus Argon Scattering Gas Pressures..... 88

G. Systematic Errors..... 94

CHAPTER SIX: CONCLUSION..... 100

A. Comparison with Other Atomic Beam Measurements of Alkali Polarizibilities..... 100

B. Comparison with Semi-empirical Calculations Employing Experimentally Determined Lifetimes and Oscillator Strengths..... 104

C. Comparison with Theoretical Calculations. 108

D. Comparison with the Stark Shift of Cesium 109

APPENDICES

A. Ideal Small Shift Deflection Theory in Atomic Beams..... 112

B. Residual Gas Scattering Distortion of the Ideal Modified Maxwellian Velocity Distribution and its Effects on the N.V.S. Polarizability Value..... 121

C. Theory of Operation of the Slotted Disk Velocity Selector..... 127

D. Total Effective Scattering Cross Section Measurements and Comparisons with Previous Experiments and Theory..... 135

E. Quadrupole Effects..... 140

BIBLIOGRAPHY..... 141

LIST OF TABLES

Table		Page
III.1.	Typical Observed Pressures.....	27
V.1	Small Shift Deflection Polarizability Measurements for Sodium.....	62
V.2	Small Shift Deflection Polarizability Measurements for Potassium.....	63
V.3	Small Shift Deflection Polarizability Measurements for Rubidium.....	66
V.4	Small Shift Deflection Polarizability Measurements for Cesium.....	68
V.5	Small Shift Alkali Polarizabilities Values and their Associated Statistical Errors.	72
V.6	Large Shift Polarizability Measurements for Na, K, Rb, and Cs.....	74
V.7	Large Shift Alkali Polarizability Values and their Associated Statistical Errors.	76
V.8	Summary of Measured Alkali Polarizability Values.....	77
V.9	Percent Fractional Decrease in Low-Velocity Beam Atoms as Compared to the Theoretical Velocity Profile.....	82
V.10	Non-velocity Selected Polarizability Measurements Corrected for Scattering Effects on the Velocity Distribution of the Beam Atoms.....	93
V.11	Systematic Errors in the Alkali Polarizability Measurements.....	98
V.12	Measured Values of the Alkali Polarizabilities.....	99
VI.1	Experimental and Theoretical Values of Alkali Polarizabilities.....	101

VI.2	Alkali Resonance f Sum Values.....	107
VI.3	Upper Bound of Alkali Polarizabilities Using the One "Effective" Electron Approximation.....	107
C.1	Specifications of Velocity Selector.....	131
C.2	Normalized Intensity as a Function of Reduced Velocity.....	133
D.1	Alkali-Argon Effective Cross Section Measurements.....	137

LIST OF FIGURES

Figure		Page
III.1	Cutaway View of Polarizability Apparatus (Side-View).....	25
III.2	Cutaway View of Polarizability Apparatus (Top View).....	26
III.3	Vacuum Equipment.....	28
III.4	Oven.....	32
III.5	Cross Section of Deflecting Electrodes for Alkali Beams.....	35
III.6	Field and Collimator Mount.....	36
III.7	High Voltage Calibration Circuit.....	39
III.8	Velocity Selector Rotor Diagram.....	41
III.9	Velocity Selector and Frame Mount (Side View).....	42
III.10	Velocity Selector and Frame Mount (Top View).....	43
III.11	Circuit Diagram for Velocity Selector Rotor Motor.....	45
IV.1	Deflecting Geometry for Alkali Beam....	52
IV.2	Small Shift Data Analysis Diagram.....	55
V.1	Beam Shape.....	71
V.2	Large Shift Data Curves.....	76
V.3	K Velocity Profile.....	79
V.4	Rb Velocity Profile.....	80
V.5	Cs Velocity Profile.....	81
V.6	K-Ar Scattering Velocity Profile.....	83

V.7	Rb-Ar Scattering Velocity Profile.....	84
V.8	Cs-Ar Scattering Velocity Profile.....	85
V.9	K Polarizability-Argon Scattering Gas Measurements.....	89
V.10	Rb Polarizability-Argon Scattering Gas Measurements.....	90
V.11	Cs. Polarizability - Argon Scattering Gas Measurements.....	91

William Davis Hall

ABSTRACT

This study reports on the experimental determination of the electric dipole polarizabilities of the alkali atoms sodium, potassium, rubidium, and cesium. The measurements were made by observing the deflections of a collimated, velocity-selected atomic beam under the influence of an unhomogeneous electric field. The results are:

$$\alpha(Na) = (24.4 \pm 1.7) \times 10^{-24} \text{ cm}^3$$

$$\alpha(K) = (45.2 \pm 3.2) \times 10^{-24} \text{ cm}^3$$

$$\alpha(Rb) = (48.7 \pm 3.4) \times 10^{-24} \text{ cm}^3$$

$$\alpha(Cs) = (63.3 \pm 4.6) \times 10^{-24} \text{ cm}^3$$

The alkali polarizabilities measured in this experiment were found to differ from previous experimental polarizability determinations in which beam velocity analysis was not available. Subsequent experiments measuring alkali velocity profiles and alkali polarizabilities as a function of argon scattering gas densities have demonstrated that the discrepancy in the polarizability values arises because of the velocity dependent scattering effect of the residual gas atoms which selectively removes low velocity atoms from the beam, thus distorting the assumed ideal modified Maxwellian velocity distribution.

The polarizability values quoted here are in good agreement with recent polarizability predictions from alkali atom lifetime measurements, oscillator strength measurements, and the theoretical predictions of Sternheimer and Stone.

CHAPTER ONE

INTRODUCTION

Polarizability , a measure of the distortion suffered by the electronic charge distribution of an atom in the presence of a perturbing electrostatic field, is an atomic property which appears in the description of many important atomic processes. The van der Waals interactions, ion-atom, atom-atom, and electron-atom collision processes, optical lifetimes, and optical dispersion phenomena all directly involve or are related to the static polarizabilities of ground and excited states of neutral atoms and molecules. The direct experimental determination of atomic polarizabilities affords a very sensitive check on the accuracy of electronic wave functions used in calculating these various atomic processes in which the outer part of the electronic wave function plays an important role.

Previous atomic beam polarizability deflection measurements (Scheffers and Stark, 1934; Salop, Polack and Bederson, 1961; Chamberlain and Zorn, 1963) have yielded results which differ appreciably from each other and from the theoretically predicted polarizabilities for the alkali atoms.

The present work describes a more accurate experimental determination of the alkali polarizabilities which are obtained by observing the deflection of a collimated,

velocity selected, beam of neutral atoms in a transverse inhomogeneous electric field.

A. Methods of Calculation of Atomic Polarizabilities.

The alkali atoms are characterized by a single S valence electron outside a closed shell core. Their low ionization potential and ease of vaporization makes these atoms primary subjects for laboratory investigation. The simplicity of atomic structure and extensive laboratory investigation has stimulated a great deal of theoretical work involving alkali atoms.

The two principal approaches to the calculation of polarizabilities are (1) conventional perturbation techniques of which the Sternheimer method and the Coulomb approximation are subclasses and (2) the variation method.

A1. Perturbation Method.

The perturbation method is used in the earlier work of Unsöld (1927), Lennard-Jones (1929) and Vinti (1932). More recently, this method has been of considerable interest (Dalgarno and Lewis, 1955; Dalgarno and Stewart, 1956; Dalgarno and Kingston, 1959; and Dalgarno, 1962) and the formalism has been extended to include electron exchange effects and induced dipole effects (Langhoff and Hurst, 1965; Cohen and Drake, 1967).

Following standard perturbation techniques (Slater, 1960), the energy of an atom placed in an external electric field E is readily calculable. The second order Stark energy for an atom in a constant electric field in the z

direction is given by

$$W_o^{(2)} = e^2 E^2 \sum_{\lambda \neq 0} \frac{|(M_{o\lambda})_z|^2}{W_o^{(0)} - W_\lambda^{(0)}} \qquad \text{I.1}$$

where e is the electron charge, E is the magnitude of the electric field in the z direction, $W_o^{(0)}$ is the energy of unperturbed ground eigenstate, $W_\lambda^{(0)}$ is the unperturbed energy of the excited eigenstate specified by the quantum number λ and $(\mu_{o\lambda})_z$ is the matrix element defined by

$$(M_{o\lambda})_z = \langle o | z | \lambda \rangle \qquad \text{I.2}$$

Classically, the increment in the energy of an atom in the ground state due to a static electric field in the absence of a dipole moment is given by

$$W_o^{(2)} = - \frac{\alpha E^2}{2} \qquad \text{I.3}$$

where α is the polarizability of ground state. If we equate equations I.1 and I.3, the average polarizability of an atom in a ground S state is given by

$$\alpha = \frac{2e^2}{3} \sum_{\lambda \neq 0} \frac{|M_{o\lambda}|^2}{W_\lambda^{(0)} - W_o^{(0)}} \qquad \text{I.4}$$

where we have used relationship

$$\left|(M_{o\lambda})_x\right|^2 = \left|(M_{o\lambda})_y\right|^2 = \left|(M_{o\lambda})_z\right|^2 = \frac{1}{3}\left|M_{o\lambda}\right|^2$$

The matrix elements $\mu_{o\lambda}$ can be conveniently expressed in terms of the dimensionless oscillator strengths $f_{o\lambda}$ defined by

$$f_{o\lambda} = \frac{8\pi^2}{3}\frac{m\,(\nu_\lambda - \nu_o)}{e^2}\left|M_{o\lambda}\right|^2 \qquad \text{I.5}$$

The polarizability in terms of the oscillator strengths is given by

$$\alpha = \frac{e^2}{4\pi^2 m}\sum_{\lambda\neq 0}\frac{f_{o\lambda}}{(\nu_\lambda - \nu_o)^2} \qquad \text{I.6}$$

where $(\nu_\lambda - \nu_o)$ is the frequency separation between the ground state (0) and the excited state (λ); e and m refer respectively to the electron charge and mass. The oscillator strengths satisfy an important sum rule known as the Thomas-Reiche-Kuhn sum rule (Bethe and Salpeter, 1957). This sum rule states

$$\sum_{\lambda} f_{o\lambda} = N \qquad \text{I.7}$$

where N is the total number of electrons in the atom. The summation of equation I.7 includes all possible states of excitation and all degrees of ionization of the atom. For a one-electron atom (Hydrogen), the result of the sum

I.7 is unity; thus, the oscillator strength characterizes the intensity of the allowed transitions.

For the alkali atoms the situation occurs in which only those oscillator strengths associated with resonance transitions make appreciable contributions to the polarizability. In particular, only those transitions from the p state fine structure levels to the ground state (D_1 and D_2 lines) are significant (Dalgarno and Kingston, 1959).

If we make the one "effective" electron approximation for the alkali atoms, the sum rule of equation I.7 becomes

$$\sum_{\lambda} f_{o\lambda} = 1$$

This simplification is useful because it places an approximate upper bound on the polarizability, that is,

$$\alpha \leq \frac{e^2}{4\pi^2 m} \frac{1}{(\nu_1 - \nu_0)^2} \qquad \text{I.8}$$

where ν_j is the frequency of state closest to the ground state whose oscillator strength f_{o1} is not zero (Bederson and Robinson, 1966). This approximation neglects electron correlation and core polarization effects.

One can also calculate the expectation value of the induced dipole moment by using the corrected wave functions. If we let $|1\rangle$ be the first order correction to the unperturbed wave function $|0\rangle$, then the wave equation

for $|1\rangle$ is

$$(H_o - \mathcal{E}_o)|1\rangle = -H'|0\rangle \qquad \text{I.9}$$

where H_o is the unperturbed Hamiltonian, $\mathcal{E}_o$ is the energy eigenvalue of H_o and H' is the perturbation Hamiltonian of the atom in the presence of an electric field given by

$$H' = -\sum_{\lambda}' e\vec{r}_{\lambda}\cdot\vec{E} \qquad \text{I.10}$$

and $\vec{r}_i$ is the position of the i^{th} electron. The second order perturbation energy is given by

$$W^{(2)} = \langle 1|H'|0\rangle \qquad \text{I.11}$$

The simplest procedure is to assume that $|0\rangle$ can be represented by a product of one-electron wave functions (Hartree Approximation), and apply equation I.11 separately to each orbital. The total polarizability is then the sum of the polarizabilities of the individual one-electron wave functions (Bederson and Robinson, 1966).

A.2 Sternheimer Perturbation Method.

In essence the Sternheimer (1954) method consists of solving the radial part of equation I.9 for each unperturbed wave function. The solution is obtained numerically for all the orbitals in the configuration and the total polarizability is evaluated from the sum of polarizabilities

of the individual one-electron wave functions. The orbitals used are the most accurate ones available for each specific atom.

In Sternheimer's (1962) calculation of alkali polarizabilities, using this perturbation technique, electron correlation effects are approximately included in the unperturbed wave functions. The total dipole polarizability predicted in this calculation includes both the effect of the valence electron and the contribution of the core electrons. The core contribution involves a calculation of the electric field at the nucleus due to the dipole moment induced in the valence electron charge distribution by the external electric field. The results of Sternheimer's calculation are given in Table VI.1 for the alkali atoms Na, K, Rb, and Cs.

A.3 Coulomb Approximation.

Bates and Damgaard (1949) calculate the transition integral,

$$\int_0^\infty R_i R_f \, r \, dr \qquad \text{I.12}$$

where R_i and R_f are respectively the initial and final radial wave functions of the active electron normalized in atomic units, neglecting the departure of the potential of an atom from its asymptotic Coulomb form. This enables a general analytical expression for the transition integral to be derived and tables are compiled in which absolute

line strengths of a large number of spectral lines are tabulated. Comparison of this method with experiment (Stephenson, 1951) has shown that for atoms with a single electron outside a closed shell, the measured excited state lifetimes agree well with those predicted by the Coulomb approximation.

The absolute line strength S (atomic units) expressed in terms of the radial transition integral is given by (Bates and Damgaard, 1949)

$$S = \mathcal{L}(M)\,\mathcal{L}(L)\,\sigma^2 \qquad \text{I.13}$$

where $$\sigma^2 = \frac{1}{4l^2-1}\left(\int_0^\infty R_\lambda R_f\, r\,dr\right)^2$$

and $\mathcal{L}(M)$ and $\mathcal{L}(L)$ are factors calculated for the angular dependence of the particular transition;* and l is the greater of the two azimuthal quantum numbers. The oscillator strength is related to the absolute line strength by the expression (Bates and Damgaard, 1949)

$$f = \frac{8\pi^2 mc}{3he^2}\,\frac{1}{g_1\lambda}\,S \qquad \text{I.14}$$

where g_1 is the statistical weight of the lower level and λ is the wave length of the emitted radiation in Ångström units. Now using equation I.8 and replacing the sum rule result "unity" by the Bates-Damgaard f value for the

*Tabulated values for (M) and (L) are given in Goldberg (1935) and Russel (1936).

resonance transition we obtain the expression

$$\alpha = 6.5 \times 10^{-20} \lambda \sigma^2 \qquad \text{I.15}$$

where λ is the wave length of the resonant D_1 transition measured in centimeters and σ^2 is obtained from the tables in Bates and Damgaard (1949).

A.4 Variational Method.

As equation I.4 demonstrates, electric polarizabilities are directly related to the change in energy due to the electric field perturbation and they may be determined therefore by the application of the conventional Rayleigh-Ritz variational methods. This method for calculating polarizabilities has been applied mainly to hydrogen, alkali ions and noble gas atoms. An excellent review of these methods are found in the following papers: Hasse (1931), Slater and Kirkwood (1931), Hellman (1935), Buckingham (1937), and Wikner and Das (1957). The accuracy of this method is limited by the unperturbed wave functions available for the various atoms.

B. Polarizabilities as Related to Atomic Properties.

Polarizabilities can be related to the index of refraction of gases, spectral line strengths and oscillator strengths, Einstein coefficients of spontaneous emission and lifetimes of excited atomic states, and van der Waals forces associated with mutual polarization of atoms and

molecules.

B.1. Optical Dispersion.

Using simple classical dispersion theory in which the electrons of the atom are regarded as harmonically and isotropically bound particles to individual equilibrium positions, the dynamic polarizability is given by (Hirschfelder et al., 1954):

$$\alpha(\nu_0) = \frac{e^2}{4\pi^2 m} \sum_{\beta} \frac{f_\beta}{\nu_\beta^2 - \nu_0^2} \qquad \text{I.16}$$

where ν_0 is the frequency of the impressed electric field, ν_β is the natural frequency of the β^{th} electron, and f_β is the oscillator strength of the β^{th} level. More rigorous treatments include a damping term in the denominator which avoids the unphysical infinity in $\alpha(\nu_0)$ at resonance. Using the Clausius Mossotti relationship it is shown (Korff and Breit, 1932) that for low gas densities and close to the absorption line but not within it, one may use the approximate formula

$$\eta = 1 + \frac{e^2 N}{4\pi m c^2} \frac{\lambda_1^3 f_1}{(\lambda - \lambda_1)} \qquad \text{I.17}$$

to relate the oscillator strength f_1 of the absorption line to the index of refraction η of the gas, where N is the number of gas atoms per cubic centimeter and λ_1 is the wave length of the absorption line in centimeters. Korff and Breit (1932) discuss several methods for measuring η

in the region of an absorption line, e.g., Hook method, from which absolute oscillator strengths can be derived provided one knows the gas density accurately (Kvater and Meister, 1952; Minkowski and Mühlenbruch, 1930). Then using equation I.6 (Dalgarno and Kingston, 1959) polarizability values can be predicted from resonance oscillator strength data.

B.2 Lifetimes, Einstein Spontaneous Emission Coefficients and Oscillator Strengths.

The lifetime of a state m is related to the various depopulating transitions by the usual relation

$$\tau_m = \left[\sum_n A_{mn} \right]^{-1} \qquad \text{I.18}$$

where A_{mn} is the Einstein spontaneous emission coefficient and the sum over n covers all states that are lower than state m. The f value for absorption from state n to state m is given by (Bethe and Salpeter, 1957)

$$f_{nm} = \frac{g_m}{g_n} \frac{\lambda^2 A_{mn}}{8\pi^2 c r_o} \qquad \text{I.19}$$

where g_m and g_n refer respectively to the statistical weights of the upper and lower states, λ is the wave length of the transition (centimeters), c is the velocity of light and r_o the classical radius of the electron (e^2/mc^2). For the resonance transitions in the alkali metals f_{nm} can be

calculated directly from τ_m. Thus, using equation I.6 lifetime measurements (Link, 1966; Stephenson, 1951; Gallagher, 1967) can be used to infer polarizability values.

B.3 Van der Waals Forces.

The van der Waals force is best characterized as that force which gives rise to the constant a in the van der Waals equation of state; the pressure constant a is a measure of the specific interaction strength between gas atoms. The van der Waals force between two neutral nonpolar gas atoms was explained by Debye (1920), but his calculation of the intermolecular energies, based upon an electrostatic molecular induction model, did not meet with great success because it predicted far too small an intermolecular force in comparison with experiment. London and Eisenschitz (Margenau, 1939) presented a method of calculating the interaction energy in which the intermolecular energies appear as a series of second order perturbation terms. The classical explanation of the "London dispersion force" between two neutral atoms is as follows. Consider two hydrogen atoms sufficiently far apart such that their electron clouds do not overlap. Electrons in their lowest stationary states move and thus each atom has an instantaneous dipole moment capable of inducing an additional dipole moment antiparallel to itself in the other atom. Classically we would say the atoms have a tendency to rotate in phase giving rise to an attractive force between them.

The leading term in the series representation for the interaction energy, between two neutral atoms a and b, is a dipole-dipole interaction term (Margenau, 1939), that is

$$W^{(2)} = -\frac{C_{ab}}{R^6} \qquad \text{I.20}$$

where C_{ab} is the van der Waals force constant and R is the distance of separation between the two atoms. There are many approximate formulae for the constant C_{ab}. In the variational approach taken by Slater and Kirkwood (1931), the two atoms are considered to have N(a) and N(b) electrons respectively, each in a single shell. The force constant in terms of the polarizabilities of the particular atoms is given by

$$C_{ab} = \frac{3eh}{2(m_e)^{1/2}} \left[\frac{\alpha(a)\,\alpha(b)}{\left(\frac{\alpha(a)}{N(a)}\right)^{1/2}+\left(\frac{\alpha(b)}{N(b)}\right)^{1/2}}\right] \qquad \text{I.21}$$

Similar expressions have been derived by Helmann (1935), Buckingham (1937), and Chang (1967).

Another expression involving the force constant C_{ab} is Q, the total elastic scattering cross-section for neutral atoms derived by Massey and Mohr (1934). In Appendix D the results from experimental measurements of Q for K-Ar, Rb-Ar and Cs-Ar are compared to the theoretical predictions of Massey and Mohr using the new values of the alkali polarizabilities obtained in this experiment.

A knowledge of van der Waals force constants is also

useful in calculating pressure broadening of spectral lines and hfs frequency shifts due to buffer gases in alkali vapor gas cells (Margenau, Fontana, and Klein, 1959; Herman and Margenau, 1961).

C. Atomic Beam Deflection Measurements of Alkali Polarizabilities.

The first atomic beams measurement of the alkali polarizabilities was performed by Scheffers and Stark (1934) in which they measured the polarizabilities of Li, K and Cs by passing beam atoms through a strong inhomogeneous radial electric field. Chamberlain and Zorn (1963) repeated the electrostatic deflection measurements for Li, Na, K, Rb and Cs using a two wire type deflecting field which provided a more uniform and better known deflecting force than the radial field of Scheffers and Stark. Both of these experiments require a precise knowledge of the apparatus geometry beam shape and velocity distribution of the beam atoms to obtain accurate polarizability values. The most serious systematic uncertainty arises because of the lack of knowledge about the actual beam velocity distribution.

Salop, Pollack and Bederson (1961) measured the alkali polarizabilities of Li, Na, K, Rb and Cs using a unique congruent electric and magnetic deflecting field, atomic beam balance method. The advantage of their method is that the balance condition is independent of the beam

velocity distribution, specific values of the field gradients, and the apparatus geometry (except where it enters into the calculation of the electric field). The polarizability values obtained in this experiment and the experiment of Chamberlain and Zorn agree fairly well with each other and are consistent with the semi-empirical calculations of Dalgarno and Kingston (1959). *

The experimental determination of the alkali polarizabilities described in this thesis is an extension of the Chamberlain-Zorn experiment with the added feature of beam velocity analysis. The polarizability values obtained in the present experiment, in particular for cesium, are systematically larger than the values obtained in the previous atomic beam measurements. The origin of these larger polarizability values, with respect to the Chamberlain-Zorn experiment, are thoroughly investigated and shown to be attributable to the removal of low-velocity atoms from the beam by residual gas scattering. The larger polarizability values obtained in the present experiment are also shown to correlate better with recent alkali lifetime and oscillator strength measurements.

---

*See Table VI.1.

CHAPTER TWO

PRINCIPLES OF THE EXPERIMENT

Introduction

The atomic polarizabilities of the alkali atoms sodium, potassium, rubidium and cesium are determined by observing the deflection of a highly collimated velocity selected neutral beam in a transverse inhomogeneous electric field. The beam is formed by methods standard in atomic and molecular beam work (Ramsey, 1956). The deflection field used is the two wire field which generates a uniform deflection force over the dimensions of the field. The velocity selector is of the classic slotted disk type constructed to eliminate any sideband contributions. Comparisons between earlier non-velocity selected (NVS) measurements and the present velocity selected (VS) measurements are made and a residual gas scattering mechanism is used to explain the different values for the atomic polarizabilities obtained by these two methods.

A. Polarizability.

Polarizability is a parameter used to measure the deformation of an atom when it is placed in an electric field. If a neutral atom is placed in an electric field, E^*, a relative separation of the charge centers takes

---

*Note $|\vec{E}| \equiv E$

place, giving rise to an induced dipole moment μ which for small fields may be written as

$$\vec{\mu} = \alpha \vec{E} \qquad \text{II.1}$$

where α is the proportionality constant between the applied electric field and the induced dipole moment. This quantity α is called the polarizability and is in general a tensorial quantity. For the case of the alkali atoms, where the orbital angular momentum is zero in the ground state, the polarizability is a scalar. The potential energy of an atom in an electric field with a scalar polarizability may be written as

$$U = -\frac{1}{2} \alpha E^2 \qquad \text{II.2}$$

The force on such an atom in a non-uniform electric field is given by

$$\vec{F} = -\nabla U \qquad \text{II.3}$$

The z component of the force can be written as

$$F_z = -\frac{\partial U}{\partial z} = \alpha E \frac{\partial E}{\partial z} \qquad \text{II.4}$$

where $\frac{\partial E}{\partial z}$ is the electric field gradient in the z direction.

B. Non-Velocity Selected Small Shift Theory.

From equation II.4 we see that if an atom is placed in a non-uniform electric field it suffers a transverse force.

As a result of this force each atom suffers a deflection S in traversing the apparatus given by

$$S = \frac{\alpha}{2mv^2} E \frac{\partial E}{\partial z} L \qquad \text{II.5}$$

where L is a constant depending upon the apparatus geometry and v is the velocity of the atom. The deflection S, although not the force, is velocity dependent and the resultant deflection pattern is smeared out due to the distribution of velocities among the atoms. Thus the determination of the polarizability using this technique requires a knowledge of the velocity distribution of the atoms in the beam.

If one assumes that the velocity distribution is the ideal Maxwellian effusion velocity distribution, it can be shown* that the observed average deflection $\bar{S}$ of the beam atoms at the detector plane is given by

$$\bar{S} = \frac{\alpha}{4kT} E \frac{\partial E}{\partial z} L \qquad \text{II.6}$$

where T is the temperature of the source in ^{o}K, k is Boltzmann's constant, and L, which equals $l_1(l_1+2l_2)$, is a geometrical quantity determined by the apparatus parameters**. To obtain equation II.6 from II.5, the substitution $v = \sqrt{\frac{2kT}{m}}$ is used where m is the mass of the atom.*

---

*See Appendix A.

**See Figure IV.1.

In the method of small shifts the applied voltage is kept low enough such that the deflection S is small compared to the detector wire width W_D, i.e.,($S \leq 0.1\ W_D$). This condition is necessary if one assumes the beam shape is negligibly distorted upon deflection (Chamberlain, 1962). Now with the detector positioned at approximately the half maximum point of the beam shape, at an intensity I, a change in intensity dI occurs when the field voltage is turned on due to the deflection of the beam atoms relative to the fixed detector. In the small shift approximation $\bar{S}$ is determined from the relation

$$\bar{S} = \frac{dI}{\gamma} \qquad \text{II.7}$$

where γ is the beam shape slope.* Thus rewriting equation II.6 and making use of this substitution we obtain

$$\frac{dI}{\gamma} = \frac{\alpha}{4kT} E \frac{\partial E}{\partial z} L \qquad \text{II.8}$$

Thus, the theoretical expression for the polarizability is given by

$$\boxed{\alpha = \frac{dI}{\gamma} \frac{4kT}{E \frac{\partial E}{\partial z} L}} \qquad \text{II.9}$$

C. Velocity Selected Small Shift Theory.

The inclusion of a velocity selector in the experimental

---

*See Figure V.1.

determination of the atomic polarizabilities enables one to neglect any assumptions about the velocity distribution in the beam. Thus the equation used to relate the deflection S to the atomic polarizability is the exact expression

$$\alpha = S \frac{2mv^2}{E \frac{\partial E}{\partial z} L} = \frac{dI}{\gamma} \frac{2mv^2}{E \frac{\partial E}{\partial z} L} \qquad \text{II.10}$$

where only a knowledge of the apparatus geometry, applied deflection voltage and transmitted velocity are required.

D. Velocity Selected Large Shift Theory.

In the large shift measurement the applied deflecting voltage is large enough such that S, the deflection, is larger than W_D, the wire width. Beam shapes are taken for the undeflected and deflected case and then the deflection S is obtained directly, by visually comparing the two beam shapes. The value for S is then substituted into equation II.10 and α, the polarizability, is calculated for the particular voltage and velocity.*

E. Velocity Profile Measurements and Effects of Residual Gas Scattering.

The detector in an atomic beams experiment measures the number of particles incident upon it in unit time. If the slit in the oven is an ideal aperture, then a Maxwellian

*See Figure V.2.

v^2 volume distribution in the oven becomes a v^3 velocity distribution at the detector neglecting any other effects that might distort the velocity distribution. An ideal aperture is one in which the dimensions of the aperture are much smaller than the mean free path of the molecules in the oven (Miller and Kusch, 1955). The oven slits used in the present experiment are designed to meet this condition within the range of experimental feasibility.

The conclusions drawn from the experimental measurements of the velocity profile, assuming an ideal aperture, indicate that scattering of beam atoms by residual gas molecules results in the preferential removal of low velocity beam atoms from the velocity distribution. This velocity-dependent effect can be understood physically by the fact that the lower velocity atoms spend a longer time in the scattering region and thus have a larger probability of being removed from the beam. This effect is also observed in the severity of the distortion of the velocity profiles of the individual alkali elements. If we characterize the velocity distribution of each alkali by its most probable velocity v_p, which is inversely proportional to its mass, then cesium should exhibit the largest velocity distribution distortion. Figures V.3, V.4 and V.5 clearly show that this is what is observed experimentally.

Velocity profiles were also measured as a function of the gas density of argon. The use of argon gas permits

comparison of the theoretically predicted and experimentally measured velocity profiles since the identity and density of the gas responsible for the scattering is known.* The results of these measurements indicate that the principal mechanism of the velocity distribution distortion is the removal of beam atoms by scattering from residual gas molecules.

F. Polarizability Measurements and the Effects of Residual Gas Scattering.

In the derivation of equation II.9, using the theory in Appendix A, it is assumed that the velocity distribution characterizing the beam atoms is the ideal modified v^3 Maxwellian distribution. This experiment has demonstrated that this basic assumption is not valid because the residual gas atoms present in the apparatus introduce a distortion in the velocity distribution characterized by a deficiency of low velocity atoms. Using simple gas kinetic theory, the effect of the velocity distribution distortion can be included in the theory to derive the corrected form of equation II.9. The details of this calculation are given in Appendix B. The result is

$$\alpha = \frac{dI}{\gamma} \frac{4kT}{E \frac{\partial E}{\partial z} L} \frac{1}{I_1(A)} \qquad \text{II.11}$$

*See Chapter V (E).

where $I_1(A)$ is the correction factor which includes the effect of the velocity distribution distortion.

Velocity selected and non-velocity selected polarizability values were measured as a function of the density of the argon scattering gas which facilitated comparison between the theoretical predictions (equation II.11) and the experimental measurements. The details and results of these measurements and their implications are discussed in Chapter V (F).

CHAPTER THREE

DESCRIPTION OF THE EXPERIMENTAL APPARATUS

Introduction.

The most important characteristic of this apparatus is its capability of yielding accurate determinations of the atomic polarizabilities of the alkali metals independent of any assumptions about the velocity distributions of the beam atoms.

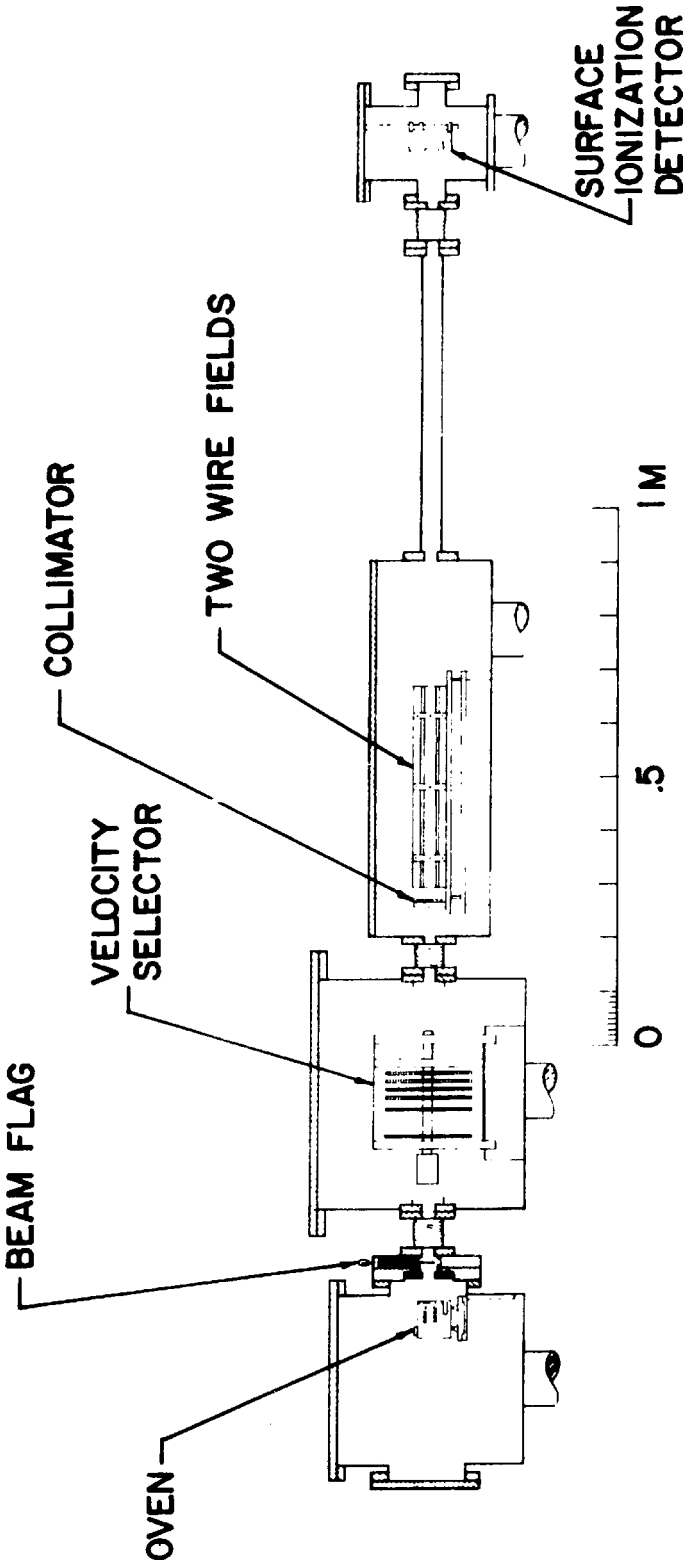
Figures III.1 and III.2 show a cutaway diagram of the apparatus and its vacuum envelope with its associated equipment, source, velocity selector, collimator, deflecting field and detector. A description of these components follows.

A. Vacuum System.

The vacuum envelope is composed of four interconnected brass chambers which house the oven, velocity selector, deflecting field and detector. A single straight through skinny high vacuum valve separates the oven chamber from the rest of the apparatus and allows one to reload the oven without letting the rest of the machine down to air.

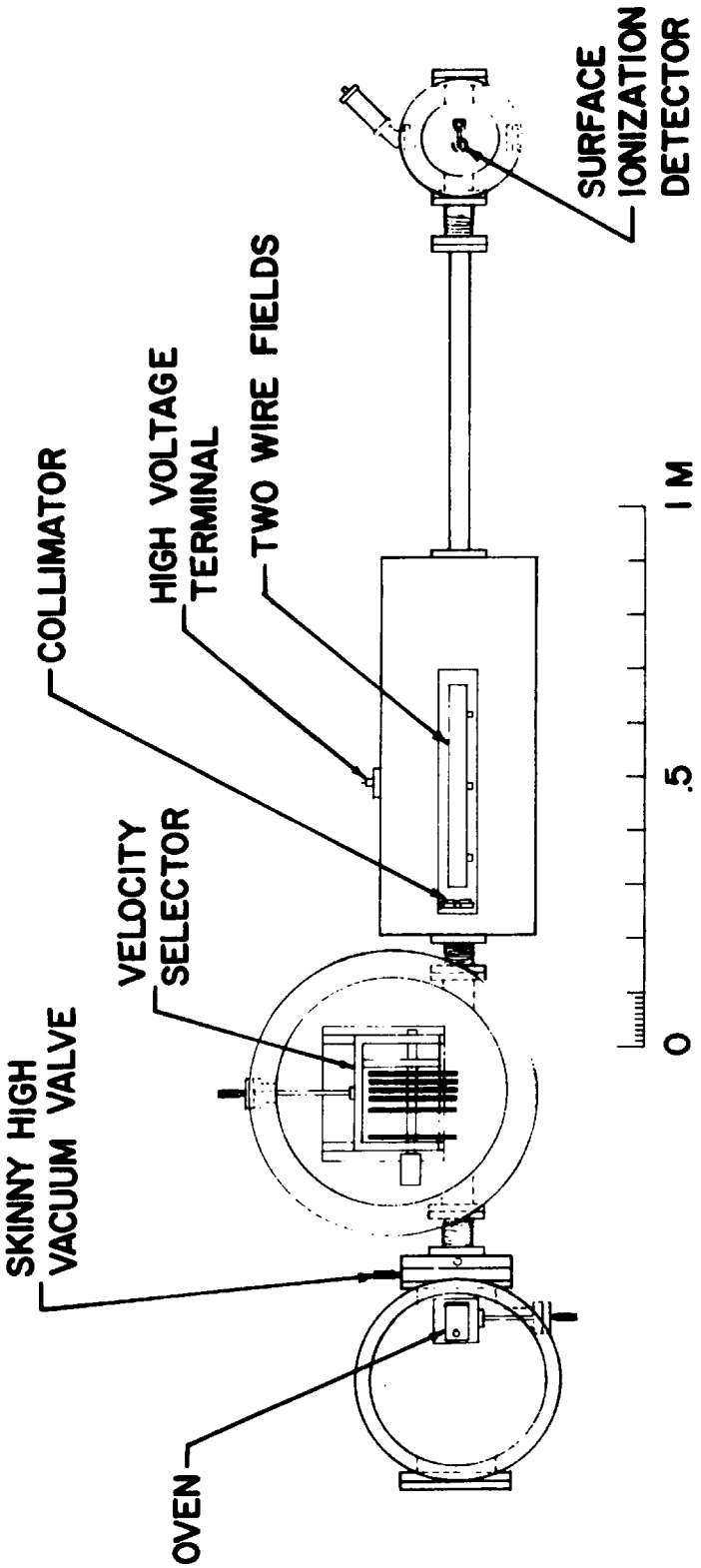
Seals are provided for the interconnecting chambers and lids by O-rings lightly coated with Apiezon "L" grease. Since brass was the primary construction material, no bake out procedures were even used.

The vacuum is maintained by four HK 750 N.R.C. oil



(SIDE VIEW)

FIG. III.1.--CUTAWAY VIEW OF POLARIZABILITY APPARATUS



(TOP VIEW)

FIG. III.2:-CUTAWAY VIEW OF POLARIZABILITY APPARATUS

diffusion pumps using DC 705 silicon pump fluid. In addition, three liquid nitrogen traps are mounted on the lids of the oven, velocity selector, and deflecting field chamber; these were always filled during a run to provide additional pumping for the system. Factors of two improvement in the pressure were consistently observed when the traps were filled, thus indicating that there was an appreciable quantity of condensable vapors in the vacuum envelope. Two Cenco"Hyvac 7" forepumps are used in the forelines. Figure III.3 shows a schematic diagram of the vacuum system used for the apparatus.

The pressure of each chamber is monitored by a Bayard Alpert RG-75 Veeco ionization gauge. A single Veeco type RG-21A control unit is used to observe each gauge by means of a four-position selector switch. Table III.1 is a presentation of typical pressures observed in each chamber with liquid nitrogen in the three traps and a beam in the machine.

TABLE III.1

TYPICAL OBSERVED PRESSURES WITH BEAM ON

Section	Pressure
Oven chamber	1×10^{-6} torr
Velocity Selector Chamber	2×10^{-7} torr
Field chamber	7×10^{-8} torr
Detector chamber	1×10^{-7} torr

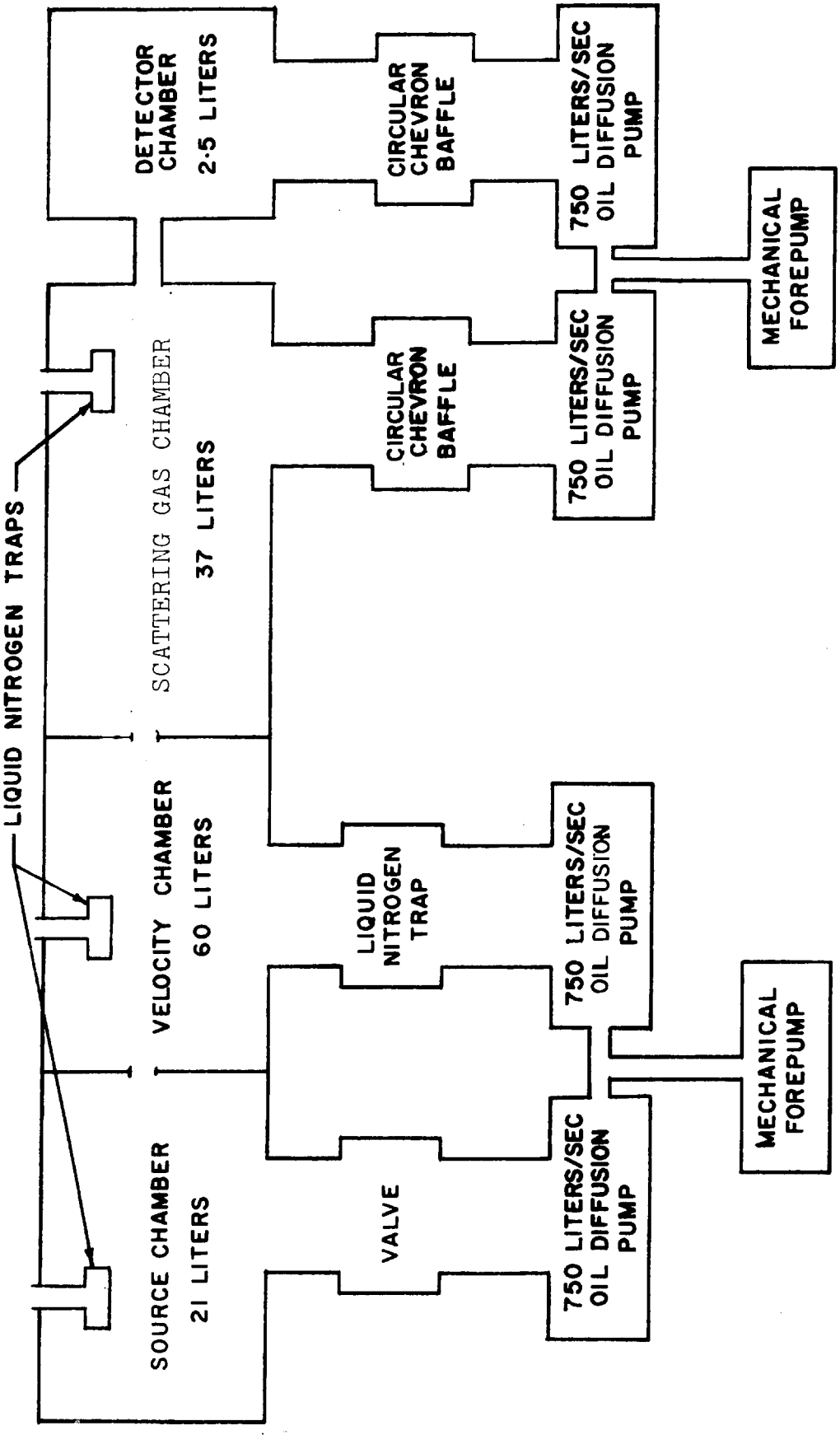


FIG. III.3.--VACUUM EQUIPMENT

B. Pressure Measurements.

Since a series of polarizability versus argon scattering gas density measurements were performed, an accurate determination of the argon partial pressure was required. This involved calibrating a Veeco RG-75 ionization gauge and control unit.

The calibration was done by the Space Physics Research Group (SPRG) by attaching our RG-75 gauge and control unit to their vacuum system upon which three calibrated Bayard Alpert Veeco ionization gauges were mounted.* The procedure was to leak in nitrogen gas after the system had reached its ultimate equilibrium pressure and compare readings between the four gauges. This was done over the pressure range of 10^{-10} torr down to 10^{-5} torr. Each individual run resulted in 60 data points for each gauge tube from which pressure comparison curves were constructed. A total of five separate runs were performed and an average correction factor for our gauge was calculated. The resulting gauge constant for our RG-75 gauge was 1.25×10^{-1} Amps/Torr as compared to a gauge constant of 1.00×10^{-1} Amps/Torr for the three calibrated gauges in a nitrogen gas atmosphere. This means that indicated pressure (P_I) must be multiplied by a factor of 0.8 to obtain the actual pressure (P_A) for nitrogen; that is,

---

*The three gauges were calibrated by using a McLeod gauge as the primary reference in a nitrogen gas atmosphere.

$$P_A = 0.8 P_I \qquad \text{III.1}$$

In order to correct the ionization gauge reading for the partial pressure of argon, results of a previous calibration run at SPRG were used in which a magnetron (constant energy electrons-90 ev) was used to compare sensitivities of the ionization gauges for nitrogen and argon gas. Thus, the following relation was used to correct the nitrogen partial pressure reading to argon gas partial pressure,

$$\frac{\sigma_{N_2}}{\sigma_{Ar}} = \frac{1}{1.148} = 0.87\ (\text{ARGON}) \qquad \text{III.2}$$

where σ_{N_2} and σ_{Ar} refer respectively to the ionization cross sections for 90 volt electrons.* Thus, the expression for the actual partial pressure of argon gas as measured by the calibrated RG-75 gauge is given by

$$P_A = 0.70 P_I \qquad \text{III.3}$$

The calibrated gauge was then placed on the field chamber (effective scattering cell) and the pressure reading between the original ionization gauge and the calibrated ionization gauge were compared under simulated running conditions. The result of the calibration check indicated that the original pressure reading has to be multiplied

*Private communication, D.D. Buglia, Ultek Corporation

by a factor of .78 to obtain the true pressure for argon in the field chamber, that is

$$P_A = 0.78 P_{I\,(ARGON)} \qquad \text{III.4}$$

A comparison of the gauges for typical vacuum conditions indicated that our original gauge read a consistent 15% lower pressure than the calibrated gauge. The results of this calibration procedure is estimated to be accurate to ± 25%.

C. Alkali Oven.

The oven source for the alkali runs is of the standard design (Kusch-Hughes, 1959) and is shown in Figure III.4. All the alkali measurements are made in a nickel oven using nickel knife edge slits gapped at 25.4 X 10^{-3} cm. The slit height is 1 cm. A coil of tungsten wire, inserted in ceramic tubing, is used as the heater element for the oven. The power supply for the oven is a Superior Electric Powerstat directly connected via vacuum-feed-throughs to the tungsten heater coil. Typical currents required for a run never exceeded 1.5 amps for the alkali metals.

The oven is located on three stainless steel pins mounted to a dove tail unit which allows the oven to be translated perpendicular to the beam trajectory by means of an external rotary micrometer-drive unit. It was observed that after thermal equilibrium had been achieved

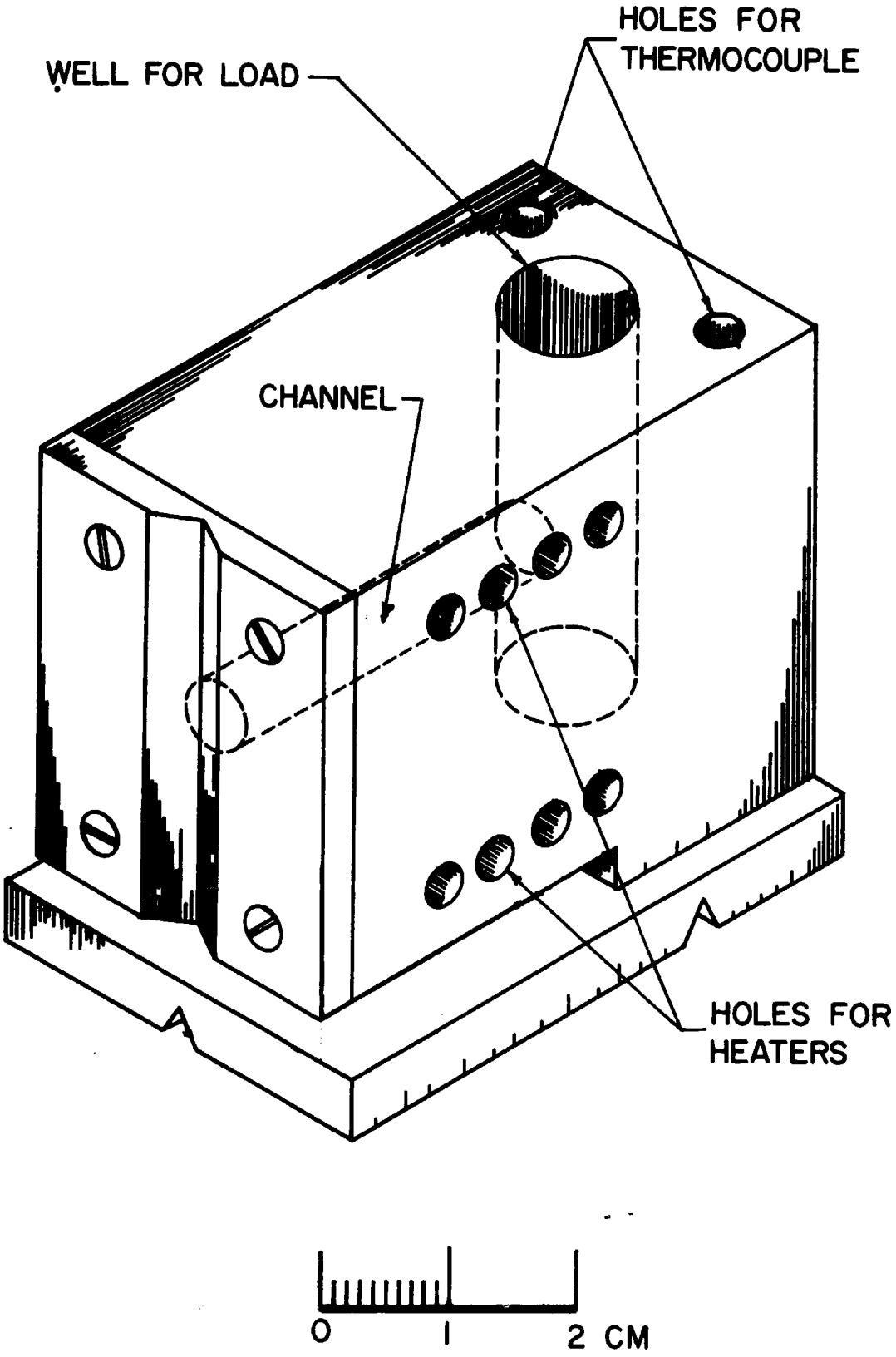


FIG. III.4.--OVEN

readjustment of the oven position was necessary due to thermal shifts which caused the beam to move off the optical axis. Changes in oven position as large as 10^{-2} cm were observed at oven temperatures around 500° K.

D. Temperature Measurement.

A pair of Chromel-P-Alumel thermocouples are used to monitor the temperature of the oven. The thermocouples are inserted in the oven receptacles at the back of the oven shown in Figure III.4. The indicated temperature as measured from each thermocouple was found to agree within 5° K. No attempt was made to measure the temperature drop across the oven (front to back) but, according to Chamberlain (1963), a 0.2% temperature gradient was observed in an identical nickel oven.

The reference junctions for the thermocouples are monitored by a mercury thermometer placed in thermal contact with the reference junctions. The emf of each thermocouple is measured by a Minneapolis-Honeywell Rubicon Potentiometer (Model No. 2732). The accuracy of the potentiometer and thermocouple circuit was checked by measuring the temperature at the ice point and the boiling point of water. The temperatures recorded were 0.07°C for the ice point of water and 100.09°C for the boiling point of water.

The Weston Standard Cell of the potentiometer was checked by the University of Michigan Electrical Engineering Department and found to be 1.01880 volts at 25°C.

This potentiometer is used later as a secondary laboratory voltage reference (Section G).

E. Collimator.

The collimator slit is constructed of stainless steel razor blade edges. The height of the slit is 1 cm and the width was maintained at 7.6×10^{-3} cm for all runs. The collimator slit assembly is itself rigidly mounted on the deflecting fields assembly as shown in Fig. III.6. The collimator slit cannot be adjusted from outside the vacuum enclosure. Thus, it was necessary to optically check its alignment before each run, as described in Chapter IV.

F. Deflecting Field and High Voltage Power Supply.

The deflecting field used for the polarizability measurements is the well-known two wire deflecting field. (Ramsey, 1956). The field is constructed such that its surfaces are equivalent to the equipotential surfaces produced by having two line charges of equal and opposite sign located a distance 2a apart. These equipotential surfaces are circular cylinders passing through the point $\pm$ a. In Figure III.5 the ideal two wire field is shown as established between two intersecting cylindrical equipotentials (in practice, the electrodes obviously cannot intersect when a potential is applied between them). The trough radius r_2 is continued by the dashed lines shown to

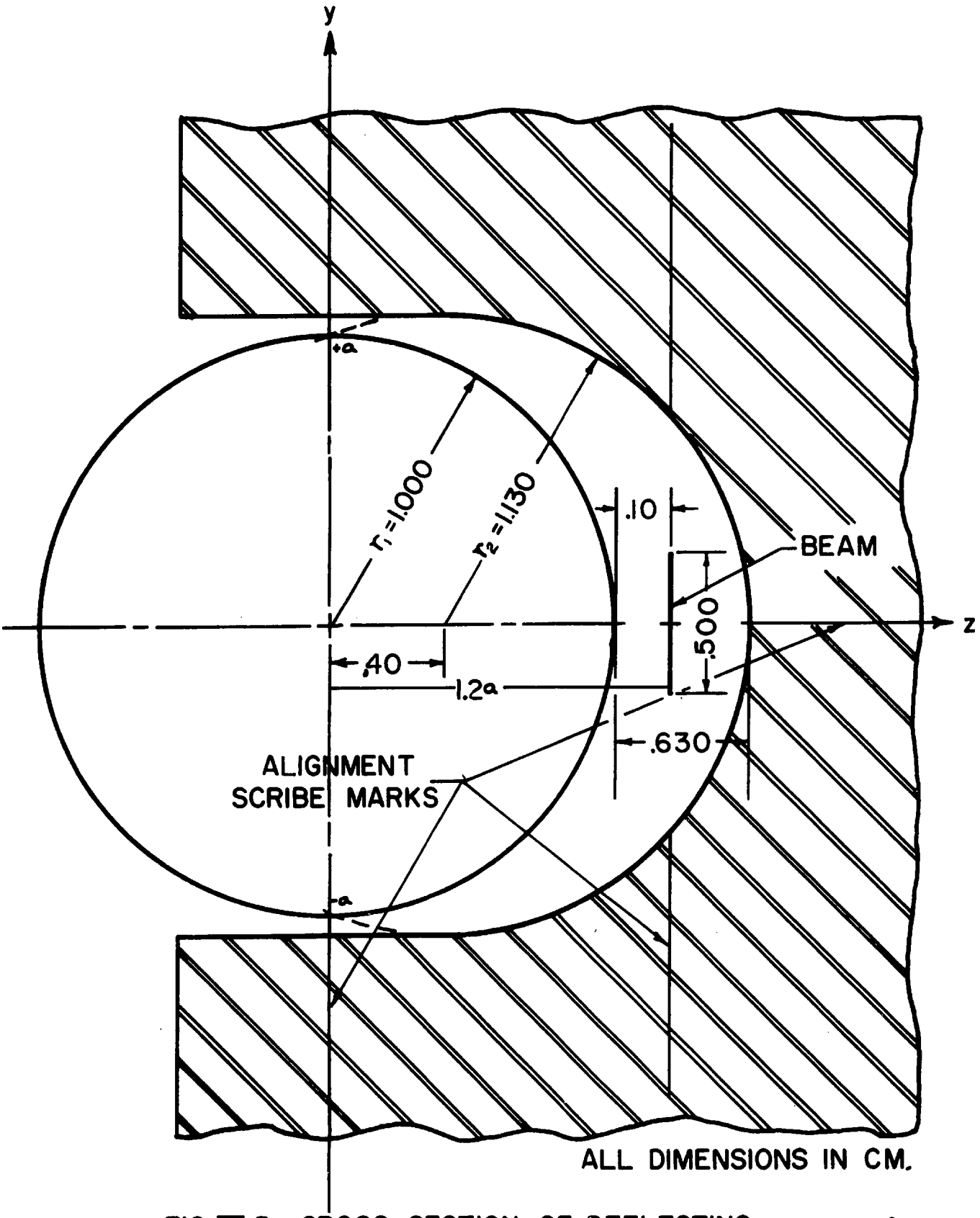


FIG. III.5.--CROSS SECTION OF DEFLECTING ELECTRODES FOR ALKALI BEAMS

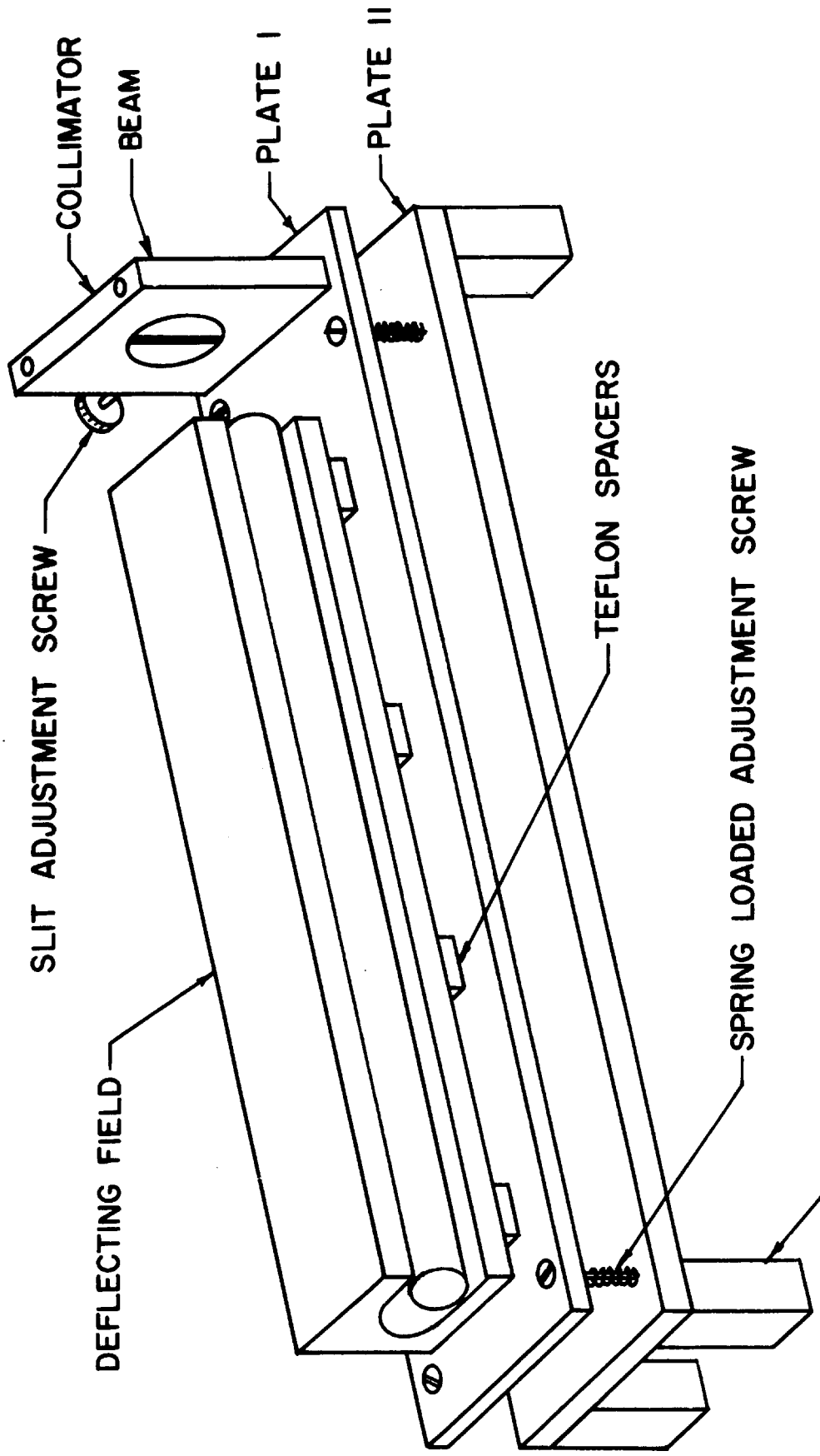


FIG. III.6.--FIELD AND COLLIMATOR MOUNT

the points of intersection with the bead radius r_1. The points of intersection defines the y axis and are located a distance 2a apart. This quantity "a" characterizes the two wire field.

The electrode trough is machined from a bar of aluminum 40 cm long and the inside is polished. The bead is a polished, 2.54 cm diameter, 304 stainless steel rod. The bead is mounted to the trough with four teflon spacers. The trough and bead are scribed with the lines shown in Figure III.5 to insure proper alignment. The horizontal and vertical scribe marks to the right of the bead located at Z = 1.2 a define the position of the beam during a run. The other scribe marks are used to check for any misalignment of the bead-trough relation due to creep of the teflon over a period of time.

The field mount is shown in Figure III.6 with the collimator mounted on plate I. The spacer blocks are rigidly mounted to the fields chamber via 1/4-20 stainless bolts. Plate I, upon which the field is mounted, is attached by four spring loaded adjustable screws to plate II. This arrangement makes possible the optical alignment of fields electrodes with respect to the beam path. To insure proper alignment of the back of the field, a jig was constructed which slides over the trough of the field and has two 3×10^{-3} cm cross hairs which coincide with the scribe marks, thus allowing optical alignment.

The maximum voltage applied to the field electrodes

never exceeded 10 kv. It was found that the field was able to hold this voltage with no apparent current drain. Two "Advac" high voltage vacuum feed throughs were used to pass the deflecting field voltage into the vacuum chamber.

The power supply used to provide the deflecting voltage for all measurements was a Fluke Model 410B D.C. Power Supply (Serial No. 123). The output voltage was 0 to ± 10,000 volts with a quoted accuracy of ± 0.25%. The recovery time for the supply is 50 microseconds.

The calibration of the supply was checked using a voltage divider network consisting of a $10^9\Omega$ high precision resistor in series with the $10^6\Omega$ input resistance of a Dymec Integrating Digital Voltmeter Model No. 2401C (Serial No. 501-00034). The circuit is shown in Figure III.7.

The procedure for the calibration measurement is as follows. The division factor of the bridge (δ) was determined by taking the ratio of the output voltage of bridge to output voltage of the supply in integral steps from 10 volts to 1000 volts. The division factor δ was found to be constant to 2 parts in 10^4 in a series of measurements over the previously mentioned voltage range. The output voltage of the supply in the voltage range 1000 - 10,000 volts is now determined by multiplying the indicated output voltage of the bridge by the reciprocal of the division factor δ where $\delta = (904 \pm 2) \times 10^{-3}$. Using this method, the output voltage was found to be accurate to

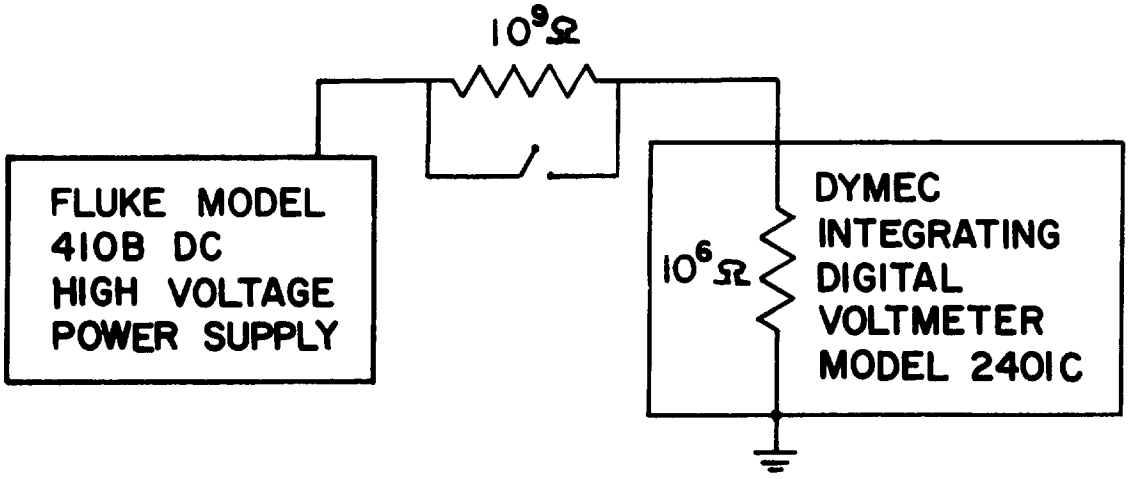


FIG. III.7.--HIGH VOLTAGE CALIBRATION CIRCUIT

within 0.5% of its rated output voltage.

The Dymec Integrating Digital Voltmeter calibration was checked by using the Rubicon Potentiometer No. 2732, whose Weston Standard cell calibration was checked by the University of Michigan Electrical Engineering Department and found to be 1.01880 volts at 25° C. The Dymec unit was found to be accurate to 0.001% using the potentiometer as a secondary voltage standard.

Before each run, the calibration of the high voltage power supply was checked by measuring the output voltage on the 1000 volt gauge and comparing the values to voltage obtained in the calibrated measurements described above.

G. Velocity Selector.

The velocity selector used in the polarizability, scattering and velocity profile measurements consists of six slotted disks spaced such that the beam is completely free of sidebands (Bernstein and Hostettler, 1960). The dimensions and general details of the rotor assembly are shown in Fig. III. 8.

The disks are all mounted on a single shaft and Syntorque Corporation Two Pole Hysteresis Motor (Type 17H71) provides the necessary torque to rotate the disks in the range from zero to thirteen thousand revolutions per minute. Figures III.9 and III.10 show the entire velocity selector assembly with the rotor unit mounted in the supporting frame. The base of the velocity selector frame

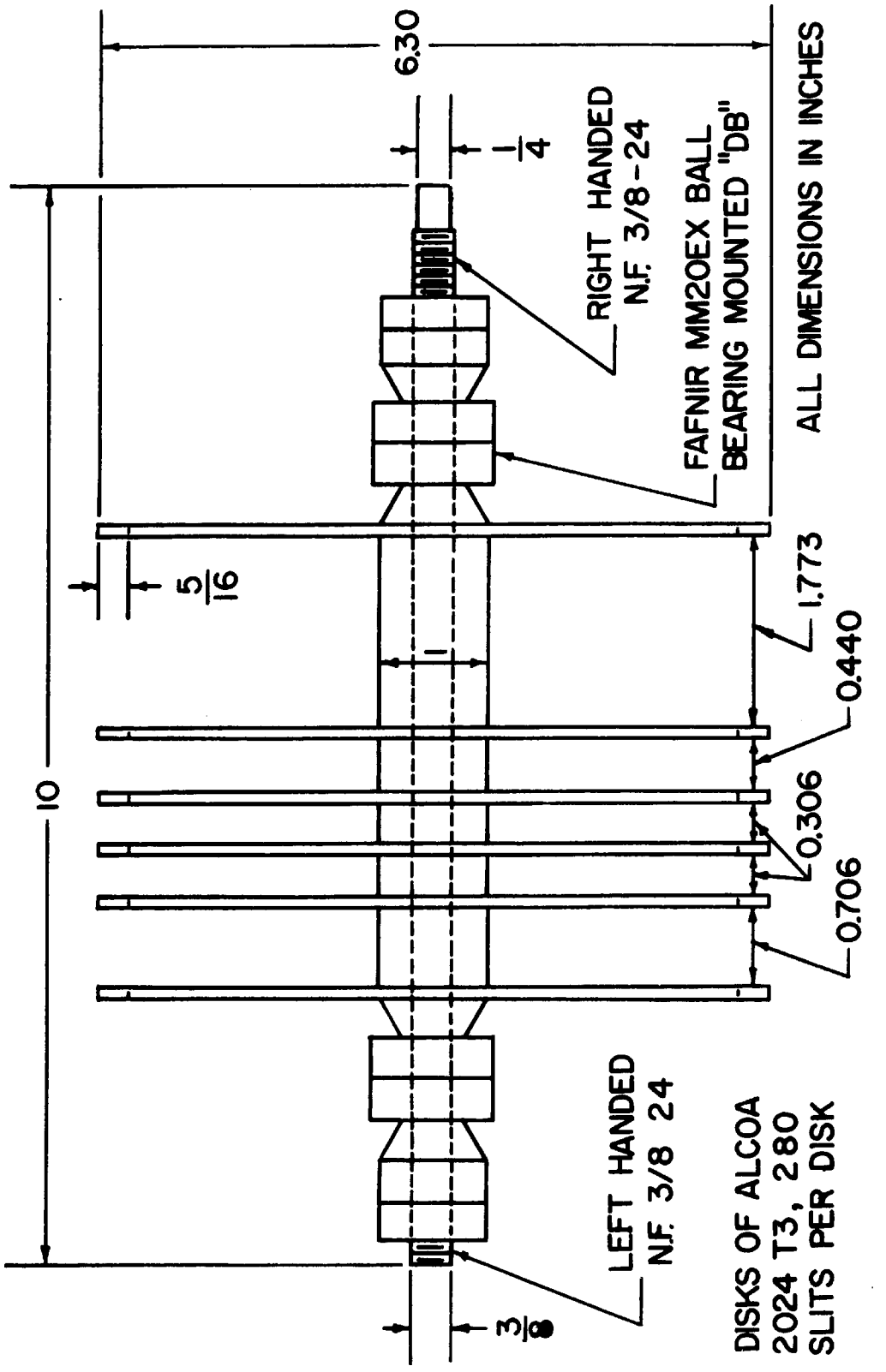


FIG. III.8. VELOCITY SELECTOR ROTOR DIAGRAM

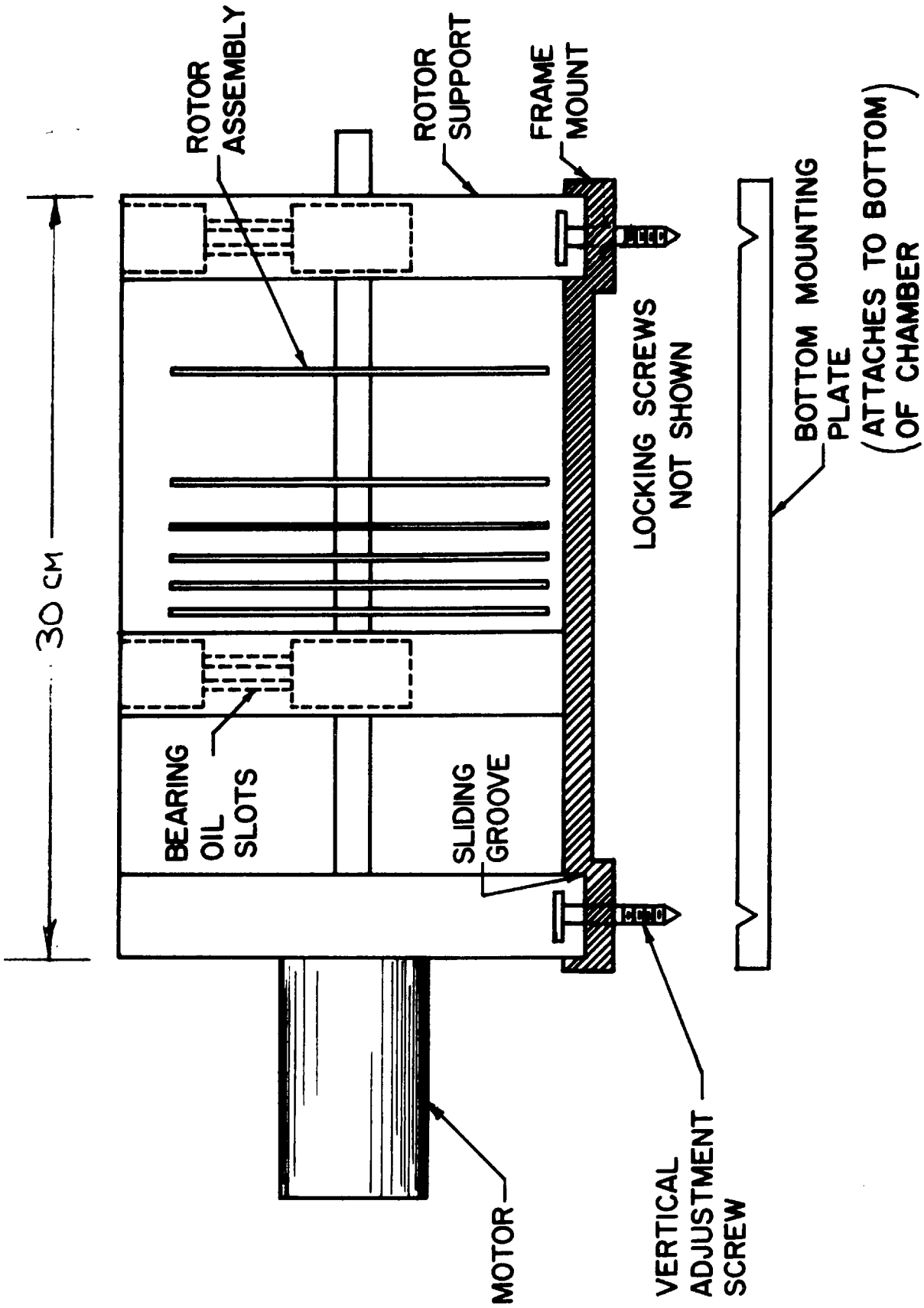


FIG. III.9--VELOCITY SELECTOR AND FRAME MOUNT (SIDE VIEW)

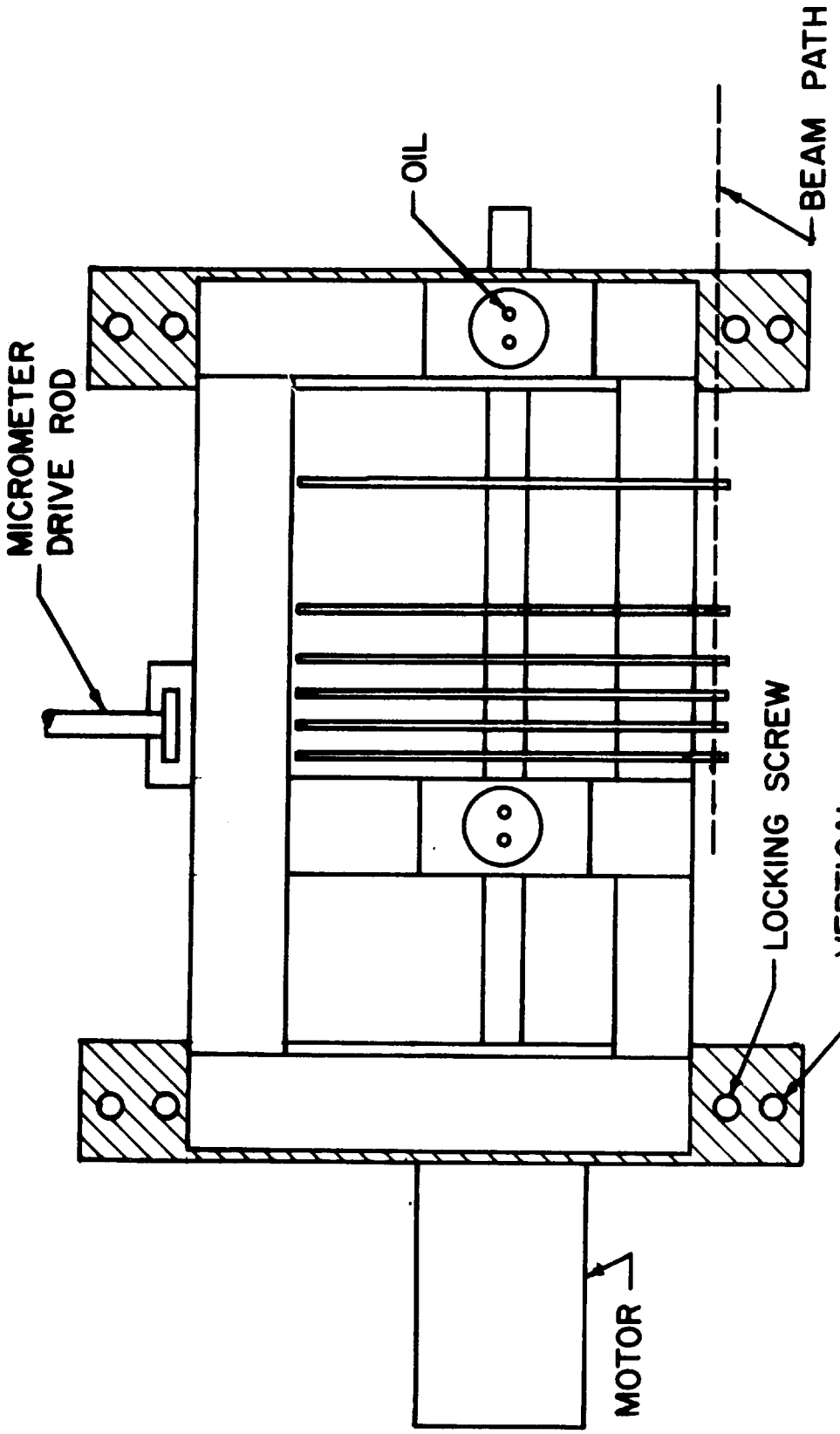


FIG. III.10.--VELOCITY SELECTOR AND FRAME MOUNT
(TOP VIEW)

is mounted in an adjustable table which provides both vertical and horizontal position alignment. The table also served as a dovetail slide groove which allows the velocity selector to be moved in and out of the beam by means of an external rotary micrometer drive unit. The table has a set of stops which provides a means of accurately repositioning the selector unit in the beam. For initial alignment procedures a set of precision pins are placed in the velocity selector frame in the exact line the beam should follow. Then the entire velocity selector assembly is aligned to a predetermined optical axis which the beam will follow during the course of a run. The position of the velocity selector is checked before and after each run. For details of the theory of operation of the velocity selector, see Appendix C.

Power is supplied to the rotor motor by a Hewlett-Packard Audio Oscillator Model 200AB whose signal is amplified by a Dynakit ST-70 Stereo Amplifier. The circuit used is shown in Fig. III.11. The phase shifter is necessary because the reactance of the motor changes as a function of rotor speed. The scope is used to observe the phase relation of the two input signals (Lissajous figure; circle for 90° phase difference), thus allowing correct adjustment of the phase shifter to maintain the 90° phase difference.

A General Radio Strobotac Model 1531-A was used to check the angular motion of the velocity selector rotor.

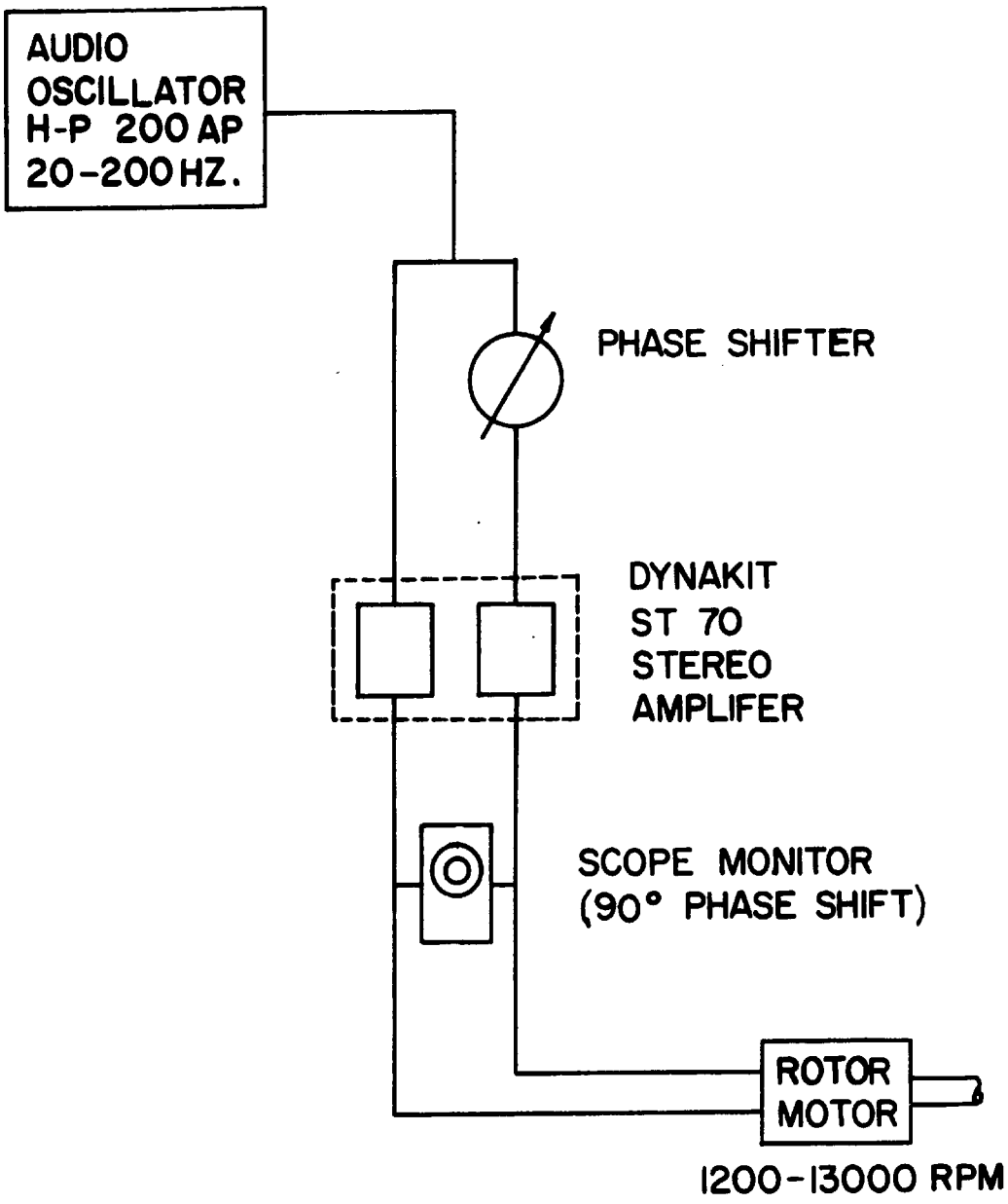


FIG. III. 11.--CIRCUIT DIAGRAM FOR VELOCITY SELECTOR ROTOR MOTOR

The relationship of the indicated RPM by the Strobotac and that of the audio oscillator was checked by using a beat frequency method in conjunction with a H-P 524L frequency counter. The positions on the dial face of the audio oscillator were calibrated with respect to the 524L frequency counter and found to be accurate to 0.1% of the indicated settings.

H. Detector.

The detector used in the experiments with the alkali metals is the standard surface ionization detector (Ramsey 1956, p. 379) with a 7.6×10^{-3} cm diameter heated tungsten filament 3 cm long. The positive ions which are formed at the surface of the wire are drawn off by a 45 volt potential difference and collected with a semi-cylindrical electrode in front of the wire. A Keithley Model 610BR Electrometer is used to monitor the positive ion current which is proportional to the total beam incident on the wire (in the case of the alkali metals the proportionality constant is effectively unity). The collector in front of the wire has slot machined in it, through which the neutral beam passes. The height of the slot is 0.50 cm. The linearity of the electrometer through the ranges of application has been measured as better than 0.1%.

The entire detector is mounted on a spring-loaded table which can be manually translated perpendicular to beam trajectory. The position of the table (detector wire)

is recorded on a Starrett dial indicator (Model No. 655-341) to ± 0.3 X 10^{-3} cm. To insure reproducibility, the readings are always taken in the same direction of translation.

I. Telescope.

The telescope used to align the apparatus is a Keuffel and Esser 9092-22 Paragon Jug Transit with a 9092-7 optical micrometer. The resolving power of the telescope is 0.4 seconds of arc according to the N.B.S. test procedure. The resolving power was checked and found to be 4.7 seconds of arc (Thomas C. English Thesis, 1965). This corresponds to one mil at six feet.

J. Leak.

The leak used in the gas scattering experiments is a Nupro Very Fine Metering Valve (Series S). It was possible to obtain leak rates as low as 10^{-3} torr liters per second using argon gas. The valve itself consists of a needle point stem tapered at one degree which sits in an orifice 0.031 inches in diameter. Finger tip tightening will close the valve leak tight.

The leak is attached to the field chamber which is used as the scattering cell in all experiments.

K. Scattering Gas.

Argon was used for all scattering experiments unless otherwise noted. The argon is rated 99.9% pure by the

supplier. A Nupro Filter was used to remove water vapor and dust particles from the gas.

L. Alkali Metal Purity.

The samples of the alkali metals used in the runs were obtained from the A.D. Macay Company with a quoted purity of 99.9% with the exception of potassium, which was obtained from an existing supply in the laboratory and had a quoted purity of 99.95%. In order to be absolutely sure that the elements used during various runs were what they were stated to be, it was decided to investigate the emission spectra of the alkali metals used in the runs by putting samples in a hollow carbon electrode and using a double prism spectrograph to record the emission lines in the visible region. The results of this check were gratifying in that they indicated the samples were free of any impurities to within 2%. Details of this check are contained in an internal laboratory report (Bechtel, 1967).

CHAPTER FOUR

EXPERIMENTAL PROCEDURE

A. Alignment Procedure.

One of the parameters which is extremely important in the experimental determination of the alkali polarizabilities is the electric field seen by the atom in the fields region. Consequently the position of the beam as it traverses the deflection fields must be well known. A knowledge of the beam position is also fundamental to the operation of the velocity selector because,as it is shown in Appendix C, the parameters characterizing the operation of the velocity depend on r, the radius of the disk at which the beam passes. Thus, correct alignment is crucial to the accuracy of the experiment.

The alignment procedure of the apparatus can best be described in the following series of steps.

1. The optical axis of the telescope is aligned to the reference marks on the field with the collimator removed from the field mount.
2. The telescope is now focused on the oven, and the oven is adjusted until the geometrical center of the rectangular slits falls on the optical axis.
3. Precision alignment pins are inserted in the velocity

selector frame and the table is adjusted until the pins are level and lie on the optical axis. The velocity selector is then translated until it reaches the table stops and the pins are again checked for alignment. The position of the optical axis on the rotor disks is now marked and measured to determine the radius r.

4. The detector wire is now placed on the optical axis and the dial indicator is adjusted to read zero.

5. The collimator is placed in position and aligned on the optical axis.

6. The 7.6×10^{-3} cm stop wire in front of the fields is now positioned on the optical axis and then translated out of the way. Its position is recorded by reading its micrometer drive setting. The above six steps are all performed with the apparatus open to air.

The next set of steps are performed with the system evacuated.

7. The stop wire position is rechecked and realigned because changes of the field chamber wall position under vacuum produce changes in the stop wire position on the order of 7.6×10^{-3} cm.

8. The detector wire position is rechecked with the wire heated to 1200° K. Position changes on the order of 5×10^{-3} cm are observed which are due to thermal shifts of the wire.

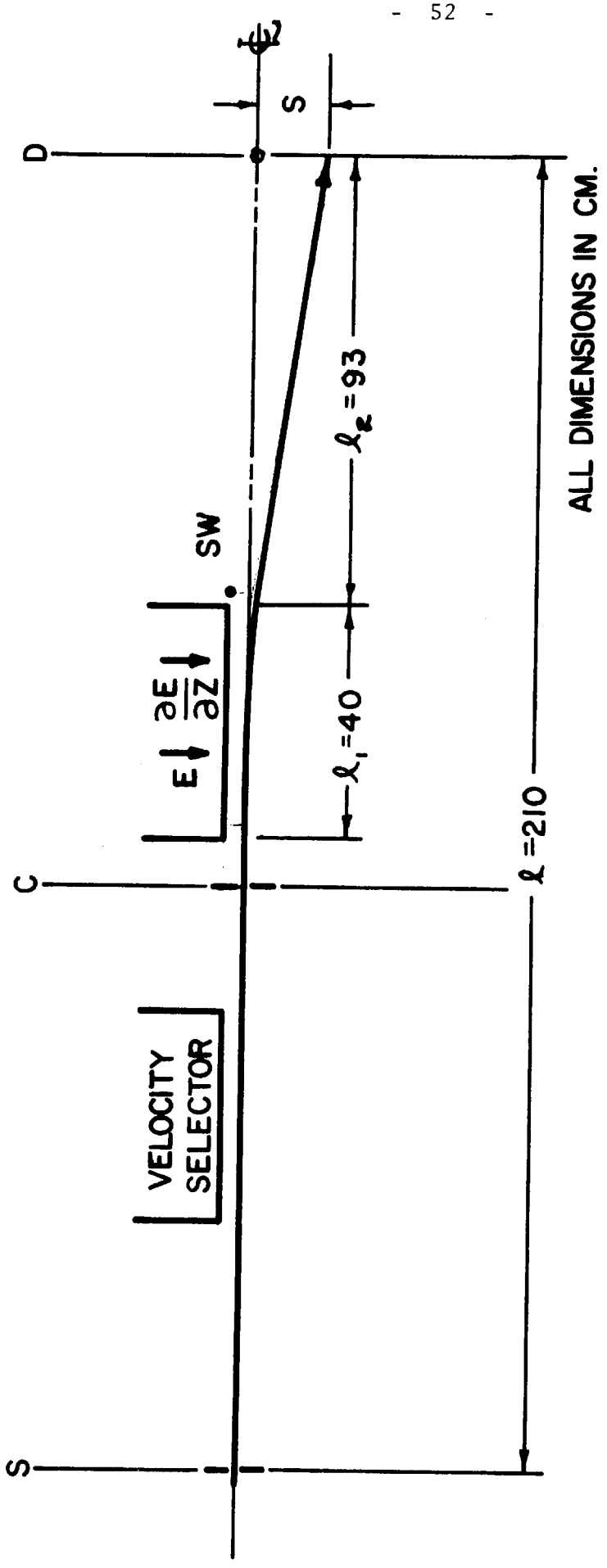
9. Now, with the wire position recalibrated and after the oven has been heated to operating temperature

(400° K) and reached thermal equilibrium, the oven is translated until an intensity maximum is observed. Typical shifts in oven position are on the order of 9×10^{-3} cm at 400° K.

10. As a final check, the stop wire is moved into position and a symmetrical minimum in the intensity is checked for about the zero setting on the dial indicator.

After completion of the above steps, the center of the undeflected beam is estimated to be located at Z = (1.2 ± 0.003) cm. Figure VI.1 indicates the alkali beam deflecting geometry.

Prior to taking data, the oven temperature, oven current, wire current and pressures in the four chambers are recorded and periodically checked. Then a preliminary beam shape (a plot of beam intensity versus detector wire position) is taken and the full width at half maximum (FWHM) is compared to the theoretically predicted FWHM which is calculated from the geometrical parameters of the apparatus. This check insures against extreme vertical slit misalignment with respect to the detector wire, collimator slit, and oven slit. Theory predicts 38×10^{-3} cm and experimental measurements yield 43×10^{-3} cm FWHM. This slight broadening of the beam can be explained by scattering of the beam atoms in the region between the collimator and detector. The beam shapes are always measured in the same direction of translation.



$$S = \frac{\alpha\, E\, \partial E/\partial Z}{2\, m\, v^2}\, \ell_1 (\ell_1 + 2\ell_2)$$

FIG. IV. 1 :- DEFLECTING GEOMETRY FOR ALKALI BEAM

B. Small Shift Analysis.

In the small shift measurements, the beam shape is carefully recorded on graph paper in order to determine γ, the slope of the beam shape. Checks on the reproducibility of the beam shape indicate that the short term stability of the beam and the reproducibility of the detector wire coordinate introduce systematic differences of less than 0.5% in the measured value of γ.

In making the deflection measurements, the detector is placed near the half maximum position on the beam shape which represents the central portion of the linear region of the beam shape.* After the placement of the detector, the deflection measurements consist of recording changes in the intensity (dI) when a voltage is alternately applied to the deflecting fields. This procedure is carried out on both sides of the beam shape for three different voltages and nine data points are recorded at each voltage. This corresponds to a total of 54 data points for each beam shape at three different deflecting voltages.

Data are obtained in the manner described above for both velocity selected (VS) and non-velocity selected (NVS) beams. When the velocity selector was used, the overall beam intensity was reduced by a factor of approximately sixty for the peak intensity I_o on the velocity profile.

*See Figure V.1.

This reduction in intensity limited the lower and upper velocities at which data could be obtained because of small spurious background signals due to wire noise and current leaks from the detector bias voltages. Signal intensities of less than 1×10^{-13} amps were not measured because of these background signals.

The voltages applied to the fields were such that the beam deflections were always less than the diameter of the detector wire (7.6×10^{-3} cm) for all small shift measurements.

The acquisition of data for the small shift analysis is greatly simplified by the following system. A programable circuit using an industrial timer and a set of relays is used to provide a series of signals which initiate the automatic recording of nine data points for a particular deflecting field voltage. The signal from the electrometer is fed into an integrating digital voltmeter and the high voltage power supply is turned on and off, and the difference in beam intensity is averaged and recorded on a digital recorder. The circuit diagram is shown in Figure IV.2.

The timer sequence is such that the high voltage is cycled on and off every 10 seconds. The digital voltmeter records the signal intensity 7 seconds after the high voltage is cycled and the reading is stored in the memory circuit. Ten seconds later the next reading is subtracted from the previously stored input reading and the print command signal allows the printer to record the difference. This printed difference reading corresponds to the change in beam intensity

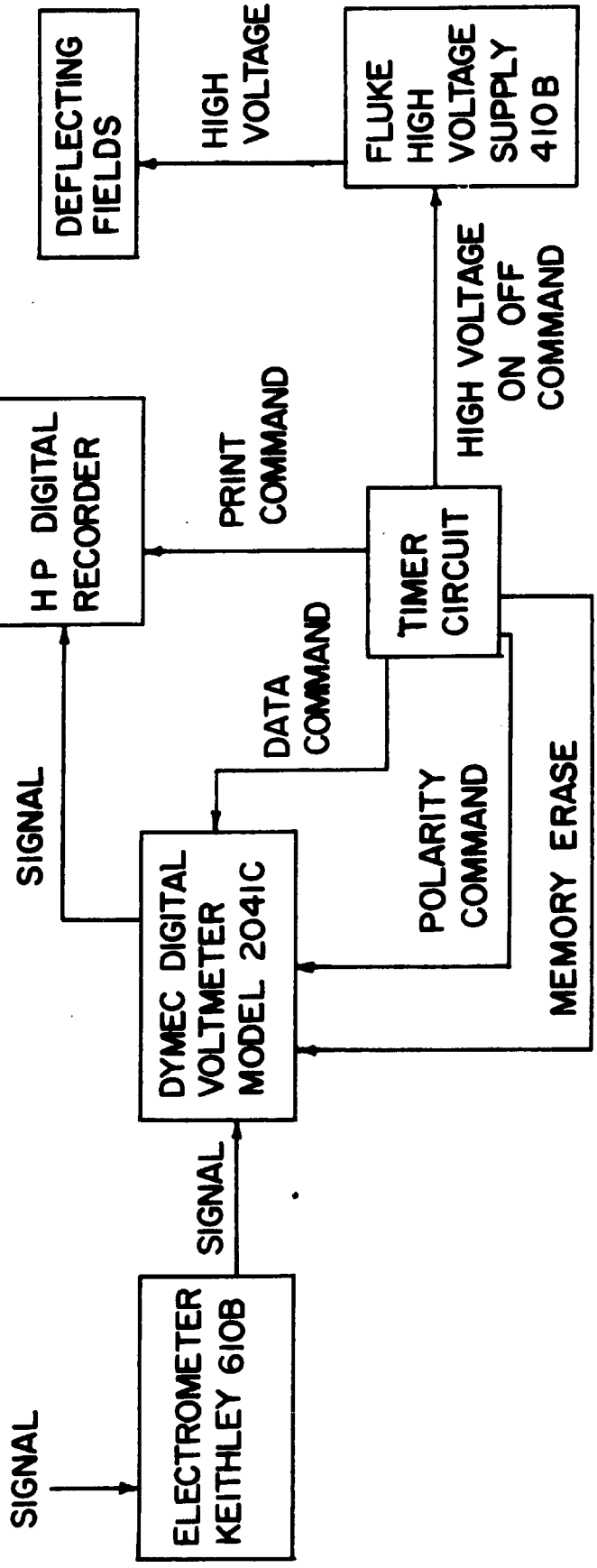


FIG. IV. 2.--SMALL SHIFT DATA ANALYSIS DIAGRAM

dI. The memory erase signal clears the memory circuit and the whole sequence is repeated 18 times, giving a total of 9 printed data points at a particular voltage. The on-off cycling of the power supply introduces no long-lived transients since, as reported in Chapter Three, G, the recovery time is less than 50 microseconds. All small shift data was taken using the above system.

C. Large Shift Analysis.

All the data obtained in the large shift measurements was for a velocity selected beam. This eliminates the difficult problem of distortion in the beam shape which would arise due to the velocity distribution in the non-velocity selected beam.

The data obtained using this method is quite straightforward. An undeflected beam shape is carefully recorded and then, with 10 kv on the deflecting field, the deflected beam shape is recorded. The deflection is obtained directly by comparison of the two beam shapes.

Large shift measurements were obtained for all runs except run 6K and for at least three different velocities in the course of an individual run. Most of the data obtained using this method was for the lowest possible velocities since the smaller the velocity the larger the observable deflection. Shifts varying from 7.5×10^{-3} cm to 20×10^{-2} cm were observed.

D. Velocity Profile Measurements.

Velocity profile measurements refer to velocity versus intensity measurements which were obtained by holding the detector position fixed and varying the angular speed of the velocity selector rotor. Each point obtained on the velocity profile curve is the result of averaging ten data points taken at a particular velocity. Typical intensities ranged from 1×10^{-13} amps to 3×10^{-12} amps. The statistical fluctuations associated with each point were on the order of 1×10^{-15} amps. The representative curves are plotted and normalized to unit intensity to afford a comparison with the theoretical velocity profile curve described in Appendix C.

In later runs, velocity profiles were measured as a function of the argon scattering gas pressure. In all profile measurements the pressures and oven temperatures were carefully recorded.

With the exception of potassium, velocity profile measurements were made over a major portion of the velocity distribution. The limiting factor for the potassium runs was the maximum allowable angular speed of the velocity selector rotor which was set at 13,000 RPM, which corresponds to about 67,000 cm/sec. Thus for potassium it limited the data to only a few points on the high velocity side of the most probable velocity v_p.

E. Scattering Cross Section Determination.

The measurement of the total scattering cross section

for the interaction of the alkali metals potassium, rubidium, and cesium with argon gas were made by observing a reduction in the intensity of the beam species after it passes through a region (scattering cell) containing the scattering gas (Rosin and Rabi, 1935). The scattering gas pressures and beam intensities were recorded and later used to calculate the total scattering cross section. The angular resolution of the apparatus for a single scattering event is calculated to be 5×10^{-5} radians at the center of the scattering cell (Kusch, 1962).

The assumptions made in calculating the total cross sections are as follows:

1. The density of the scattering gas is constant in the scattering cell.
2. The length of the scattering cell is taken to be the linear dimension of the field chamber (76 cm).
3. Multiple scattering events are not considered.
4. Scattering of beam particles back into the detected beam are neglected.
5. The resolution of the apparatus is considered constant.
6. All scattering events are considered to originate in the scattering cell, and are exclusively attributed to the argon scattering gas.

F. Polarizability Measurements Versus Argon Scattering Gas Pressures.

Polarizabilities for the alkali metals were measured for a non-velocity selected beam as a function of the scattering gas pressure in the field chamber. The polarizabilities were recorded using the small shift method. During the runs the field chamber pressure and oven temperature were carefully recorded.

Velocity-selected small shift and large shift measurements were also made at the same scattering gas pressures as a check for consistency in the velocity selected polarizabilities. Velocity profiles as mentioned in Section D were also recorded as a function of scattering gas pressure.

CHAPTER FIVE

EXPERIMENTAL RESULTS OF ALKALI POLARIZABILITY AND SCATTERING MEASUREMENTS

The symbols used in the tables have the following definitions:

T_S = Source temperature (K^o).

S = (1) indicates measurements taken on side (1) of the beam shape.

S = (2) indicates measurements taken on side (2) of the beam shape.

γ = Beam slope (Amps/cm).

V = Voltage applied to deflecting field (esu).

v = velocity of beam particles (m/sec).

α_i = polarizability measured for the i^{th} deflection (A^3).

$\bar{\alpha}$ = average of measured polarizability on S(1) and S(2).

$\bar{\alpha}_{LS}$ = total average large shift polarizability.

$\bar{\alpha}_{vs}$ = total average small shift velocity selected polarizability.

$\bar{\alpha}_{NVS}$ = total average small shift non-velocity selected polarizability.

$\overline{\alpha_T}$ = total average measured polarizability for individual run.

LS = observed large shift (10^{-3} cm).

P = pressure in apparatus during run (torr).

$\dot{n}$ = the number of polarizability values measured.

A. Small Shift Polarizability Results for Na, K, Rb, and Cs.

The experimental small shift results and corresponding values of α for the alkali metals Na, K, Rb, and Cs are summarized in Tables V.1, V.2, V.3, and V.4. The tables actually represent a reduction of considerably more extensive data than shown. In particular, the number of measurements performed is indicated by the symbol n.

A typical beam shape is shown in Figure V.1. The slope γ is obtained by drawing a line tangent to the linear portions of the curve, as indicated in the figure. In general, the sides of the beam shape are linear over a distance of 20×10^{-3} cm for a full width at half maximum (FWHM) of 32×10^{-3} cm. The small shift data was obtained with the detector centered about the linear portion of the beam as indicated by the stars in Figure V.1. The maximum deflection allowed in the small shift analysis corresponded to a shift of 0.8×10^{-3} cm at the detector.

B. Statistical Analysis.

The deflections from which the individual values of α_i are calculated are assumed to be normally distributed. A mean value, standard deviation, and standard error of the mean (SEM) are calculated (Young, 1963). In a sample of n values $\alpha_1 \text{---} \alpha_n$ taken from an infinite population with normal distribution, the most probable value of the measured

TABLE V.1

SMALL SHIFT DEFLECTION POLARIZABILITY MEASUREMENTS FOR SODIUM

Run	Date	T_S	S	γ	V^2	v	α_i	$\bar{\alpha}$	$\bar{\alpha}_T$
		^oK		$\frac{amps}{cm}$ $X10^{-10}$	esu^2	m/sec	$Å^3$	$Å^3$	$Å^3$
1Na	8/8/66	560	1	.195	100	--	22.02	22.38	
			2	.190	178	--	22.74		22.56
P = 6 X 10^{-8} torr			1	.238	278	--	22.55	22.73	
			2	.236	400	--	22.92		
			1	.092		301.2	23.14	23.53	
			2	.092		301.2	24.00		
			1	.147		338.8	23.72	24.20	
			2	.145		338.8	24.65		24.35
			1	.245		376.5	24.53	24.80	
			2	.250		376.5	25.06		
			1	.381		414.1	24.75	24.90	
			2	.391		414.1	25.00		

TABLE V.2

SMALL SHIFT DEFLECTION POLARIZABILITY MEASUREMENTS FOR POTASSIUM

Run	Date	T_S	S	γ	V^2	v	α_i	$\bar{\alpha}$	$\bar{\alpha}_T$
		^oK		$\frac{amps}{cm}$ $X10^{-10}$	esu^2	m/sec	$Å^3$	$Å^3$	$Å^3$
6K	9/22/66	457	1	.472		--	42.10	42.22	
			2	.488	100	--	42.25		42.22
P = 1 X 10^{-7} torr			1	.15	178	338.8	47.44	46.11	
			2	.16	278	338.8	44.79		44.27
			1	.279		414.1	45.90	44.36	
			2	.281		414.1	42.82		
			1	.336		476.9	47.83	45.58	
			2	.396		476.9	43.33		
			1	.443		558.4	44.98	43.51	
			2	.433		558.4	42.06		
7K	9/29/66	443	1	.167		--	42.32	42.22	
			2	.168		--	42.11		42.51
P = 6 X 10^{-8} torr			1	.168		--	44.36	42.80	
			2	.158		--	41.15		
			1	.098	100	348.8	44.08	45.61	
			2	.090	136	348.8	47.15		
			1	.148	178	423.5	46.75	45.40	
			2	.154		423.5	45.53		45.58
			1	.221		514.5	45.21	44.22	
			2	.210		514.5	43.23		

TABLE V.2 (CONT.)

Run	Date	T_S	S	γ	V^2	v	α_i	$\bar{\alpha}$	$\bar{\alpha}_T$
		^oK		$\frac{Amps}{cm}$ $X10^{-10}$	esu^2	m/sec	$Å^3$	$Å^3$	$Å^3$
7K			1	.210		596.1	47.21	47.11	
			2	.210		596.1	46.92		
8K	10/29/66	465	1	26.5	100	--	41.67	42.54	42.54
			2	27.4	178	--	43.41		
P = 7 X 10^{-8} torr			1	.032	278	257.2	45.70	45.00	
			2	.035		257.2	44.30		
			1	.086		313.7	42.50	43.50	
			2	.086		313.7	44.31		
			1	.140		376.5	45.76	45.73	
			2	.143		376.5	45.70		44.88
			1	.223		445.5	44.81	45.30	
			2	.230		445.5	45.74		
			1	.271		502.0	45.32	45.37	
			2	.284		502.0	45.42		
9K	2/18/67	456	1	34.7	178	--	42.39	41.70	41.70
			2	36.4	278	--	41.00		
P = 6 X 10^{-8} torr			1	.029	400	225.9	47.33	45.90	
			2	.033		225.9	44.48		45.43
			1	.063		263.5	44.65	44.60	
			2	.059		263.5	44.55		

TABLE V.2 (CONT.)

Run	Date	T_S	S	γ	V^2	v	α_i	$\bar{\alpha}$	$\bar{\alpha}_T$
		^oK		$\frac{Amps}{cm}$ $X10^{-10}$	esu^2	m/sec	$Å^3$	$Å^3$	$Å^3$
9K			1	.096		301.2	46.31	46.10	
			2	.099		301.2	45.90		
			1	.142		338.8	45.09	44.87	
			2	.147		338.8	44.63		45.43
			1	.206		376.5	45.03	45.70	
			2	.198		376.5	46.37		
			1	.159		357.6	45.75	45.70	
			2	.154		357.6	45.65		

TABLE V.3

SMALL SHIFT DEFLECTION POLARIZABILITY MEASUREMENTS FOR RUBIDIUM

Run	Date	T_S	S	γ	V^2	v	α_i	$\bar{\alpha}$	$\bar{\alpha}_T$
		^oK		$\frac{amps}{cm}$ $X10^{-10}$	esu^2	m/sec	$Å^3$	$Å^3$	$Å^3$
1Rb	10/20/66	453	1	.030	44.5	263.5	47.20	47.74	
			2	.031	69.6	263.5	48.28		
			1	.051	100.2	326.3	49.51	48.20	
P = 8 X 10^{-8} torr			2	.056		326.3	46.91		47.57
			1	.079		489.4	47.54	48.01	
			2	.072		489.4	48.48		
			1	.063		527.1	46.78	46.45	
			2	.065		527.1	46.11		
			1	.015		225.9	47.45	47.45	
2Rb	11/18/66	444	1	.022	178	225.9	48.80	49.02	
			2	.019	278	225.9	49.25		
			1	.058	400	263.5	50.25	50.52	
P = 7 X 10^{-8} torr			2	.058		263.5	50.79		49.79
			1	.102		301.2	50.48	50.40	
			2	.103		301.2	50.32		
			1	.171		338.8	50.31	49.60	
			2	.172		338.8	48.08		
			1	.283		451.8	48.96	49.40	

TABLE V. 3 (CONT.)

Run	Date	T_S	S	γ	V^2	v	α_i	$\bar{\alpha}$	$\bar{\alpha}_T$
		^oK		$\frac{Amps}{cm}$ $X10^{-10}$	esu^2	m/sec	$Å^3$	$Å^3$	$Å^3$
2Rb			2	.281		451.8	49.87		
			1	.227		376.5	48.84	49.80	
			2	.227		376.5	50.77		
4Rb	3/31/67	473	1	.070	178	263.5	50.93	49.41	
			2	.071	278	263.5	47.94		
P = 6 X 10^{-8} torr			1	.132	400	338.8	48.48	47.71	
			2	.138		338.8	46.94		48.11
			1	.299		376.5	48.58	48.24	
			2	.343		376.5	47.90		
			1	.141		225.9	47.81	47.10	
			2	.142		225.9	46.38		
5Rb	5/17/67	430	1	26.6	178	--	41.97	42.27	42.27
			2	25.6	278	--	42.58		
P = 6 X 10^{-8} torr			1	.010	400	225.9	49.28	49.25	
			2	.010		225.9	49.22		49.39
			1	.014		263.5	48.76	49.22	
			2	.013		263.5	49.66		
			1	.016		301.2	49.72	49.72	
			2	.016		301.2	--	--	

TABLE V.4

SMALL SHIFT DEFLECTION POLARIZABILITY MEASUREMENTS FOR CESIUM

Run	Date	T_S	S	γ	V^2	v	α_i	$\bar{\alpha}$	$\bar{\alpha}_T$
		^oK		$\frac{Amps}{cm}$ $X10^{-10}$	esu^2	m/sec	$\mathring{A}^3$	$\mathring{A}^3$	$\mathring{A}^3$
1Cs	10/13/66	411	1	26.7	44.5	--	48.19	48.29	
			2	26.9	69.6	--	48.39		48.77
P = 7 X 10^{-8} torr			1	24.3	100.2	--	50.33	49.25	
			2	25.6		--	48.16		
			1	.093		188.2	59.69	60.19	
			2	.091		188.2	60.69		
			1	.264		257.2	60.80	62.54	
			2	.259		257.2	64.29		
			1	.351		30].2	61.66	60.42	
			2	.351		301.2	59.17		61.98
			1	.312		357.6	69.57	66.45	
			2	.326		357.6	64.35		
			1	.228		432.9	59.07	60.32	
			2	.227		432.9	61.56		
2Cs	11/2/66	413	1	17.1	44.5	--	47.97	47.52	
			2	17.9	69.6	--	47.07		48.12
P = 6 X 10^{-8} torr			1	13.9	100.2	--	48.72	48.72	
			2	14.4		--	48.72		

TABLE V.4 (CONT.)

Run	Date	T_S	S	γ	V^2	v	α_i	$\bar{\alpha}$	$\bar{\alpha}_T$
		^oK		$\frac{Amps}{cm}$ $X10^{-10}$	esu^2	m/sec	$Å^3$	$Å^3$	$Å^3$
2Cs			1	.069		188.2	66.08	65.11	
			2	.065		188.2	64.14		
			1	.213		244.7	64.08	65.45	
			2	.201		244.7	66.82		64.90
			1	.281		294.9	64.66	64.85	
			2	.281		294.9	65.03		
			1	.268		376.5	64.13	64.79	
			2	.250		376.5	64.45		
			1	.145		445.5	64.78	64.32	
			2	.141		445.5	63.87		
3Cs	12/18/66	401	1	17.6	178	--	48.99	48.55	
			2	18.9	278	--	48.12		
			1	.105	400	188.2	62.89	63.13	
P = 6 X 10^{-8} torr			2	.110		188.2	63.38		62.69
			1	.138		225.9	63.41	62.73	
			2	.150		225.9	62.05		
			1	.076		205.0	61.67	62.32	
			2	.077		205.0	62.97		

TABLE V.4 (CONT.)

Run	Date	T_S	S	γ	V^2	v	α_i	$\bar{\alpha}$	$\bar{\alpha}_T$
		^oK		$\frac{Amps}{cm}$ $X10^{-10}$	esu^2	m/sec	$Å^3$	$Å^3$	$Å^3$
4Cs	5/1/67	416	1	26.1	100	--	46.32	47.12	47.12
			2	26.4	178	--	47.81		
P = 7 X 10^{-8} torr			1	.152	278	225.9	63.30	64.11	
			2	.155		225.9	65.25		63.72
			1	.075		338.8	65.42	63.80	
			2	.076		338.8	62.17		
			1	.187		376.5	62.48	63.25	
			2	.190		376.5	64.00		

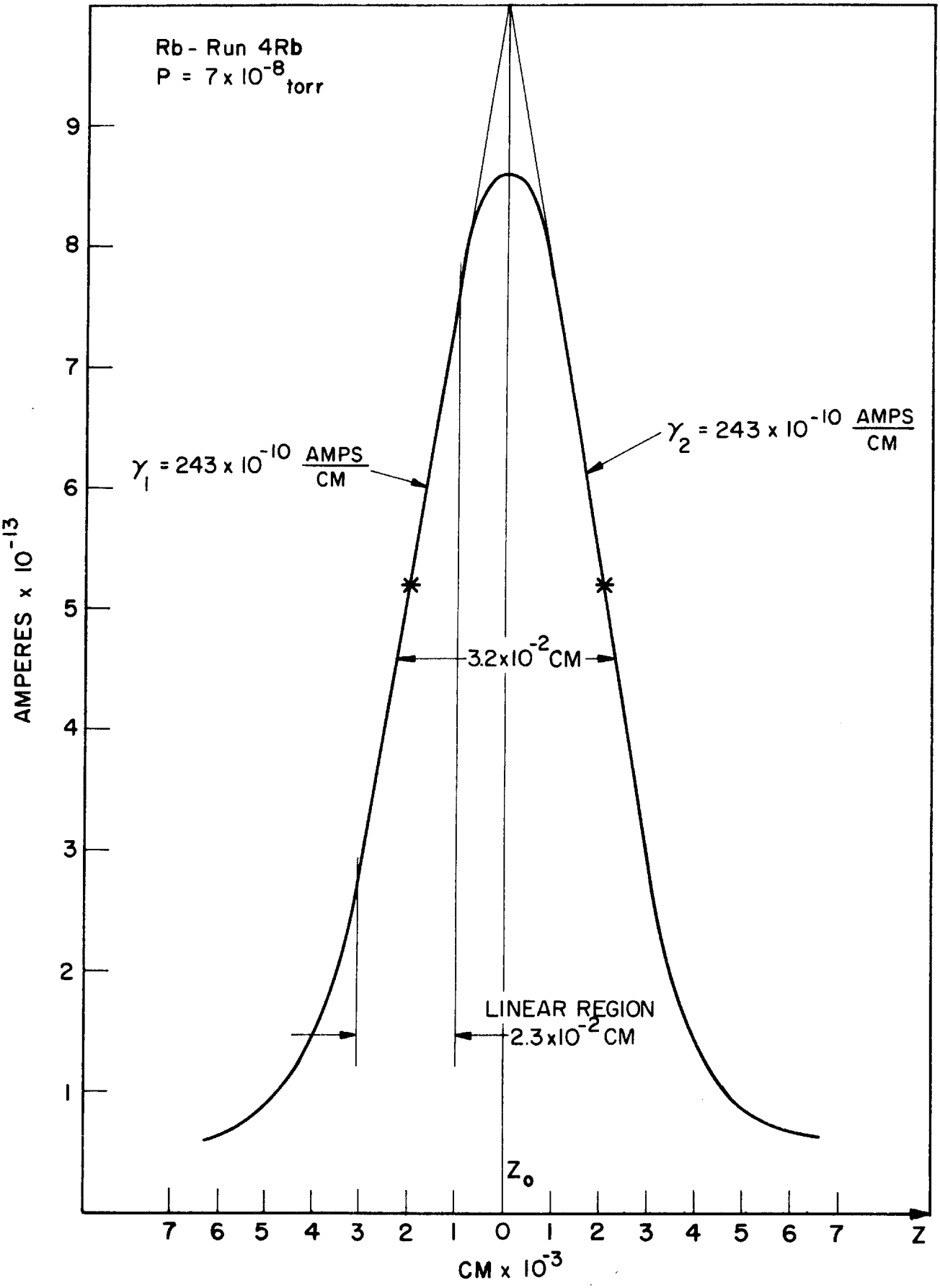


FIG. V.1 BEAM SHAPE

quantity is the arithmetic mean

$$\bar{\alpha} = \frac{1}{n} \sum_{\lambda=1}^{n} \alpha_\lambda \qquad \text{V.1}$$

The standard deviation σ is given by

$$\sigma^2 = \frac{1}{n-1} \sum_{\lambda=1}^{n} (\alpha_\lambda - \bar{\alpha})^2 \qquad \text{V.2}$$

and the standard error of the mean β is

$$\beta = \frac{\sigma}{\sqrt{n}} \qquad \text{V.3}$$

These values are calculated for the small shift measurements given in Tables V.1 to V.4 and presented in Table V.5 along with the total mean polarizability value $\bar{\alpha}_T$.

TABLE V.5

		Sodium	Potassium	Rubidium	Cesium
Non-Velocity Selected	$\bar{\alpha}_T$	22.56	42.08	42.27	48.14
	σ	1.8%	2%	1%	1.7%
	β	0.17%	0.12%	0.13%	0.10%
	n	100	270	54	324
Velocity Selected	$\bar{\alpha}_T$	24.35	45.24	48.74	63.32
	σ	2.7%	3%	2.7%	3.4%
	β	0.16%	0.09%	0.09%	0.12%
	n	270	1026	918	864

Small Shift Alkali Polarizability Values

and Their Associated Statistical Errors

C. Large Shift Polarizability Measurements for the Alkali Metals Na, K, Rb, and Cs.

The large shift measurements were all made with a velocity selected beam, thus eliminating any problems of velocity distributions distorting the beam shapes. The measurements were conducted at very low velocities and at very high voltages on the deflecting field to give the largest deflection. The principal source of scatter is the background noise from the hot tungsten detector wire. The data obtained for the alkali metals is presented in Table V.6. The statistical analysis is the same as that outlined in Section B and is presented in Table V.7.

A typical data curve is shown in Figure V.2. In determining the actual deflection, two beam shapes corresponding to the deflecting field voltage on and off were recorded on separate sheets of graph paper and then compared by physically matching the two curves. The accuracy of this method is estimated to be better than $\pm$ 0.3 X 10^{-3} cm.

TABLE V.7

LARGE SHIFT ALKALI POLARIZABILITY VALUES AND THEIR ASSOCIATED STATISTICAL ERRORS

	Sodium	Potassium	Rubidium	Cesium
$\bar{\alpha}(A^3)$	24.44	44.88	49.60	64.46
σ	1.6%	3.1%	2.0%	3.2%
β	0.96%	1.2%	0.7%	1.2%
n	3	6	9	9

TABLE V.6

LARGE SHIFT POLARIZABILITY MEASUREMENTS FOR NA, K, RB AND CS

Run	Date	T_S	LS	V^2	v	α_i	$\overline{\alpha_T}$
		^oK	10^{-3}cm esu^2		m/sec	$\mathring{A}^3$	$\mathring{A}^3$
8K	10/29/66	465	13.7	1113.3	257.2	43.47	43.96
			9.9	1113.3	313.7	42.54	
			7.6	1113.3	376.5	45.93	
9K	2/18/67	486	11.43	1113.3	301.2	45.78	
			15.0	1113.3	263.5	45.80	45.80
			10.2	1113.3	225.9	45.80	
2Rb	11/18/66	444	7.6	1113.3	263.5	50.10	
			8.0	1113.3	282.3	49.80	49.71
			10.3	1113.3	320.0	49.25	
5Rb	5/17/67	430	7.2	901.8	301.2	48.44	48.94
			8.1	901.8	263.5	49.45	
1Rb	10/20/66	453	12.7	1113.1	188.2	49.03	
			9.1	1113.1	263.5	49.51	49.84
			8.1	1113.1	326.3	50.51	
			10.4	1113.1	225.9	50.31	
1Cs	10/13/66	411	9.4	1113.1	188.2	60.53	64.44
			7.8	1113.1	225.9	68.36	

TABLE V.6 (CONT.)

Run	Date	T_S	LS	V^2	v	α_i	$\overline{\alpha}_T$
		^oK	10^{-3}cm esu^2		m/sec	$Å^3$	$Å^3$
2Cs	11/2/66	413	19.9	1113.3	145.6	62.19	
			13.2	1113.3	181.9	64.40	64.17
			8.9	1113.3	225.9	65.93	
4Cs	5/1/67	416	6.4	113..3	263.5	64.77	
			12.4	1113.3	188.2	64.93	64.79
			6.4	1113.3	263.5	64.72	
			6.4	1113.3	263.5	64.77	
1Na	8/8/67	560	8.7	1113.3	257.2	24.60	
			7.6	1113.3	313.7	24.40	24.44
			6.5	1113.3	320.0	22.33	

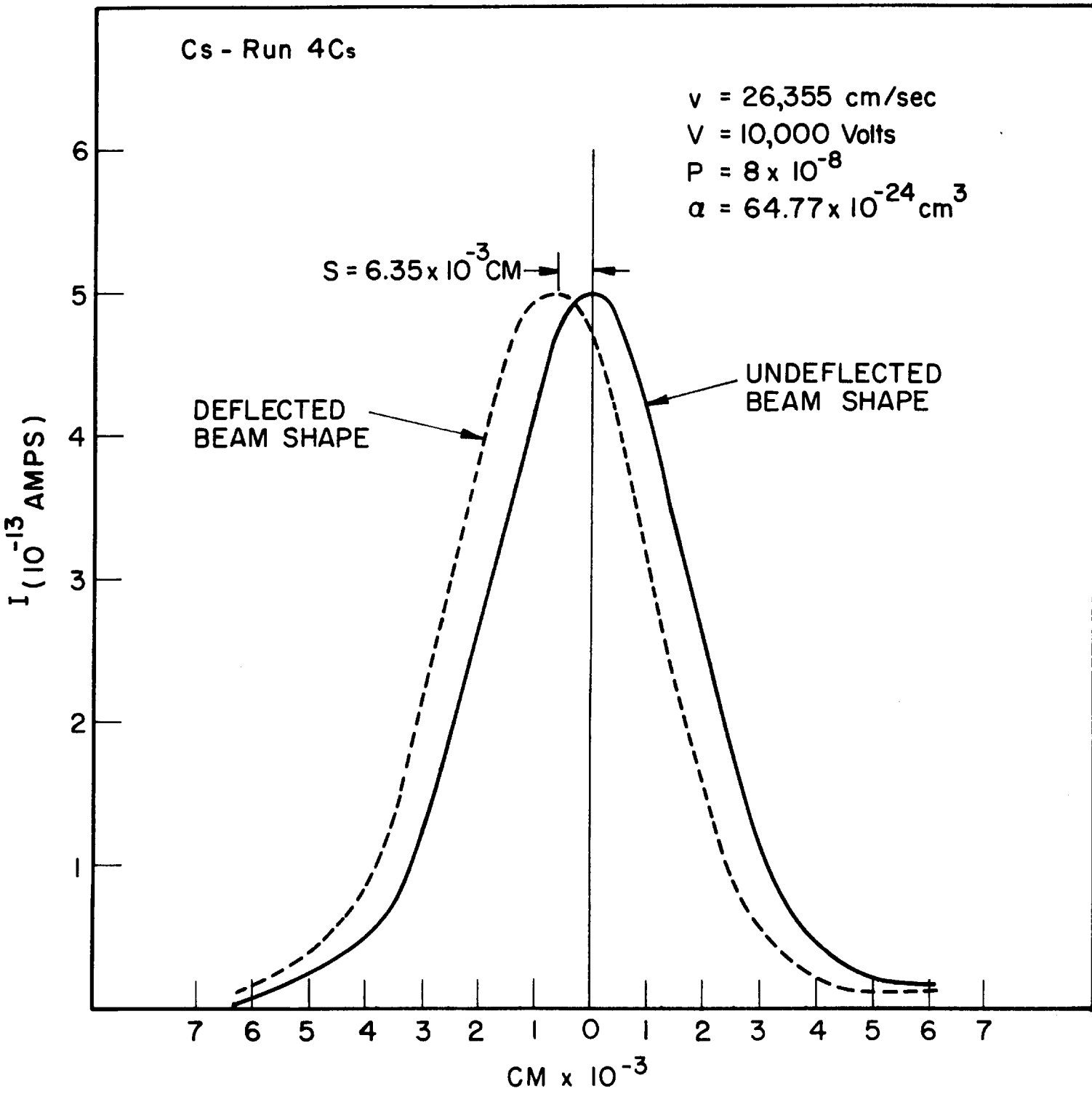


FIG. V.2 LARGE SHIFT DATA CURVES

In addition to the statistical errors presented in Tables V.5 and V.6, two other random errors associated with the velocity selected measurements must be included. The first additional error arises because of the uncertainty in the velocity of the beam atoms. Using the value for the resolution of the velocity selector, this error is estimated to be ± 2.1%. Secondly, in the large shift measurements the error in the observed shift is estimated to be less than ± 0.3 X 10^{-3} cm, which corresponds to ± 3% for the lowest observed shift of 7.6 X 10^{-3} cm. Table V.8 summarizes the polarizability values obtained for both large and small shift, velocity and non-velocity selected measurements, including the total estimated random errors.

TABLE V.8

SUMMARY OF MEASURED ALKALI POLARIZABILITY VALUES

Element	$(\bar{\alpha}_{NVS} \pm \sigma)\text{Å}^3$	$(\bar{\alpha}_{VS} \pm \sigma)\text{Å}^3$	$(\bar{\alpha}_{LS} \pm \sigma)\text{Å}^3$
Sodium	22.5 ± 0.3	24.4 ± 0.9	24.4 ± 0.8
Potassium	42.5 ± 0.9	45.2 ± 1.6	44.6 ± 1.9
Rubidium	42.3 ± 0.4	48.7 ± 1.7	49.6 ± 1.6
Cesium	48.1 ± 0.9	63.3 ± 2.5	64.4 ± 2.7

D. Velocity Profile Measurements.

At the end of each run the oven temperature and pressure of each chamber were carefully measured and then a point-by-point measurement of the velocity profile curve was made for the alkali metals K, Rb and Cs. Except for potassium, the velocity profile was measured over a large range of velocities extending on both sides of peak velocity v_p. Figures V.3, V.4 and V.5 are plots of the experimentally measured velocity profile along with the theoretically predicted velocity profile curve, as discussed in Appendix C. The statistical error associated with each point on the experimental curve is less than 0.1%.

The important feature to compare in Figures V.3, V.4, and V.5 is the fractional decrease in the beam intensity on the low velocity portion of the curve in comparison to the theoretical curve. Table V.9 is a presentation of the measured percent fractional decrease for each element as a function of the reduced velocity V. The reduced velocity V is defined as the ratio of the actual measured velocity v to the theoretically predicted, most probable velocity v_p. The symbols T_S, v_p and v_{p_E} refer respectively to the source temperature, the theoretically predicted most probable velocity and the experimentally measured most probable velocity.

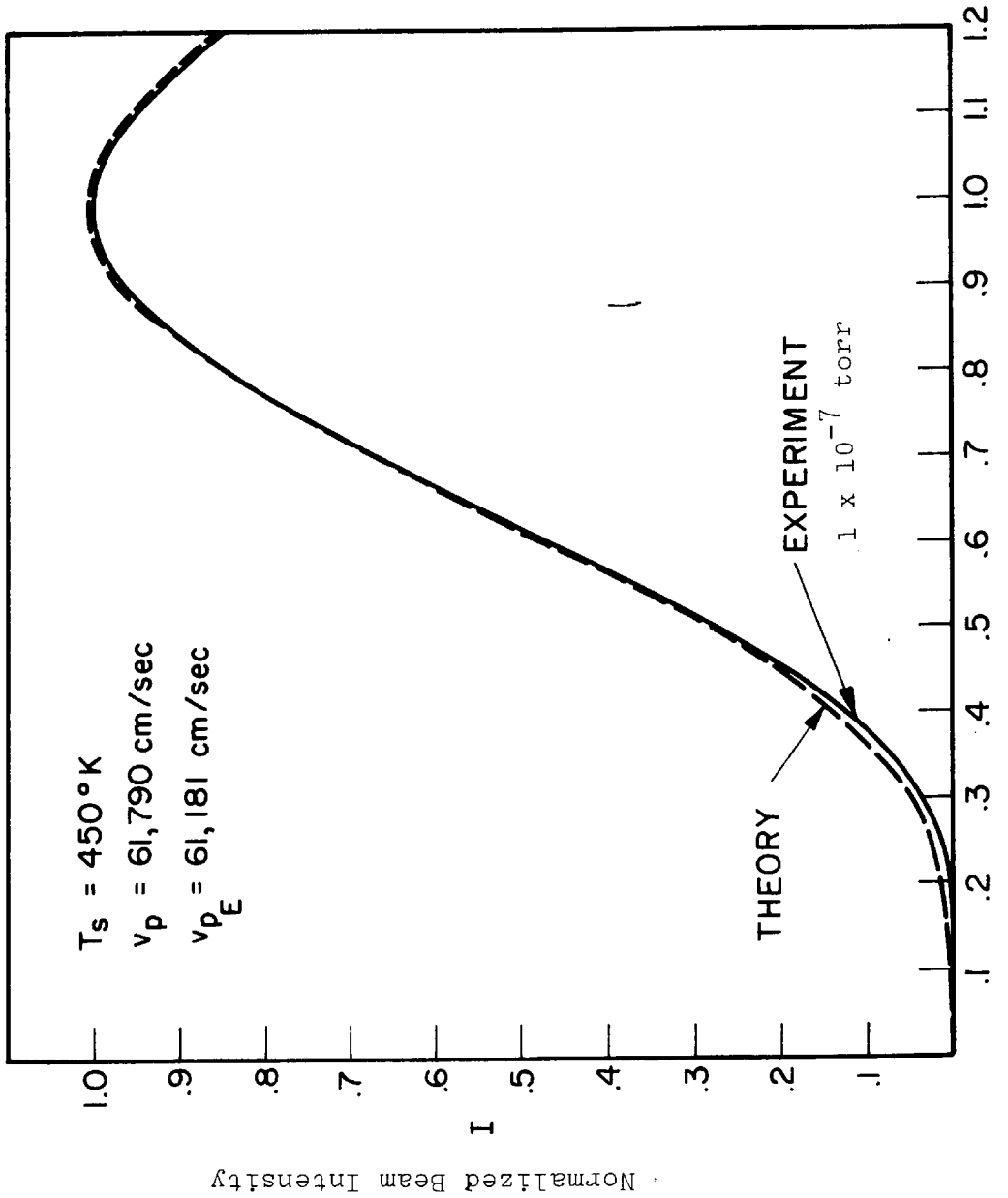


FIG. V.3 K VELOCITY PROFILE

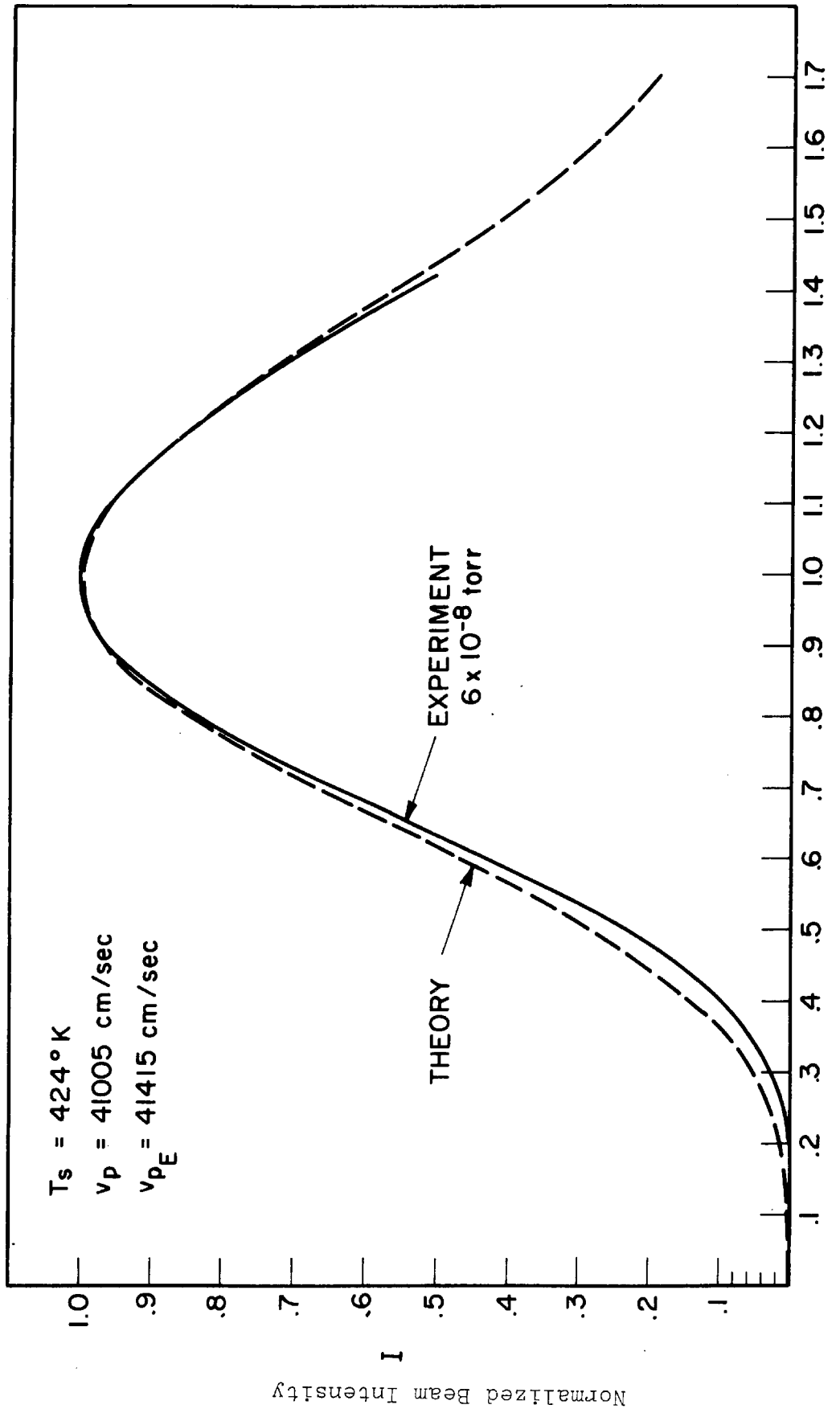


FIG. V.4 Rb VELOCITY PROFILE

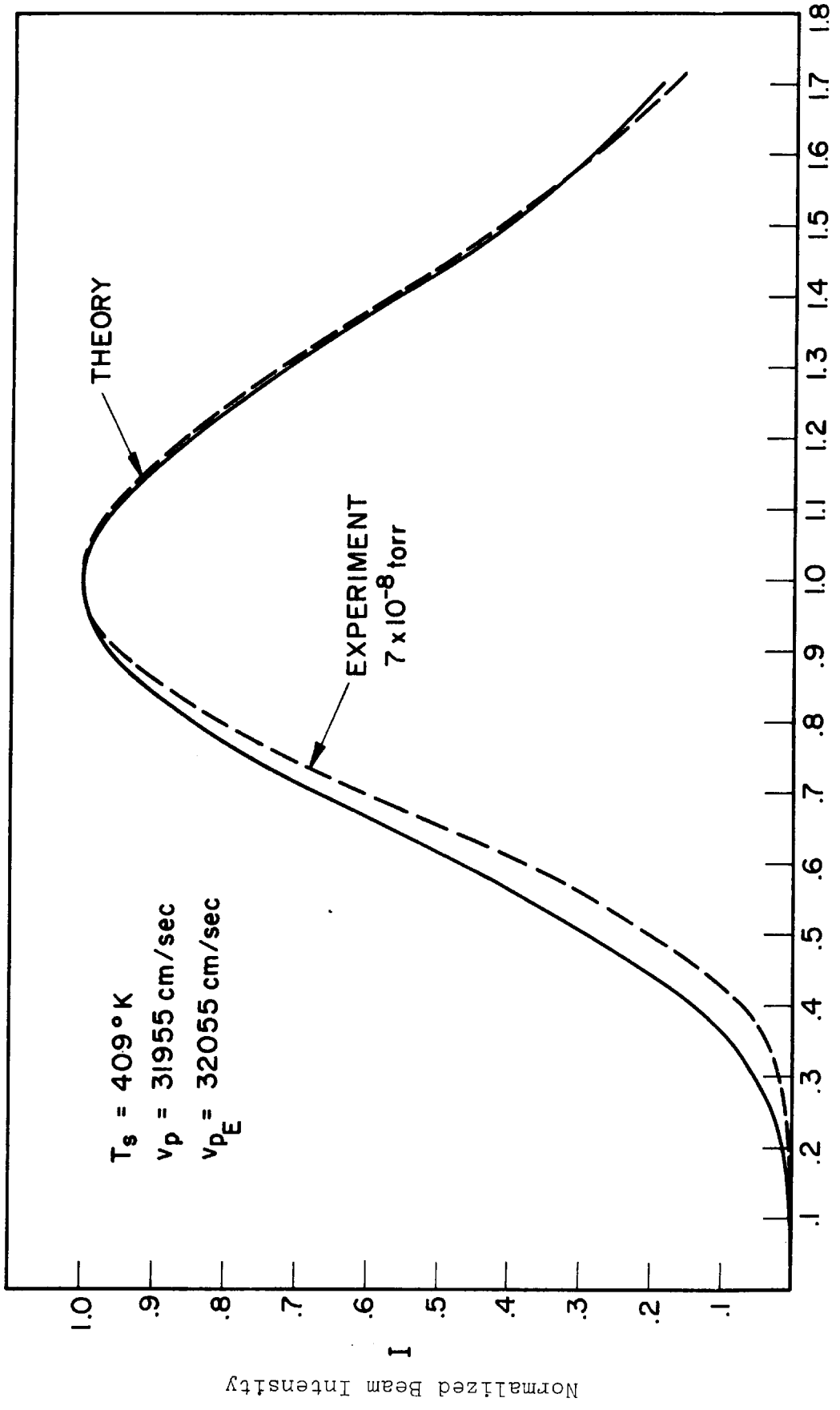


FIG. V.5 Cs VELOCITY PROFILE

TABLE V.9

PERCENT FRACTIONAL DECREASE IN LOW VELOCITY BEAM ATOMS AS COMPARED TO THE THEORETICAL VELOCITY PROFILE

V	Potassium	Rubidium	Cesium
1.0	0.00%	0.00%	0.00%
0.9	0.00%	0.00%	0.00%
0.8	0.00%	0.50%	3.70%
0.7	0.10%	3.80%	9.60%
0.6	1.50%	10.30%	19.2%
0.5	3.70%	16.7%	30.0%
0.4	9.70%	28.9%	46.5%
0.3	23.0%	50.0%	74.7%
0.2	47.0%	--	--
0.1	--		

E. Scattering Velocity Profile Measurements.

In runs 9K, 5R, and 4C, argon gas was introduced into the field chamber by means of a mechanical leak (Chapter II, K), and velocity profiles were obtained for the three alkali metals K, Rb, and Cs as a function of the argon scattering gas pressures. The results of these measurements are presented in Figures V.6, V.7, and V.8. The solid curve represents the experimentally measured curve normalized such that unit intensity corresponds to

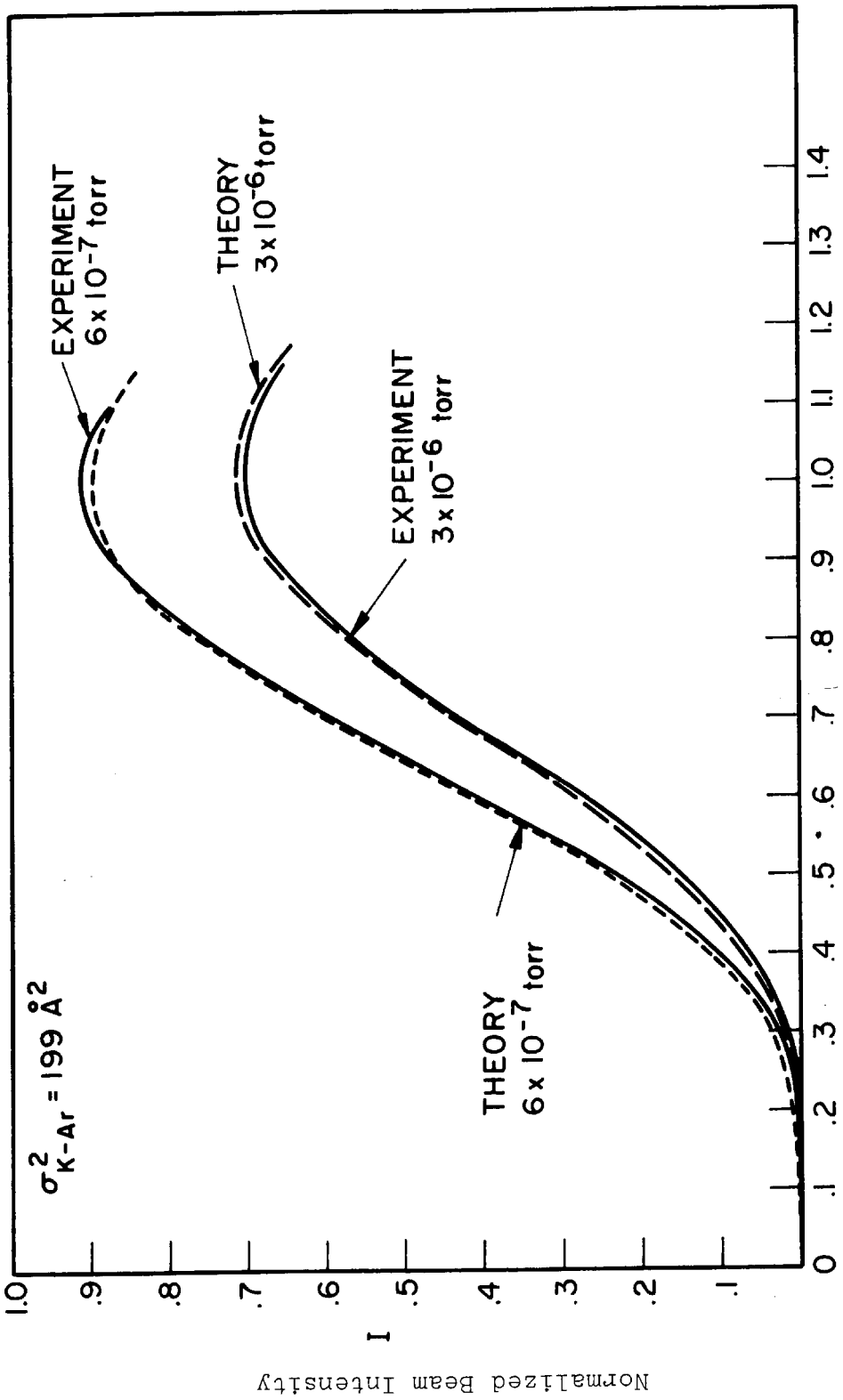


FIG. V.6. K - Ar SCATTERING VELOCITY PROFILE

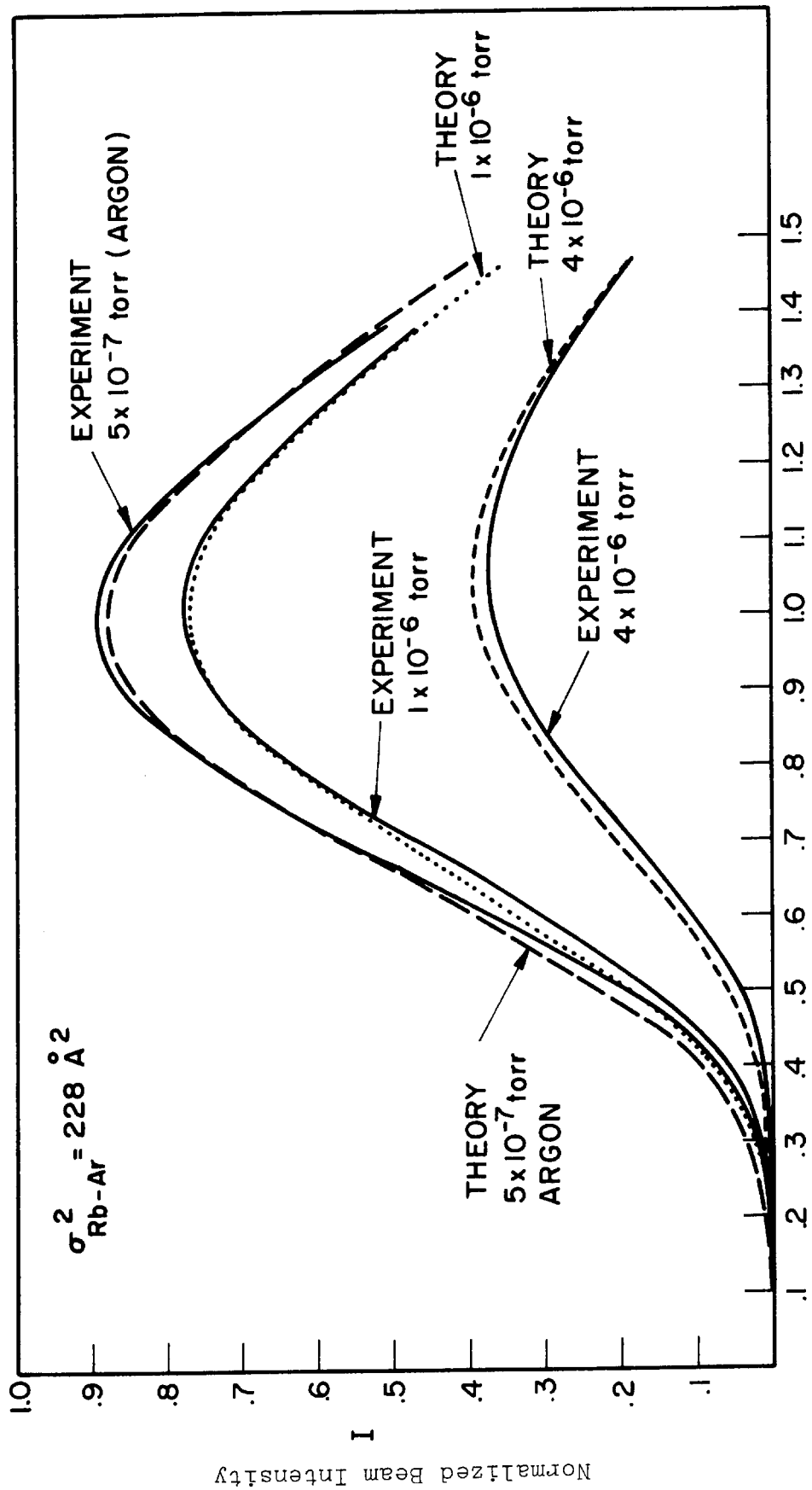


FIG. V.7. Rb SCATTERING VELOCITY PROFILE

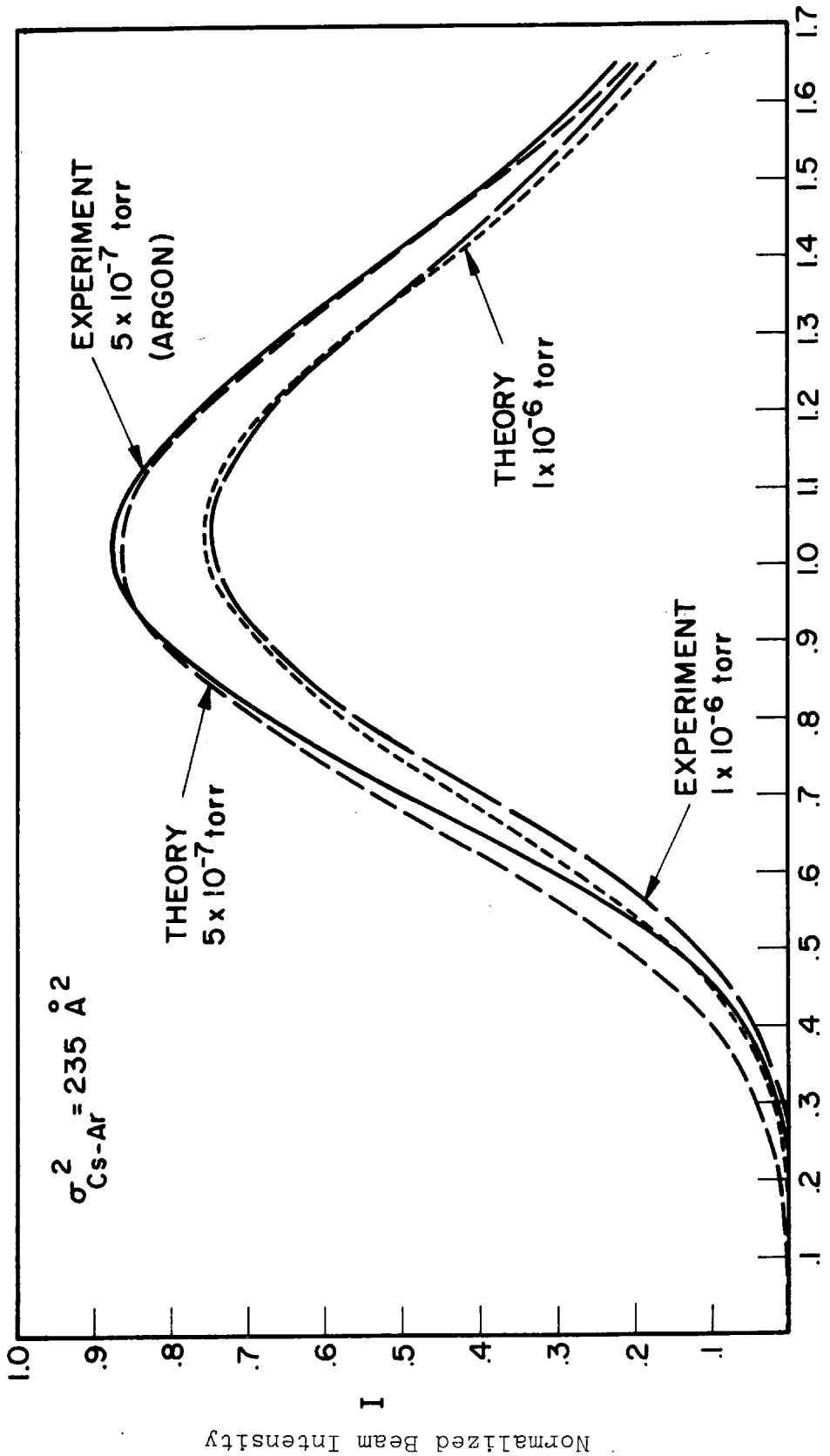


FIG. V.8. Cs - Ar SCATTERING VELOCITY PROFILE

no argon in the scattering cell. The dashed curve is the theoretically predicted velocity profile curve which is derived by taking into account the removal of atoms from the beam by scattering.

The explicit relationship for this phenomenon is as follows: The normalized ideal velocity distribution function, after passing through the velocity selector, is given by (Appendix C)

$$T(V)dV = 7.39\,V^4 e^{-2V^2} dV \qquad V.4$$

where V is the reduced velocity. To obtain the scattering velocity profile curve, we must multiply equation V.4 by the probability that an atom of velocity V arrives at the detector after traveling a distance ℓ through the scattering region. This probability is given by the expression

$$P(v) = e^{-\ell/\lambda(v)} \qquad V.5$$

The theoretical scattering velocity profile curve is then obtained from the following expression (product of equations V.4 and V.5)

$$T(v)dV = 7.39\,V^4 e^{-(2V^2 + \ell/\lambda(v))} dV \qquad V.6$$

where ℓ is the length of the scattering chamber and $\lambda(v)$ is the mean free path of a beam atom of reduced velocity

V in the scattering gas argon given by

$$\lambda(V) = \frac{V^2}{\pi^{1/2} N_G \sigma_{BG}^2 \Psi(V)} \qquad V.7$$

Thus the theoretical curves are obtained by evaluating equation V.6 as a function of the experimentally measured argon scattering gas density N_G, the reduced velocity V and the total scattering cross section σ_{BG}^2.*

The comparison of the theoretical and experimental scattering velocity profile curves is complicated by several effects which are difficult to include in the theory. The first effect is a result of the fact that the experimental curves have the residual gas scattering contribution to the removal of atoms, whereas the theoretical curves do not. The second and more serious effect is the observation that the scattering cell length ℓ is not a constant independent of the scattering gas pressure. This second effect was experimentally observed. When the partial pressure of argon in the scattering cell reached 10^{-6} torr, an increase in the pressures of the adjacent detector and velocity selector chambers occurred, thus indicating that the argon scattering cell length ℓ increased as the argon partial pressure increased. Consequently, the deviation of the experimentally measured curves from the theoretically

---

*See Appendix D.

predicted curves can be understood in light of the above observations.

F. Polarizability Measurements Versus Argon Scattering Gas Pressures.

As a final check on the velocity distortion effect and its influence on the electrostatic deflection method of measuring polarizabilities, a series of polarizability measurements were performed with various argon pressures in the scattering cell. These measurements were made for both velocity selected and non-velocity selected beams at the same argon pressures. Figures V.9, V.10, and V.11 present the results of these measurements.

The interesting features which these particular experiments indicate are (1) the velocity selected measurements are insensitive to the presence of argon in the scattering cell, (2) the observed non-velocity selected polarizabilities are very sensitive to the presence of argon in the scattering cell, and (3) if one draws a smooth curve connecting the data points for the non-velocity selected measurements, the curve approaches the velocity selected polarizability value in the limit of zero argon partial pressure in the scattering cell.

The error bars on the graphs represent the statistically determined root mean square deviation (σ) in the measured polarizability values as functions of the argon partial pressure for each individual alkali run. The triangular

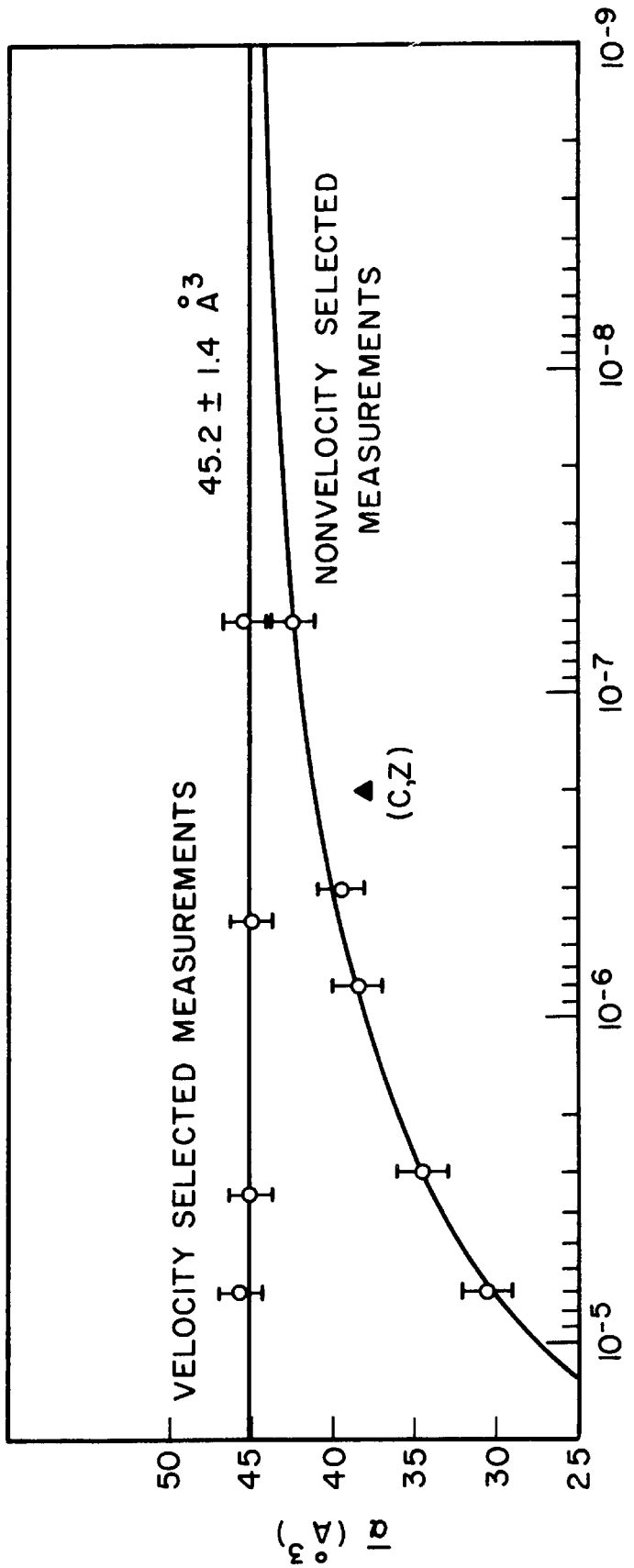


FIG. V.9 K POLARIZABILITY MEASUREMENTS VS NOMINAL ARGON SCATTERING GAS PRESSURES

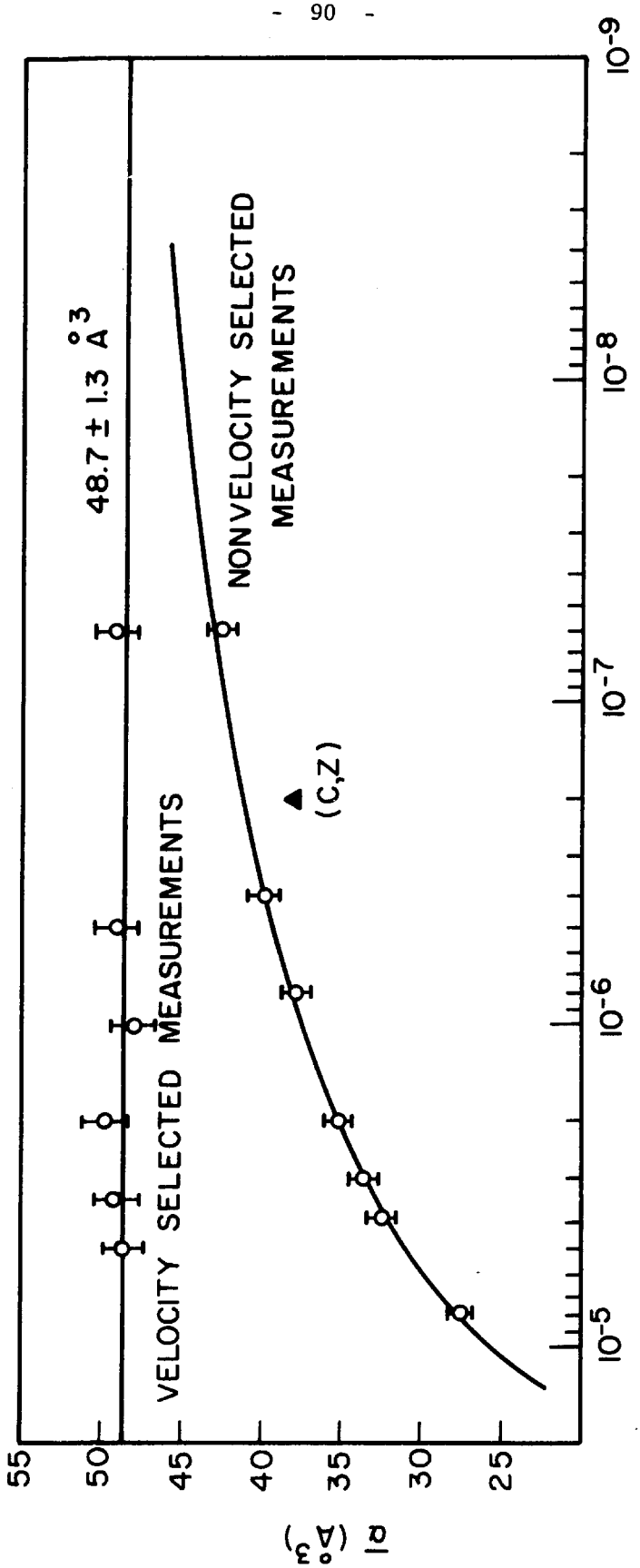


FIG. V. 10 Rb POLARIZABILITY MEASUREMENTS VS NOMINAL ARGON SCATTERING GAS PRESSURES

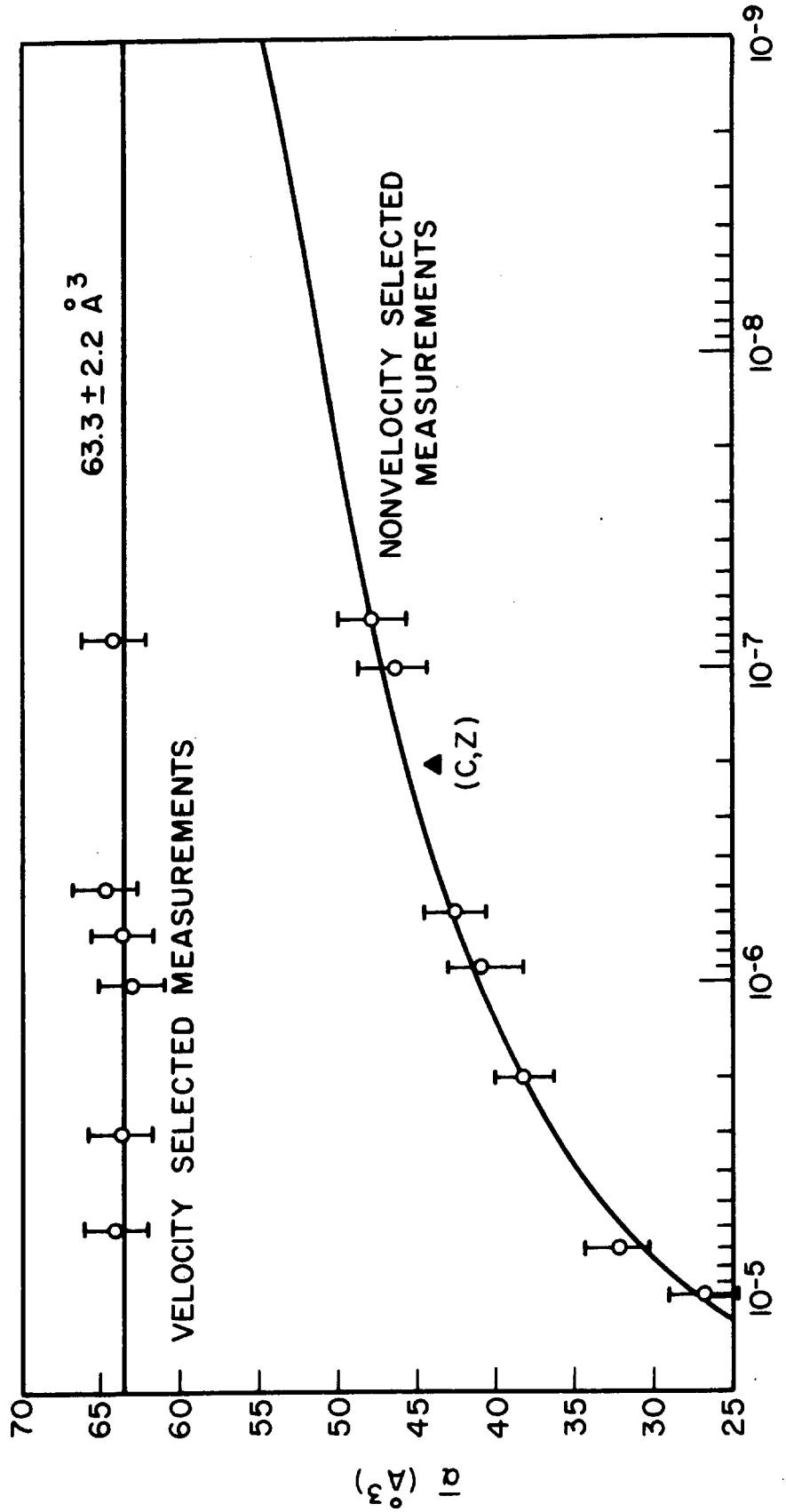


FIG. V.11. Cs POLARIZABILITY MEASUREMENTS VS NOMINAL ARGON SCATTERING GAS PRESSURES

point on the figures at 2 X 10^{-7} torr indicates the polarizability as measured by Chamberlain and Zorn (1963) using the non-velocity selected small shift deflection method.

Table V.10 is a presentation of the results of the non-velocity selected polarizability measurements corrected for the scattering effects on the velocity distribution of the beam atoms. The polarizabilities in the column under α (experimental) refer to the NVS values of the polarizability measured at the indicated argon partial pressures in the scattering cell. The polarizabilities in the column under α(corrected) are obtained by using the arguments developed in Appendix B to account for the selective removal of slow velocity beam atoms by scattering. The explicit relationship between α(experimental) and α(corrected) is given by the following expression

$$\alpha(\text{corrected}) = \frac{\alpha(\text{experimental})}{I_1(A)} \qquad \text{V.8}$$

where $I_1(A)$* is the correction factor which arises to account for the velocity distortion effect in the beam atoms. The correction factor $I_1(A)$ is evaluated using the experimentally measured scattering gas density N_G, the scattering cross section σ^2_{BG}, and the scattering cell length ℓ . The polarizability values under the column α(velocity selected) represent the measured values

*See equation B.18

TABLE V.10

NON-VELOCITY SELECTED POLARIZABILITY MEASUREMENTS CORRECTED FOR SCATTERING EFFECTS ON THE VELOCITY DISTRIBUTION OF THE BEAM ATOMS

Element	Pressure	α(Experimental)	α(Corrected)	α(Velocity Selected)
Cs	7×10^{-8} torr*	48 Å^3	57 Å^3	
	6×10^{-7} torr (Argon)	42 Å^3	61 Å^3	63 Å^3
	9×10^{-7} torr (Argon)	40 Å^3	63 Å^3	
	2×10^{-6} torr (Argon)	38 Å^3	82 Å^3	
Rb	6×10^{-8} torr*	42 Å^3	46 Å^3	
	4×10^{-7} torr (Argon)	40 Å^3	47 Å^3	48 Å^3
	8×10^{-7} torr (Argon)	37 Å^3	49 Å^3	
	2×10^{-6} torr (Argon)	33 Å^3	69 Å^3	
K	6×10^{-8} torr*	42 Å^3	44 Å^3	
	4×10^{-7} torr (Argon)	39 Å^3	45 Å^3	45 Å^3
	8×10^{-7} torr (Argon)	38 Å^3	46 Å^3	
	3×10^{-6} torr (Argon)	34 Å^3	64 Å^3	

of the alkali polarizabilities which were observed to be independent of the argon partial pressure in the scattering cell.

The starred entry in Table V.10 represents the results of evaluating the correction factor $I_1(A)$ for $\sigma^2_{BG} = 200$ Å^2 and ℓ = 210 cm, which corresponds to a mixture of water vapor, carbon monoxide, nitrogen, argon, and carbon dioxide as the residual gas components. The polarizability value quoted is an approximate result because of the uncertainty in the residual gas components.

In all cases where the argon partial pressure exceeded 1×10^{-6} torr, the corrected value of the polarizability is considerable larger than the measured, velocity selected polarizability. This arises because the argon pressure distribution begins to seriously affect the pressure in the rest of the apparatus and also because of the nature of the approximations used in arriving at the correction factor $I_1(A)$.

It appears that the lower values for the experimental alkali polarizabilities as determined by Chamberlain and Zorn (1963) can, for the most part, be explained by the velocity distortion effect due to the selective removal of low velocity atoms from the beam.

G. Systematic Errors.

In determining α, systematic errors are allowed for in the evaluation of the constants k_1, L, Z, and V for velocity

selected and non-velocity selected small shift and velocity selected large shift measurements.

The constant k_1 has the following definition:

$$K_1 = \frac{E \frac{\partial E}{\partial z}}{V^2}$$

It is useful to express k_1 in terms of the field parameters (Ramsey, 1956):

$$E = \frac{V a}{r_1^2 r_2^2 \left(\tan^{-1}\left(\frac{z_2}{a}\right) - \tan^{-1}\left(\frac{z_1}{a}\right) \right)^2}$$

$$\frac{\partial E}{\partial z} = \frac{V a z (r_1^2 + r_2^2)}{r_1^3 r_2^3}$$

$$K_1 = \frac{a^2 z (r_1^2 + r_2^2)}{r_1^5 r_2^5 \left(\tan^{-1}\left(\frac{z_2}{a}\right) - \tan^{-1}\left(\frac{z_1}{a}\right) \right)^2}$$

where r_1 is the radius of the bead, r_2 is the radius of the trough, z_1 and z_2 are where the electrode surfaces intersect the y = 0 plane (See Figure III.5) and z = 1.2a. In order to determine the error in evaluating k_1, it is useful to express the field parameters in terms of the assembly parameters which are r_1, r_2, and D, the field gap ($z_2 - z_1 = D$). It can be shown that

$$a^2 = \frac{D(2r_2 - D)(2r_1 + D)(D + 2r_1 - 2r_2)}{4(D + r_1 - r_2)^2}$$

$$z_1 = \frac{r_2^2 - r_1^2 - (r_1 - r_2 + D)^2}{2(r_1 - r_2 + D)}$$

$$z_2 = \frac{r_2^2 - r_1^2 + (r_1 - r_2 + D)^2}{2(r_1 - r_2 + D)}$$

The sources of error in the evaluation of k_1 arise from the error in r_1 ($\pm$ 0.0012 cm), r_2 ($\pm$ 0.0012 cm), D ($\pm$ 0.005 cm), the errors due to machining and assembly of the electrodes. The combined error in k_1 is estimated to be $\pm$ 4%.

The error in z which arises from the uncertainty in the beam position is estimated to be $\pm$ 1% which is consistent with the accuracy of the optical line up procedure.

In estimating the geometrical error of L, in addition to the error in physical measurements, an allowance of two field gap widths (1.26 cm) is included to account for the fringing effects of the field, which introduces an uncertainty in the effective deflecting lengths of the field. The estimated geometric error L is a generous $\pm$ 3%.

The voltage calibration of the Fluke high voltage power supply leads to an estimated error of $\pm$ 0.5% in V.

In all the velocity selected measurements there is an additional systematic error in the beam velocity measurement. The estimated error in the velocity measurements is less than $\pm$ 0.1 % and can be neglected.

The small shift non-velocity selected measurements have three additional systematic errors. The first error

originates from uncertainties in the oven temperature measurement T. The differences in the two thermocouple readings for the nickel oven were never greater than 0.2 mv, and an error of ± 0.2 mv corresponding to ± 5° K is quoted. The reference junction temperature measured on the laboratory mercury thermometer is assumed to be better than ± 2° K. This corresponds to a ± 2% error in T for cesium at 405° K, the lowest oven temperature used. The second error arises in the small shift approximation for a non-velocity selected beam. It can be shown (Chamberlain, 1963) that the observed intensity change dI in the small shift limit ($S = 0.1\ W_D$) is about 3% smaller than assumed. This effect occurs because of the smearing out of the beam shape due to the velocity distribution in the beam atoms. Finally, the most important systematic error in the non-velocity selected small shift measurements arises because of the distortion in the modified Maxwellian velocity distribution in the beam. The present experiment has shown that the systematic error introduced by this effect can be as large as 25% in the case of cesium. The size of this error can be estimated by comparing the non-velocity selected and velocity selected polarizability values.

The purity of the alkali metals used in the polarizability experiments has been spectrally investigated and shown to be in accord with the specifications of the supplier.

The dimerization of the alkalis has also been found to be negligible. It is estimated from velocity profile

measurements that the dimer content in the alkali beams is less than 1% (Miller and Kusch, 1955; present experiment, 1967).

Finally, the deflection due to an induced quadrupole is too small to be observed (Appendix E).

The systematic errors are summarized in Table V.11

TABLE V.11

SYSTEMATIC ERRORS IN THE ALKALI POLARIZABILITY MEASUREMENTS

Source of error	Percentage error in source	Percentage error in α
z	$\pm$ 1.0 %	$\pm$ 1.0%
L	$\pm$ 3.0%	$\pm$ 3.0%
T	$\pm$ 2.0%	$\pm$ 2.0%
V	$\pm$ 0.5%	$\pm$ 1.0%
k_1	$\pm$ 4.0%	$\pm$ 4.0%
dI	+ 3.0%	+ 3.0%

It is not possible to say with certainty how the errors will collectively affect the polarizability measurements. If one adds the errors, the error is $^{+14\%}_{-11\%}$ for the non-velocity selected small shift measurements and the maximum error for the velocity selected measurements is $\pm$ 9%.

If we assume that the systematic errors with the $\pm$ sign are random with respect to one another, then we can combine them quadratically by taking the square root of

the sum of the squares of the systematic errors. The resulting total systematic error for the velocity selected measurements is ± 5% and $^{+9\%}_{-6\%}$ for the small shift non-velocity measurement not including the velocity distortion effect.

Now assuming the systematic and statistical errors are random with respect to one another, they can be combined quadratically. The results of this quadratic combination are presented in table V. 12 for the measured values of the alkali polarizabilities in this experiment. It must be emphasized that the systematic error arising from the distortion in the modified Maxwellian velocity distribution is not included in the errors quoted for the NVS small shift measurement in table V.12. This error can be estimated by comparing the differences in the polarizability values for NVS and VS measurements.

TABLE V.12

MEASURED VALUES OF THE ALKALI POLARIZABILITIES

Element	$\alpha_{NVS}(\mathring{A}^3)$	$\alpha_{VS}(\mathring{A}^3)$	$\alpha_{LS}(\mathring{A}^3)$
Sodium	$22.6\ ^{+2.10}_{-1.42}$	24.4 ± 1.7	24.4 ± 1.7
Potassium	$42.5\ ^{+\ 3.9}_{-\ 2.7}$	45.2 ± 3.2	44.9 ± 3.3
Rubidium	$42.3\ ^{+\ 3.8}_{-\ 2.5}$	48.7 ± 3.4	49.6 ± 3.5
Cesium	$48.1\ ^{+\ 4.5}_{-\ 3.0}$	63.3 ± 4.6	64.4 ± 4.8

CHAPTER SIX

CONCLUSION

The results for the alkali polarizability values measured in this experiment using beam velocity analysis are given in table VI.1 along with the experimental and theoretical values obtained by others.

A. Comparison with Other Atomic Beam Measurements of Alkali Polarizabilities.

The Scheffers and Stark (1934) values for potassium and cesium polarizabilities are included for historical interest and can be considered in the same class as the more refined Chamberlain-Zorn (1963) experiment. The systematically higher polarizability values obtained in the present experiment, in comparison to the values measured by Chamberlain and Zorn (1963) have been explained by the velocity distribution distortion effect caused by the selective removal of low velocity atoms from the beam due to scattering by residual gas molecules (Chapter V).

In the atomic beam E-H gradient balance measurements (Salop et al., 1961), alkali polarizabilities were obtained by observing a zero deflection condition for the beam atoms. In their E-H gradient balance method the electric deflecting force is made to balance the magnetic deflecting force on the paramagnetic alkali atoms for particular magnetic substates. Congruent electric and magnetic fields are

INVESTIGATOR	METHOD	Na	K	Rb	Cs
Present Experiment (1967)	Atomic Beam Deflection with Velocity Selector	24.4 ± 1.7	45.2 ± 3.2	48.7 ± 3.4	63.3 ± 4.6
Scheffers and Stark (1934	Atomic Beam Deflection	-----	34 ± 1.7	----	42 ± 2.1
Chamberlain and Zorn (1963)	Atomic Beam Deflection	21.5 ± 2	38 ± 4	38 ± 4	48 ± 6
Salop, Pollack and Bederson (1961)	Atomic Beam E-H Gradient Balance Method	20 ± 2.5	36.5 ± 4.5	40 ± 5	52.5 ± 6.5
Dalgarno and Kingston (1962)	Semi-Empirical Calculation	24.6 ± 1.2	41.6 ± 2.1	43.8 ± 2.2	53.7 ± 5.4
Sternheimer (1962)	Theoretical, Valence Wave Functions	22.9	44.4	49.1	67.7
Stone and Reitz (1963)	Theoretical Oscillator strength calculation	-----	-----	-----	66.5

TABLE VI.1

EXPERIMENTAL AND THEORETICAL VALUES OF ALKALI POLARIZABILITIES

INVESTIGATOR	METHOD	Na	K	Rb	Cs
Bates and Damgaard (Hall) (1949)	Coulomb Approximation	23	43	46	56
Link (1966) (Hall)	Phase shift Lifetime measurement	24.2	41.4	44.5	60.0
Kavater and Meister (1952) (Hall)	Hook Method Oscillator strength measurement	-----	-----	-----	65.2
Mizushina (1965)	Theoretical and Experimental Stark Shift for Cesium	-----	-----	-----	53.8 (65.07)*

TABLE VI.1 (CONT.)

*See text

established in the same region using a two wire type field similar to the one discussed in the present experiment. The condition that atoms in a particular magnetic substate* suffer zero deflection in such a field region is given by

$$\alpha E \frac{\partial E}{\partial z} = \mu_{eff} \frac{\partial H}{\partial z}$$

where α is the atomic polarizability, μ_{eff} is the effective magnetic moment in a field H, and $\frac{\partial E}{\partial z}$ and $\frac{\partial H}{\partial z}$ are the transverse components of the gradients of the electric and magnetic field. If we assume congruency of the electric and magnetic fields, that is,

$$\frac{\partial E}{\partial z} = CE$$

$$\frac{\partial H}{\partial z} = CH$$

where C is a geometry factor, then the atomic polarizability is given by

$$\alpha = \mu_{eff} \frac{H}{E^2}$$

The values of the atomic polarizability obtained using this method are presumably independent of the velocity distribution in the beam, the specific values of the field gradients,

---

*that substate for which the effective magnetic moment μ_{eff} is negative in the sense of being opporite to the magnetic field direction.

and the apparatus geometry (except where it enters into the calculation of the electric field).

There is a factor of 1.2 inconsistency between the alkali polarizabilities reported in their experiment and the present experiment; the origin of this discrepancy is not understood.

B. Comparison with Semi-Empirical Calculations Employing Experimentally Determined Lifetimes and Oscillator Strengths.

The alkali polarizability values for Na, K, Rb, and Cs quoted by Dalgarno and Kingston (1959) are semi-empirical values obtained using the lifetime measurements of Stephenson (1951) for Na, K, and Rb and the oscillator strength data of Minkowski and Mühlenbruch (1930) for Cs. In evaluating the oscillator strength sum in the semi-empirical formulae (equation I.6), only two terms are used, corresponding to the f values for the resonance transitions from the $P_{3/2}$ and $P_{1/2}$ states to the ground $S_{1/2}$ state. The other terms in the sum are neglected since they contribute less than 2% to the total oscillator strength sum (Dalgarno and Kingston, 1959; M. Cohen, 1967). The error quoted for the polarizability values by Dalgarno and Kingston reflects the uncertainty in the oscillator strength measurements and the estimated uncertainty introduced by terminating the oscillator strength sum.

Absolute oscillator strength values are very difficult to obtain accurately employing the Hood Method (Kvater and

Meister, 1952) or the Magnetic Rotation Method (Minkowski and Mühlenbruch, 1930) since they both require a knowledge of the alkali vapor density (Kroff and Breit, 1932).

The cesium oscillator strengths for the $P_{3/2}$-$S_{1/2}$ and $P_{1/2}$ - $S_{1/2}$ transitions measured by Minkowski and Mühlenbruch (1930)were found to be 0.66 ± 0.07 and 0.32 ± 0.03 respectively. Dalgarno and Kingston (1959) used these values in their semi-empirical calculation to derive the value of 53.7 ± 5.4 A^3 for the polarizability of cesium.

The later experiments of Kvater and Meister (1952), however, gave values of 0.79 ± 0.008 and 0.39 ± 0.004 for the resonance transition oscillator strengths. Their values are supported by the recent lifetime measurements of Link (1966) and Gallager (1967) and the theoretical calculations of Stone (1962). If the Kvater and Meister oscillator strength values are used in the semi-empirical calculation, we find the polarizability of cesium to be 65.0 A^3, which is in excellent agreement with the present experiment.

The discrepancy between the M-M and K-M oscillator strengths is well beyond the reported probable errors for both experiments and its source is not well understood. Link (1966) has used the recent vapor pressure data of Hultgen et al. (1963) to recalculate the absolute oscillator strengths for both experiments and found them not to be significantly different from those originally reported.

Thus, with the exception of cesium, the polarizability values obtained in the present experiment and the values quoted by Dalgarno and Kingston agree within the reported probable errors. The anomalous cesium result can be attributed to the oscillator strength data used in evaluating the semi-empirical formulae (equation I.6).

The lifetimes of the resonance excited states of the alkalis Na, K, Rb and Cs have been measured using the phase shift method (Link, 1966). The measured lifetimes of Na, K, and Rb are in good agreement with the earlier measurements of Stephenson (1951) and the Rb and Cs lifetimes are in excellent agreement with the recent Hanle-effect measurements of Feichtner (1965) and Gallagher (1967).* The polarizability values are calculated using the relationship between lifetimes and oscillator strengths (equation I.19) and the semi-empirical formulae (equation I.6). The errors in Link's lifetime measurements are estimated to be ± 2%. The polarizability values inferred from Link's lifetime measurements are in excellent agreement with the values obtained in the present experiment.

One further experimental observation that should be noted is the fact that the f values derived from Link's lifetime measurements, Kvater and Meister's oscillator strength measurements and the f-values inferred from the

---

*Private communication.

present experimental polarizabilities sum to a value greater than unity which contradicts the one "effective" electron approximation. Table VI.2 is a presentation of oscillator strength sums for the resonance transitions.

TABLE VI.2

ALKALI RESONANCE f SUM VALUES

Source	Na	K	Rb	Cs
Link	.975	.957	1.01	1.10
Kvater and Meister	--	--	--	1.21
Hall	.987	1.06	1.11	1.20

The f value sums inferred from the present experiment are obtained using equation I.8 and the experimentally determined polarizabilities. If we use the one "effective" electron approximation and equation I.8 for the upper bound on the alkali polarizabilities which corresponds to an oscillator strength sum of unity, we obtain the polarizability values given in Table VI.3.

TABLE VI.3

UPPER BOUND ON ALKALI POLARIZABILITIES USING THE ONE "EFFECTIVE" ELECTRON APPROXIMATION

Element	$\alpha(\mathring{A}^3)$
Na	25
K	42
Rb	43
Cs	52

The implication is that for small Z alkali atoms, Na (11) and K (19), the polarizabilities predicted from the one "effective" electron approximation are in agreement with the present experimental polarizabilities, but for the large Z alkali atoms, Rb (37) and Cs (55), there is a substantial interaction of the optical electron with the closed shell electrons leading to an f-sum larger than unity and consequently a larger polarizability value than predicted from the one "effective" electron approximation.

C. Comparison with Theoretical Calculations.

The theoretical treatment of Sternheimer and of Bates and Damgaard have been discussed in Chapter One and will not be developed further. The observation is that the polarizability values predicted using these treatments are in excellent agreement with the values obtained in the present experiment.

In the Stone-Reitz (1963) cesium polarizability calculation, wave functions obtained from numerical solutions of the Schrodinger equation with a central, symmetric potential and with the spin-orbit term, are used to calculate cesium oscillator strengths (Stone, 1962) from which polarizability values are derived using equation I.9. The validity of the wave functions used are demonstrated by comparison of experimental and calculated values of (1) ratios and magnitudes of principal series oscillator strengths, (2) fine structure splittings of the doublets, (3) binding energies

of the 40 lowest spectroscopic levels, and (4) hyperfine splitting of the cesium ground state (Stone, 1962). The result of this calculation for the cesium polarizability value is in excellent agreement with the Sternheimer calculation, the value inferred from Link's lifetime measurements, the semi-empirical Kvaster-Meister value, and, finally, the value obtained in the present experiment.

There are available in the current literature many other approximate methods for calculating alkali electric dipole, quadrupole, and octapole polarizabilities. The reader is referred to the review by Dalgarno (1962) and papers by Langhoff and Hurst (1965), M. Cohen (1966; 1967) and M. Cohen and Drake (1967) for a more detailed discussion of these methods and results. All methods of polarizability calculations are strongly dependent on the form of the approximate unperturbed wave function. Errors for such calculations are very difficult to estimate and can really be obtained only by comparison with reliable experimental values.

D. Comparison with the Stark Shift of Cesium.

The change in the hyperfine-structure separation energy caused by an electric field has been measured for cesium using an atomic-beam magnetic-resonance method. The shift of the ground state ($F = 4$, $m_F = 0$) $\longrightarrow$ ($F = 3$, $m_F = 0$) transition frequency in an electric field E (volts/cm) is given by (Haun and Zacharias, 1957)

$$\Delta W^{(2)} = -2.29 \times 10^{-6} (1 \pm 0.03) E^2 \quad Hz.$$

Mizushima et al.(1965) calculated the theoretical ground state hyperfine Stark shift and corresponding cesium ground state polarizability using the wave functions of Stone (1962). The value obtained for the Stark shift including hyperfine mixing is

$$\Delta W^{(2)} = -2.25 \times 10^{-6} E^2 \quad Hz.$$

which is in excellent agreement with the experimental measurements of Haun and Zacharias. The polarizability value calculated for cesium corresponding to the predicted Stark shift is

$$\alpha(Cs) = 65.07 \text{ Å}^3$$

The final result quoted for the theoretical Stark shift is

$$\Delta W^{(2)} = -1.9 \times 10^{-6} (1 \pm 0.1) E^2 \quad Hz.$$

which Mizushima et al.derive by multiplying the original Stark shift prediction by the ratio (53.8/65.07), where according to Mizushima the most appropriate polarizability value for cesium was the Dalgarno-Kingston (1959) result ($\alpha(Cs) = 53.8$) which agreed with the recent experimental determinations of Salop et al.(1961) and Chamberlain and Zorn (1963). If we neglect this correction and use the polarizability value for cesium obtained in the present

experiment, we retain internal consistency between experiment and theory. In addition, recent experiments by Marrus, McColm and Yellin (1966) have demonstrated that excited state polarizabilities of cesium, determined by observing the Stark shift of excited states, are in agreement with theoretical predictions using Stone's wave functions.

In view of the preceding comparisons and discussions, it appears that the values of the alkali polarizabilities obtained in the present atomic beam deflection experiment are in excellent agreement with the values derived from related properties such as oscillator strengths, lifetimes of excited states, Stark shifts, and with calculations done from first principles.

APPENDIX A

IDEAL SMALL SHIFT DEFLECTION THEORY IN ATOMIC BEAMS*

In the ideal case let us assume that atoms emerge from the source with a Maxwellian effusion velocity distribution characteristic of the oven temperature T. The distribution function N(v)dv describing the number of atoms in the velocity interval v and v + dv which arrive at the detector per unit area is given by

$$N(v)\,dv = \frac{2N}{\alpha_B^4}\, v^3 e^{-v^2/\alpha_B^2}\, dv \qquad \text{A.1}$$

where N is the total number of atoms per unit area in the detection plane and $\alpha_B = \left(\frac{2kT}{m}\right)^{1/2}$ is the most probable velocity for atoms of mass m in an isothermal container at temperature T.

The expression for the deflection S_v for atoms of velocity v at the detector plane, for the geometry shown in Figure IV.1, is given by

$$S_v = \frac{\alpha E \frac{\partial E}{\partial z}\, l_1 (l_1 + 2l_2)}{2mv^2} \qquad \text{A.2}$$

where α is the polarizability of the atom, E is the electric field strength in the field region, $\frac{\partial E}{\partial z}$ is the gradient of

*Zorn, Chamberlain and Hughes (1962).

the electric field in the field region, v the velocity of the beam atoms and m is the mass of the beam atom. For convenience, let us define

$$G = \frac{\alpha E \frac{\partial E}{\partial z} l_1(l_1+2l_2)}{2m} \qquad A.3$$

thus

$$S_v = \frac{G}{v^2} \qquad A.4$$

The quantity we shall be interested in calculating is S_v when we take into account the velocity distribution of the beam.

In the following calculation we shall derive the expression for the relationship between beam shift and the change in observed signal at the detector plane assuming the beam can be described by the ideal modified Maxwellian velocity distribution neglecting any mechanisms which could distort the velocity distribution.

Since the oven collimator and detector are of finite width, the signal due to atoms incident at the detector will have the beam shape shown in Fig. V.1. Typical experimental values for the source width S_W, collimator width C_W, detector width D_W and W_{FWHM} (full width of the beam at half maximum) are as follows:

$S_W = 1.5 \times 10^{-2}$ cm

$C_W = 7.6 \times 10^{-3}$ cm

$D_W = 7.6 \times 10^{-3}$ cm

$W_{FWHM} = 3.5 \times 10^{-2}$ cm

The signal (Intensity) obtained from a detector of finite width will be designated as $I(Z,\phi)$, where Z is the coordinate indicating the position of the center of the detector and ϕ is the value of the deflecting field in the electrode gap. At each position Z the contribution of atoms of velocity v to this signal is designated as $I_v(Z,\phi)$; thus the observed signal can be written as

$$I(z,\phi) = \int_v I_v(z,\phi)\, dv \qquad \text{A.5}$$

The signal obtained when the deflecting fields are on is equivalent to shifting the detector a distance S_v:

$$I_v(z,\phi) = I_v(z+S_v,0) \qquad \text{A.6}$$

where S_v is given by equation A.2. Substituting this result A.6 into equation A.5 and rewriting equation A.5 we obtain

$$I(z,\phi) = \int_v I_v(z+S_v,0)\, dv \qquad \text{A.7}$$

The intensity $I_v(Z,0)$ is of the same general shape as $I(Z,0)$ but of reduced amplitude and can be expressed as

follows:

$$I_v(z,0) = \frac{2I(z,0)}{\alpha_B^4} v^3 e^{-v^2/\alpha_B^2} dv \qquad \text{A.8}$$

The change in detected intensity at the detector position Z due to the shift in beam position as the deflecting field ϕ is applied, is defined as $\delta(Z,\phi)$ where

$$\delta(z,\phi) = I(z,0) - I(z,\phi) \qquad \text{A.9}$$

or

$$\delta_v(z,\phi) = I_v(z,0) - I_v(z,\phi)$$

Thus the total shift at position Z due to the applied deflection field ϕ as a function of the velocity v of the deflected atoms can be written as

$$\delta(z,\phi) = \int_{v=0}^{v=\infty} \delta_v(z,\phi)\,dv = \int_{v=0}^{v=v_1} \delta_v(z,\phi)\,dv + \int_{v=v_1}^{v=\infty} \delta_v(z,\phi)\,dv \qquad \text{A.10}$$

where v_1 is a small velocity of order 0.1 α_B. The reason for introducing v_1 is to investigate the contribution of slow atoms to the total beam shift since physically one might expect these slow atoms to introduce large effects since they are deflected substantially further than the faster atoms in the velocity distribution. Also, as we will see later, this breaking of the integral into two specific parts avoids the unphysical presence of any infinities arising from the lower bound v = 0.

The contribution of these slow atoms to the total shift of the beam can now be shown to be negligibly small. The change in signal due to the shift of atoms of velocity v ($\delta_v(Z,\phi)$) must clearly be less than $I_v(Z_0,0)$, which is the maximum signal obtained at position Z_0 (See Fig.V.1). Thus

$$\int_{v=0}^{v=v_1} \delta_v(z,\phi)\,dv < \int_{v=0}^{v=v_1} I_v(z_0,0)\,dv \qquad \text{A.11}$$

Now using equation A.8

$$\int_{v=0}^{v=v_1} I_v(z_0,0)\,dv \rightarrow \int_{v=0}^{v=0.1\alpha_B} 2I(z_0,0)\left(\frac{v}{\alpha_B}\right)^3 e^{-v^2/\alpha_B^2}\,\frac{dv}{\alpha_B}$$

and letting $v/\alpha_B = \lambda$ and $dv = \alpha_B d\lambda$, we obtain

$$2I(z_0,0)\int_{\lambda=0}^{\lambda=0.1} \lambda^3 e^{-\lambda^2} d\lambda$$

and integrating by parts

$$\int_{v=0}^{v=0.1\alpha_B} I_v(z_0,0)\,dv = \frac{I(z_0,0)}{2}\left(0.1\right)^4 = 5\times10^{-5} I(z_0,0)$$

Clearly this contribution from the slow velocity atoms is negligible.

Now in order to discuss the contribution from the second part of the expression in equation A.10, i.e., the integral from v_1 to infinity, it is convenient to expand ($I_v(Z + S_v,0)$) in a Taylor series for small S_v. This is

the small shift limit of applicability.

$$I(z+s_v,0) = I(z,0) + \frac{\partial I(z,0)}{\partial z} s_v + \frac{1}{2!}\frac{\partial^2 I(z,0)}{\partial z^2} s_v^2 + \cdots \quad \text{A.12}$$

Thus

$$\delta_v(z,\phi) = \frac{\partial I_v(z,0)}{\partial z} s_v + \frac{1}{2!}\frac{\partial^2 I_v(z,0)}{\partial z^2} s_v^2 + \cdots \quad \text{A.13}$$

Now using the relationships expressed in equation A.4 and A.8 we can rewrite equation A.13 as follows:

$$\delta_v(z,\phi) = \sum_{n=1}^{\infty} \frac{1}{n!}\frac{\partial^n I(z,0)}{\partial z^n}\left(\frac{G}{v^2}\right)^n \frac{2v^3 e^{-v^2/\alpha_B^2}}{\alpha_B^4}\, dv \quad \text{A.14}$$

Rearranging terms in equation A.14 we obtain

$$\delta_v(z,\phi) = \sum_{n=1}^{\infty} \frac{1}{n!}\frac{\partial^n I(z,0)}{\partial z^n}\left(\frac{G}{\alpha_B^2}\right)^n \frac{2e^{-v^2/\alpha_B^2}}{(v/\alpha_B)^{2n-3}}\,\frac{dv}{\alpha_B} \quad \text{A.15}$$

and

$$\int \delta_v(z,\phi)\,dv = \sum_{n=1}^{\infty} \frac{1}{n!}\frac{\partial^n I(z,0)}{\partial z^n}\left(\frac{G}{\alpha_B^2}\right)^n \int_{v=v_1}^{v=\infty} \frac{2e^{-v^2/\alpha_B^2}}{(v/\alpha_B)^{2n-3}}\,\frac{dv}{\alpha_B} \quad \text{A.16}$$

It is now apparent that the use of a lower limit $v_1 \neq 0$ eliminates the question of convergence in the integrals in equation A.16. Making use of the small shift criteria (that is, $S_v \leq 10^{-4}$ cm), only the first term (n = 1) of the series is important.

Proof

For n = 1, equation A.14 becomes

$$\int_{v=v_1}^{v=\infty} \delta_v(z,\phi)\,dv = \frac{\partial I(z,0)}{\partial z}\,\frac{G}{\alpha_B^2}\int_{v=0.1\alpha_B}^{v=\infty} v\,\frac{e^{-v^2/\alpha_B^2}}{\alpha_B^2}\,dv$$

$$\cong \frac{\partial I(z,0)}{\partial z}\,\frac{G}{\alpha_B^2}\left(\frac{1}{2}\right)$$

$$= T_1$$

$$\left(\frac{G}{\alpha_B^2}\right) << 1$$

For n = 2 we obtain

$$\int \delta_v(z,\phi) = T_1 + \frac{\partial^2 I(z,0)}{\partial z^2}\left(\frac{G}{\alpha_B^2}\right)^2 \int_{v=0.1\alpha_B}^{v=\infty} e^{-v^2/\alpha_B^2}\,\frac{dv}{v}$$

$$= T_1 + \frac{\partial^2 I(z,0)}{\partial z^2}\left(\frac{G}{\alpha_B^2}\right)^2 (4.04)$$

$$T_2 \hat{=} T_1^2 \quad , \; T_1 < 1$$

$$\therefore \; T_2 << T_1$$

Now we must make clear the identification of G/α_B^2 with S_v, the deflection for an atom of velocity v. Recall from equation A.4 that ($S_v = G/v^2$) refers to the deflection at the detector plane for an atom of specific velocity v, whereas in equation A.15 we are taking into account the velocity distribution and effectively averaging the net deflection over the velocity distribution in the beam. Thus G/α_B^2 refers to the deflection that an atoms of velocity $v = \alpha_B = (2kT/m)^{1/2}$ will experience at the detector plane due to the applied field ϕ. Now we can

identify G/α_B^2 as $\bar{S}$ (the average observable deflection of all the beam atoms). Thus in the case where we require $\bar{S}$ to be small ($\bar{S} \leq 10^{-4}$ cm), only the first term of the series is important. The net change in detected intensity at the detector position Z due to a shift in the beam position as the field ϕ is applied is given by

$$\delta(z,\phi) = \int_{v=v_1}^{v=\infty} \delta_v(z,\phi)\,dv + \frac{\partial I(z,\phi)}{\partial z}\bar{S} + \sum_{n=2}^{\infty} \frac{1}{n!}\frac{\partial^n I(z,\phi)}{\partial z^n}\bar{S}^n \int_{v=v_1}^{v=\infty} \frac{2e^{-v^2/\alpha_D^2}}{(v/\alpha_D)^2}\,dv \qquad \text{A.17}$$

which to an excellent approximation is

$$\delta(z,\phi) \cong \frac{\partial I(z,\phi)}{\partial z}\bar{S} \qquad \text{A.18}$$

where $\frac{\partial I(Z,0)}{\partial z}$ is the slope of beam shape (γ) at position Z and $\bar{S}$ the deflection at the detector plane of atoms whose velocity is α_B. The expression for the deflection of a single velocity atom in the polarizability determination (equation A.3) may now be replaced by the total averaged expression $G/\alpha_B^2 = \bar{S}$. Consequently, equation A.3 is modified to read

$$\bar{S} = \frac{\alpha E \frac{\partial E}{\partial z} l_1(l_1+2l_2)}{4kT} \qquad \text{A.18}$$

where $v^2 = \alpha_B^2 = 2kT/m$.

Thus the expression for α, the polarizability, becomes

$$\alpha = \frac{4kT\,\bar{S}}{E\frac{\partial E}{\partial z}\,l_1(l_1+2l_2)} \qquad \text{A.19}$$

but

A.20

$$\bar{S} = \frac{\delta(z,\phi)}{\frac{\partial I(z,0)}{\partial z}} = \frac{\text{Experimentally observed Intensity Change}}{\text{Slope of the beam shape at position Z}} \equiv \frac{dI}{\gamma}$$

Thus the expression for α, the polarizability, in the limit of the above assumptions, can be written as

$$\boxed{\alpha = \frac{dI}{\gamma}\,\frac{4kT}{E\frac{\partial E}{\partial z}\,l_1(l_1+2l_2)}} \qquad \text{A.21}$$

which is valid for beam atoms described by the ideal Maxwellian effusion velocity distribution.

APPENDIX B

RESIDUAL GAS SCATTERING DISTORTION OF THE IDEAL MODIFIED MAXWELLIAN VELOCITY DISTRIBUTION AND ITS EFFECT ON THE N.V.S. POLARIZABILITY VALUE

For an explanation of this phenomenon we shall follow the methods presented in Appendix A with the modification that we include the possible occurrence of a distortion in the velocity distribution due to velocity-dependent scattering of beam atoms by the residual gas atoms in the apparatus.

The first step is the calculation of $\lambda(v)$, the mean free path of a beam atom of velocity v in a Maxwellian gas (Loeb, 1961). This is accomplished by finding the collision frequency F(v) defined as the mean number of collisions per second experienced by beam atoms of speed v moving in a gas of dissimilar molecules whose most probable velocity is α_G. On the average, an atom of speed v will collide in unit time with all of the molecules of speed v' contained in a cylinder whose base is $\sigma_{BG}{}^{2*}$ and whose height is the relative velocity

$$V_r = \left(v^2 + v'^2 - 2vv'\cos\theta\right)^{1/2} \qquad \text{B.1}$$

---

*σ_{BG} refers to the interaction radius of the atom and molecule involved in the collision.

where θ is the angle between v and v'.

The number of molecules in a unit volume for which v' lies between v' and v' + dv', θ between θ and $\theta + d\theta$ and ϕ between ϕ and $\phi + d\phi$ is given by

$$N_G \, dv' d\theta \, d\phi = \frac{N_G v'^2 e^{-v'^2/\alpha_G^2}}{\pi^{1/3} \alpha_G^3} \, dv' \sin\theta \, d\theta \, d\phi \qquad \text{B.2}$$

where N_G is the scattering gas density, ϕ the azimuthal angle and α_G the most probable velocity of the scattering gas molecules defined by $\alpha_G = \left(2kT_G/m_G\right)^{1/2}$ The mean number of collisions per second is given by

$$\frac{N_G \sigma_{BG}^2 V_r}{\alpha_G^3 \pi^{1/2}} \, v'^2 e^{-v'^2/\alpha_G^2} \, dv' \sin\theta \, d\theta \, d\phi \qquad \text{B.3}$$

To obtain the total number of collisions per second that an atom of velocity v experiences, equation B.3 must be integrated from

$$\begin{aligned} v' &= 0 \rightarrow \infty \\ \theta &= 0 \rightarrow \pi \\ \phi &= 0 \rightarrow 2\pi \end{aligned} \qquad \text{B.4}$$

The result of this integration is F(v), the collision frequency for an atom of velocity v. That is,

$$F(v) = \int\int 2\pi^{1/2} N_G \sigma_{BG}^2 V_r^2 e^{-v'^2/\alpha_G^2} \frac{v'}{v} \, dv' dV_r \qquad \text{B.5}$$

where the relative velocity V_r is used as an integration parameter defined by the relation

$$V_r \, dV_r = v v' \sin\theta \, d\theta \qquad \text{B.6}$$

The limits of integration are as follows:

For $\theta=0$, then $V_r = v-v'$ for $v' < v$, or $V_r = v'-v$ for $v' > v$

For $\theta=\pi$, then $V_r = v + v'$ for $v' < v$, or $V_r = v' + v$ for $v' > v$

Then F(v) is given by

$$F(v) = \pi^{1/2} N_G \sigma_{BG}^2 \alpha_G \psi(v) \qquad \text{B.7}$$

where σ_{BG}^2 is the "effective" collision cross section of the beam and gas molecules, and $\psi(v)$ is given by

$$\psi(v) = \frac{v}{\alpha_G} e^{-v^2/\alpha_G^2} + \left(2\left(\frac{v}{\alpha_G}\right)^2+1\right)\int_0^{v/\alpha_G} e^{-y^2} dy$$

The mean free path of atoms with velocity v in a Maxwellian gas of dissimilar molecules is given by

$$\lambda(v) = \frac{v}{F(v)} = \frac{v^2}{\pi^{1/2} N_G \sigma_{BG}^2 \psi(v)} \qquad \text{B.8}$$

The probability than an atom arrives at the detector in traveling a distance ℓ without suffering a collision* is given by

$$P(v) = e^{-\ell/\lambda(v)} \qquad \text{B.9}$$

The distorted Maxwellian velocity distribution $\overline{N(v)}dv$ is then obtained by multiplying the ideal distribution function equation A.1 (Appendix A) by the probability function P(v), giving

$$\overline{N(v)dv} = \frac{2N}{\alpha_B^4} v^3 e^{-v^2/\alpha_B^2} e^{-\ell/\lambda(v)} dv \qquad \text{B.10}$$

Now rearranging equation B.10, we obtain

*We are assuming that any collision will effectively remove the atom from the beam.

$$\overline{N(v)}dv = \frac{2N}{\alpha_B^4} v^3 e^{-\left(v^2/\alpha_B^2 + \frac{A}{v^2}\Psi(v/\alpha_G)\right)} dv \qquad \text{B.11}$$

where

$$A \equiv \pi^{1/2} N_G \sigma_{BG}^2 \alpha_G^2 \ell \qquad \text{B.12}$$

In order to follow the steps outlined in Appendix A, we shall rewrite equation B.11 in terms of an intensity function, that is

$$\overline{I_v(z,0)}\,dv = \frac{2I(z,0)}{\alpha_B^4} v^3 e^{-\left(v^2/\alpha_B^2 + \frac{A}{v^2}\Psi(v/\alpha_G)\right)} dv \qquad \text{B.13}$$

Thus following the procedure in Appendix A

$$\overline{\delta(z,\phi)} = \int_{v=0}^{v=\infty} \overline{\delta_v(z,\phi)}dv = \int_{v=0}^{v=v_1} \overline{\delta_v(z,\phi)}dv + \int_{v=v_1}^{v=\infty} \overline{\delta_v(z,\phi)}dv \qquad \text{B.14}$$

Now again neglecting the contribution from the slow atoms, which is certainly valid in this case since the scattering mechanism results in the preferential removal of slow velocity atoms and thus makes their contribution to the deflection less important than the ideal case. Now using the same Taylor series expansion for $\overline{\delta_V(Z,\phi)}$, we obtain

$$\overline{\delta_v(z,\phi)} = \sum_{n=1}^{\infty} \frac{1}{n!} \frac{\partial^n I(z,0)}{\partial z^n} \left(\frac{G}{\alpha_B^2}\right)^n \frac{2e^{-\left(v^2/\alpha_B^2 + \frac{A}{v^2}\Psi(v/\alpha_G)\right)}}{(v/\alpha_B)^{2n-3}\,\alpha_B} dv \qquad \text{B.15}$$

Thus

$$\overline{\delta(z,\phi)} = \int_{v=0.1\alpha_B}^{v=\infty} \overline{\delta_v(z,\phi)} = \sum_{n=1}^{\infty} \frac{1}{n!} \frac{\partial^n I(z,0)}{\partial z^n} \left(\frac{G}{\alpha_B^2}\right)^n \int_{v=0.1\alpha_B}^{v=\infty} \frac{2e^{-\left(\frac{v^2}{\alpha_B^2} + \frac{A}{v^2}\Psi(v/\alpha_G)\right)}}{(v/\alpha_B)^{2n-3}\,\alpha_B} dv \qquad \text{B.16}$$

If we now use the small shift criteria, only the term n = 1 will be important. Thus for n = 1

$$\overline{\delta(z,\phi)} = \frac{\partial I(z,0)}{\partial z}\,\overline{S}\int_{v=0.1\alpha_B}^{v=\infty} \frac{2v\,e^{-\left(\frac{v^2}{\alpha_B^2}+\frac{A}{v^2}\,\Psi(v_p)\right)}}{\alpha_B^2}\,dv \qquad \text{B.17}$$

where the correction factor $I_1(A)$ is defined by

$$I_1(A) \equiv \int_{v=0.1\alpha_B}^{v=\infty} \frac{2v\,e^{-\left(\frac{v^2}{\alpha_B^2}+\frac{A}{v^2}\,\Psi(v_p)\right)}}{\alpha_B^2}\,dv \qquad \text{B.18}$$

The expression for the polarizability in the ideal case is given by equation A.19, that is

$$\alpha = \frac{4hT\,\overline{S}}{E\frac{\partial E}{\partial z}\,l_1(l_1+2l_2)} \qquad \text{B.19}$$

where

$$\overline{S} = \frac{\delta(z,\phi)}{\frac{\partial I(z,0)}{\partial z}} \equiv \frac{dI}{\gamma} \qquad \text{B.20}$$

In the distorted case, $\delta(Z,\phi)$ becomes $\overline{\delta(Z,\phi)}$ and the expression for $\overline{S}$ is

$$\overline{S} = \frac{\overline{\delta(z,\phi)}}{\frac{\partial I(z,0)}{\partial z}} = \frac{dI}{\gamma}\,\frac{1}{I_1(A)} \qquad \text{B.21}$$

Thus, to account for the change in the velocity distribu-

tion function due to scattering, we must include the correction factor $I_1(A)$ in the expression for S. The corrected expression for the atomic polarizability in the NVS mode thus becomes

$$\alpha = \frac{dI}{\gamma} \frac{4kT}{E\frac{\partial E}{\partial z} l_1(l_1+2l_2)} \frac{1}{I_1(A)} \qquad \text{B.22}$$

In the actual experiment, argon gas was admitted into the field region and polarizability values for the NVS mode were measured as a function of the argon gas density. This approach was used because the true residual scattering gas consists of air plus various condensable vapors, including pump oil dissociation products which makes the calculation of the correction factor $I_1(A)$ complicated and inaccurate. The details of this measurement are discussed in chapter five (F).

APPENDIX C

THEORY OF OPERATION OF THE SLOTTED DISK VELOCITY SELECTOR*

The velocity selector described in Chapter Three, section F offers distinct advantages over the helical grooved cylinder selector of similar resolution. These are (1) lighter rotor assembly, thus allowing higher angular speeds and shorter rotor length, giving more intense beams, (2) straight perpendicular slots which are easy to fabricate, and (3) removal of wrong speed atoms by collision with the face of the disk rather than with the side wall of a groove.

The geometry and operation of the velocity selector may be characterized by the following parameters. (It should be noted that after final assembly of the velocity selector these parameters were rechecked by using the optical micrometer of the telescope [Chapter Three, section H] with the velocity selector unit mounted on the table of a high precision mill in the instrument shop.)

$$\beta = d/L \qquad \text{C.1}$$

$$\gamma = \ell_1/r_\phi \qquad \text{C.2}$$

$$\eta = \ell_1/\ell_1 + \ell_2$$

β is the ratio of the disk thickness d to the length L of the rotor, γ is the ratio of the slit width ℓ_1 to the length of the arc subtended by ϕ, and η is the fractional open area expressed in terms of ℓ_1 and ℓ_2 (the wall thickness between slits). In positioning the disks along the rotor axis

*Bernstein and Hostettler (1960).

the slits should coincide or fall exactly between one another. This restriction causes ϕ to satisfy the equation

$$\phi r = n\bar{\ell} \qquad \text{C.4}$$

where $\bar{\ell} = (\ell_1 + \ell_2)/2$ and n is an integer. The choice of γ is now obviously restricted to discrete values according to the formula

$$\gamma = 2\eta/n \qquad \text{C.5}$$

The design of the present rotor is based on the values n = 15, η = 1/2 and β = 0.0234 such that γ = 1/n = 1/15 = 0.0667.

The transmitted beam consists of atoms within a defined velocity bandwidth. The limiting velocities correspond to the subscripts v_{max} and v_{min} where v_o is the nominal center velocity for a given angular speed ω of the rotor. Equating the transit time of an atom of speed v_o with the time required for the rotor to turn through the angle ϕ , one obtains the basic equation

$$v_o/L = \omega/\phi \qquad \text{C.6}$$

Using this result we can now derive the formulas for the limiting velocities

$$v_{MAX} = \left(\frac{\omega}{(\phi - \ell/r)}\right)(L-d) \qquad \text{C.7}$$

$$v_{MIN} = \left(\frac{\omega}{(\phi + \ell/r)}\right)(L+d) \qquad \text{C.8}$$

Rewriting the above equations in terms of equation C.6, we

obtain the following results

$$v_{MAX} = v_0\left(\frac{1-\beta}{1-\gamma}\right) = 1.046\, v_0 \qquad C.9$$

$$v_{MIN} = v_0\left(\frac{1+\beta}{1+\gamma}\right) = 0.9595\, v_0 \qquad C.10$$

In order to analyze the transmission of the rotor, we must first discuss the admittance function B(v) of the rotor for different velocities. The admittance is defined as the ratio of the effective slot aperture for an atom of velocity v to that for an atom of velocity v_o. The expression for B(v) is as follows:

$$B(v) = n\left(1 - \left[(1+\beta)\frac{v_0}{v} - 1\right]\frac{1}{\gamma}\right) \quad \text{for } v_0 > v > v_{MIN} \qquad C.11$$

and

$$B(v) = n\left(1 + \left[(1-\beta)\frac{v_0}{v} - 1\right]\frac{1}{\gamma}\right) \quad \text{for } v_{MAX} > v > v_0 \qquad C.12$$

The function B(v) has a triangular shape which is not symmetric about v_o but instead is biased toward the higher velocity atoms. Physically, this means that the higher velocity atoms $v_{max} > v > v_o$ have a larger probability of being transmitted than do the slower atoms. This results in an additional factor of v in the velocity distribution function I(v), as will be shown. The transmission of the rotor is given by

$$T(v) = \int_{v_{MIN}}^{v_{MAX}} I(v)\,B(v)\,dv \qquad \text{C.13}$$

where I(v) is the velocity distribution function of the incident beam atoms and is given by

$$I(v) = \frac{2I_0\, v^3 e^{-v^2/\alpha_B^2}}{\alpha_B^4} \qquad \text{C.14}$$

where $\alpha_B = (2kT/m)^{1/2}$. If one now assumes that the incident velocity distribution is homogeneous and the band pass for a given ω is small, then one can replace I(v) by $I(v_0)$ without introducing any appreciable error. Thus we have

$$T(v) \cong I(v_0) \int_{v_{MIN}}^{v_{MAX}} B(v)\,dv \qquad \text{C.15}$$

The result of performing the above integration for the velocity intervals $v_0 > v > v_{max}$ and $v_{max} > v > v_0$ with the restriction that β and γ are small compared to unity can be shown to yield (Bernstein and Hostettler, 1960):

$$T(v) = G\,v_0\,I(v_0) \qquad \text{C.16}$$

where $G = \eta\lambda(1-\beta/\gamma)^2 = 0.0216$ is a geometrical factor.

The resolution R corresponding to the half-intensity width is given by

$$R = \frac{v_{MAX} - v_{MIN}}{2v_0} = \frac{(\gamma-\beta)}{(1-\gamma^2)} \cong \gamma - \beta \qquad \text{C.17}$$

For convenience all the parameters previously defined, for the velocity selector used in the present experiment, are tabulated in Table C.1.

TABLE C.1

SPECIFICATIONS OF VELOCITY SELECTOR

Number of disks	6
Diameter of disks	16.0 cm
Number of slits per disk	280
Slit width $\ell_1 = \ell_2$	0.0864 cm
Average radius, r	7.620 cm
Disk thickness, d	0.2381 cm
Overall length of rotor (L + d)	10.429 cm
L	10.191 cm
ϕ	0.170 radians
γ(average)	0.0666
β	0.0234
η (average)	0.499
G	0.0216
R	0.0432

In order to compare the theoretically predicted velocity profile and experimentally measured velocity profile it is convenient to define a reduced velocity parameter V. The transmitted intensity is given by the equation

$$T(v) = G\, v\, I(v)\, dv = (0.0216)\, \frac{2I_0 v^4 e^{-v^2/\alpha_B^2}}{\alpha_B^4}\, dv \qquad \text{C.18}$$

If we now define the reduced velocity V as

$$V = \frac{v}{(2\alpha_B)^{1/2}} \qquad \text{C.19}$$

then equation C.18 becomes

$$T(v) = 8GV^4 e^{-2V^2} dV \qquad \text{C.20}$$

Normalizing equation C.20 to unity we obtain the equation

$$T(v) = 7.39 V^4 e^{-2V^2} dV \qquad \text{C.21}$$

Table C.2 is a presentation of the normalized intensity as a function of the reduced velocity V and is used to compare the experimental and theoretical velocity profiles.

In order to compare the most probable velocity ($\bar{v}$) of the Maxwellian effusion velocity distribution function (e.g., C.14) to most probable velocity (v_p) as transmitted by the velocity selector, one must introduce a factor of 1.159.

Proof

(a) v_p Derivation

$$\frac{dT(v)}{dv} = 0 \quad \rightarrow \quad \frac{v_p^2}{\alpha_B^2} = 2$$

TABLE C.2

NORMALIZED INTENSITY AS A FUNCTION OF REDUCED VELOCITY

V	T(V)
0.1	0.0007
0.2	0.011
0.3	0.050
0.4	0.140
0.5	0.282
0.6	0.468
0.7	0.665
0.8	0.842
0.9	0.961
1.0	1.000
1.1	0.960
1.2	0.851
1.3	0.716
1.4	0.561
1.5	0.411
1.6	0.285
1.7	0.191
1.8	0.116
1.9	0.070
2.0	0.040

$$\therefore \; v_p = \left(\frac{4kT}{m}\right)^{1/2} = 2^{1/2}\alpha_B$$

(b) $\bar{v}$ Derivation

$$\frac{dI(v)}{dv} = 0 \longrightarrow \frac{\bar{v}^2}{\alpha_B^2} = \frac{3}{2}$$

$$\bar{v} = \left(\frac{6kT}{2m}\right)^{1/2} = \left(\frac{3}{2}\right)^{1/2}\alpha_B$$

Thus we see that

$$\frac{v_p}{\bar{v}} = \left(\frac{2}{3/2}\right)^{1/2} = 1.1590$$

Finally, the relationship between the rotor angular speed (RPM) and the velocity of the beam atoms transmitted is given by

$$v_p = \text{RPM}\,(6.275)\,\frac{cm}{sec} \qquad \text{C.22}$$

APPENDIX D

TOTAL EFFECTIVE SCATTERING CROSS SECTION MEASUREMENTS AND COMPARISONS WITH PREVIOUS EXPERIMENTS AND THEORY

The total effective cross section for elastic scattering of the alkali atoms K, Rb, and Cs with argon atoms is determined in this experiment by observing the reduction in the intensity of the beam (NVS) atoms at the detector due to the introduction of argon gas in the scattering chamber. The details of this method are described by Rosin and Rabi (1935), and thus only a brief description will be given here.

The probability that a beam atom of velocity v_B passes through a region of length ℓ without suffering a collision and being removed from the beam is given by the expression

$$P(v_B) = e^{-\ell/\lambda(v_B)} \qquad \text{D.1}$$

where $\lambda(v_B)$ is the mean free path of a beam atom of velocity v_B in a scattering gas (argon) of pressure p. The mean free path is inversely proportional to the pressure of the scattering gas, that is,

$$p\,\lambda(v_B) = p_o\,\lambda_o \qquad \text{D.2}$$

where the product $p_o\,\lambda_o$ is assumed constant. Now observing that $P(v_B)$ can be expressed as the ratio of the detected beam intensity with argon in the scattering chamber (I_G) to the

detected beam intensity without argon in the scattering chamber (I_o), we can rewrite equation D.1 as

$$\frac{I_G}{I_o} = e^{-\frac{\ell p}{\lambda_o p_o}} \qquad \text{D.3}$$

Thus the constant $p_o \lambda_o$ can be expressed as

$$p_o \lambda_o = \frac{\ell p}{\ln\left(\frac{I_o}{I_G}\right)} \qquad \text{D.4}$$

The mean free path of beam atoms of velocity v_B is given by

$$\lambda(v_B) = \frac{v_B}{f(v)} \qquad \text{D.5}$$

where f(v) is the collision frequency defined as the number of collisions per second made by a beam atom with the atoms of the scattering gas (argon). If we assume the beam atoms can be described by the modified Maxwellian velocity distribution and average equation D.5 over this distribution in the usual way, we obtain the average mean free path of the beam atoms given by

$$\lambda = \frac{2}{\pi^{1/2} N_G \sigma_{BG}^2} \left(\frac{T_G M_B}{T_B M_G}\right)^2 \int_0^\infty \frac{x^5 e^{-\left(\frac{T_G M_B}{T_B M_G}\right)^2 x^2} dx}{\psi(x)} \qquad \text{D.6}$$

where T_G is the temperature of the scattering gas atoms (^oK), T_B is the temperature of beam atoms (^oK), σ_{BG}^2 is the effective total collision cross section, M_B is the mass of the beam atoms, N_G is the scattering gas density, x is a reduced velocity parameter defined as $x = v_B / \left(M_G/2kT_G\right)^{1/2}$

and $\Psi(x)$ is defined as

$$\Psi(x) = x e^{-x^2} + (2x^2+1)\int_0^x e^{-y^2} dy$$

Now using the ideal gas law, equation D.2 and equation D.6, the explicit expression for effective total scattering cross section is given by

$$\sigma_{BG}^2 = \frac{2kT_B}{\pi^{1/2} p_0 \lambda_0} \left(\frac{T_G M_B}{T_B M_G}\right)^2 \int_0^\infty \frac{x^5 e^{-\left(\frac{T_G M_B}{T_B M_G}\right)^2 x^2} dx}{\Psi(x)} \qquad \text{D.7}$$

The constant $p_o \lambda_o$ is evaluated by using equation D.4 and the integral in equation D.7 is evaluated from the tables given by Rosin and Rabi (1935). The results of the cross section measurements for this experiment and previous experiments are given in table D.1 for the three alkali metals K, Rb, and Cs interacting with argon gas atoms.

TABLE D.1

ALKALI - ARGON EFFECTIVE CROSS SECTION MEASUREMENTS

	Hall (1967)	Rothe and Bernstein (1959)	Rosin and Rabi (1935)
$\sigma^2_{K\text{-}Ar}$	199 $\mathring{A}^2$	234 $\mathring{A}^2$	185 $\mathring{A}^2$
$\sigma^2_{Rb\text{-}Ar}$	228 $\mathring{A}^2$	---	182 $\mathring{A}^2$
$\sigma^2_{Cs\text{-}Ar}$	235 $\mathring{A}^2$	273 $\mathring{A}^2$	182 $\mathring{A}^2$

To reduce the effect of systematic errors due to resolution factors and gas density measurements, we can compare the ratios of effective cross sections for various experimental measurements. For the Bernstein and Rothe (1959) results, we find

$$\frac{\sigma^2_{K\text{-}Ar}}{\sigma^2_{Cs\text{-}Ar}} = 0.86 \pm 0.06$$

and for the present experiment we find

$$\frac{\sigma^2_{K\text{-}Ar}}{\sigma_{Cs\text{-}Ar}} = 0.84 \pm 0.08$$

The theoretically predicted effective cross section of Massey and Mohr (1934), calculated by Massey and Buckingham (1936) for scattering of alkali atoms from argon, is

$$\sigma^2_{BG} = \frac{b}{\pi}\left(\frac{C}{V_R}\right)^{2/5} \qquad \text{D.8}$$

where V_R is the average relative velocity of the colliding atoms, and $b = 4.662 \times 10^{11}$ for the van der Waals potential constant in units of erg cm^6. The values for C can be calculated using the Slater and Kirkwood formula (Margenau, 1939)

$$C = \frac{3}{2}\frac{e\hbar}{(m_e)^{1/2}}\frac{\alpha_1\alpha_2}{\left[\left(\frac{\alpha_1}{N_1}\right)^{1/2}+\left(\frac{\alpha_2}{N_2}\right)^{1/2}\right]} \qquad \text{D.9}$$

where α, N,* e, and m_e refer respectively to the polarizability, number of outer shell electrons of each atom, electron charge,

*For argon, N = 8

and electron mass. Using the Bernstein and Rothe (1959) scattering cross section results and the polarizability measurements of this experiment, we find the theoretical ratio for effective cross sections of potassium and cesium atoms with argon to be

$$\frac{\sigma^2_{K\text{-}Ar}}{\sigma^2_{Cs\text{-}Ar}} = 0.82 \pm 0.06 \qquad \text{D.10}$$

which is also in good agreement with the experimental results.

APPENDIX E

QUADRUPOLE EFFECTS

The possible effect of a deflecting force due to induced quadrupole moments is negligible as will be shown.

Two sources of a quadrupole moment Q are the homogeneous electric field E and the electric field gradient $\frac{\partial E}{\partial z}$. The quadrupole deflecting force is

$$F_Q = Q \frac{\partial^2 E}{\partial z^2}$$

For an order of magnitude estimate, we consider the alkali atom as a conducting sphere with radius r. The induced moment per unit field gradient is $Q = r^5$ (Stratton, 1941). Let us consider the case of cesium, where r = 2.5 Å (Handbook of Chemistry and Physics). In the two wire field the derivative of the field in the z direction is the same as the magnitude of the electric field and the second derivative is one tenth this value. Thus, the ratio of quadrupole polarizability force to the dipole polarizability force is

$$\frac{F_Q}{F_D} = \frac{r^5}{r^3} \frac{\frac{\partial^2 E}{\partial z^2}}{E \frac{\partial E}{\partial z}} \cong 10^{-16}$$

Thus F_Q is negligible.

BIBLIOGRAPHY

BATES, D. R. and A. Damgaard, Phil. Trans. Roy. Soc., A242, 101 (1949).

BEDERSON, R. B. and E. J. Robinson, Advances in Chemical Physics (J. Ross, Ed., Academic Press, New York, 1966).

BERNSTEIN, R. B. and E. W. Rothe, J. Chem. Phys., 31, 1619 (1959).

BERNSTEIN, R. B. and H. U. Hostettler, R.S.I., 31, 872 (1960).

BETHE, H. A. and E. E. Salpeter, Quantum Mechanics of One and Two Electron Atoms (Academic Press, Inc., New York, 1957).

BUCKINGHAM, R. A., Proc. Roy. Soc., A160, 94 (1937).

BUCKINGHAM, A. D., C. A. Coulson, and J. T. Kewis, Phys. Soc. A69, 639 (1956).

CHAMBERLAIN, G. E., "Polarizability of Alkali and Noble Gas Atoms" (Ph.D. Thesis, Yale University, 1961).

CHAMBERLAIN, G. E., and J. C. Zorn, Phys. Rev., 129, 677 (1963).

CHANG, Tai Yup, Rev. Mod. Phys., 39, 911 (1967).

COHEN, M., Canadian J. Phys., 45, 3387 (1967).

COHEN, M., Proc. Phys. Soc., 82, 778 (1966).

COHEN, M. and G. W. F. Drake, Proc. Phys. Soc., 92, 23 (1967).

CONDON, E. U. and G. H. Shortley, The Theory of Atomic Spectra (At the University Press, Cambridge, 1957).

DALGARNO, A., Proc. Roy. Soc., A251, 282 (1959).

DALGARNO, A. and A. E. Kingston, Proc. Phys. Soc., A73, 455 (1959).

DALGARNO, A. and A. L. Stewart, Proc. Roy. Soc., A238, 269 (1956).

DALGARNO, A., Advanc. Phys., 11, 281 (1962).

DEBYE, P., Polar Molecules, (Dover Publications, N.Y., N.Y. 1929).

ESTERMANN, I., O. C. Simpson, and O. Stern, Phys. Rev. 71, 238 (1947).

GALLAGHER, A., Phys. Rev., 157, 68 (1967).

GOLDBERG, C., Astrophys. J., 82, 1 (1935).

HASSE, H. R. Proc. Camb. Phil. Soc., 27, 66 (1931).

HAUN, R. D. and J. R. Zacharias, Phys. Rev., 107, 107 (1957).

HEAVENS, O. S., J. Opt. Soc. Am., 51, 1058 (1961).

HELLMAN, H., Acta Physicochim USSR, 2, 273 (1935).

HIRSCHFELDER, J. O., C. F. Curtiss, and R. B. Bird, Molecular Theory of Gases and Liquids (John Wiley and Sons, Inc. New York, 1954).

JAHNKE, E. and F. Emde, Tables of Functions (Dover Publications, New York, 1954).

KIRKWOOD, J., Physik. Z., 33, 57 (1932).

KORFF, S. A. and G. Breit, Rev. Mod. Phys., 4, 471 (1932).

KUSCH, P., and V. W. Hughes, "Atomic and Molecular Beam Spectroscopy" in Handbuch der Physik 37/1, S. Flügge, ed. (Springer Verlag, Heidelberg, 1959).

KUSCH, P., J. Chem Phys., 40, 1 (1962).

KVATER, G. S. and T. G. Meister, Vestnik Leningradskogo Universiteta, 9, 137 (1952). (as quoted by Link, 1966).

LANGHOFF, P. W. and R. P. Hurst, Phys. Rev., 139, A1415 (1965).

LINK, J. K., J. Opt. Soc. A., 56, 1195 (1966).

LOEB, L. B., The Kinetic Theory of Gases (Dover Publications, Inc., New York, 1927).

LONDON, F., Zeitz. F. Physik, 63, 245 (1930).

MARGENAU, H., P. Fontana, and L. Klein, Phys. Rev. 115, 87 (1959).

MARGENAU, H., Rev. Mod. Phys., 11, 1 (1939).

MARRUS, R., D. Mc Colm, and J. Yellin, Phys. Rev., 147, 55 (1966).

MASSEY, H. S. and R. A. Buckingham, Nature, 138, 77 (1936).

MASSEY, S. W. and C. B. O. Mohr, Proc. Roy. Soc., 34, 188 (1934).

MILLER, R. C. and P. Kusch, Phys. Rev., 99, 188 (1955).

MINKOWSKI, R. and W. Mühlenbruck, Z. Phys., 63, 1314 (1934).

MIZUSHIMA, M., J. D. Feichtner, and M. E. Hoover, Phys. Rev., 137, A702 (1965).

MOORE, C. E., Atomic Energy Levels, U. S. National Bureau of Standards, Circular 467 (U.S. Government Printing Office, Washington, D.C., 1949).

MOTT, N. F. and I. N. Sneddon, Wave Mechanics and its Applications (At the Clarendon Press, Oxford, 1950).

RAMSEY, N. F., Molecular Beams (Oxford University Press, London, 1956).

ROSIN, S. and I. I. Rabi, Phys. Rev., 48, 373 (1935).

RUSSELL, H. N., Astrophys. 83, 129 (1936).

SALOP, A., E. Pollack, and B. Bederson, Phys. Rev., 124, 1431 (1961).

SCHEFFERS, H. and J. Stark, Physik, Z., 35, 625, 1934.

SCHWARTZ, C., Phys. Rev., 123, 1700 (1961).

SLATER, J. C., Quantum Theory of Atomic Structure, (McGraw Hill Book Co., Inc., New York, 1960).

SLATER, J. C. and J. G. Kirkwood, Phys. Rev., 37, 682, (1931).

STEPHENSON, G., Nature, 167, 156 (1951).

STEPHENSON, G., Proc. Phys. Soc. A64, 458 (1951).

STERNHEIMER, R. M., Phys. Rev., 96, 951 (1954).

STERNHEIMER, R. M., Phys. Rev., 107, 1565 (1957).

STERNHEIMER, R. M., Phys. Rev., 127, 1220 (1962).

STONE, P. M., Phys. Rev., 127, 1151 (1962).

STONE, P. M., and J. R. Reitz, Phys. Rev., 131, 2101 (1963).

STRATTON, J. A., Electromagnetic Theory (McGraw-Hill Book Company, Inc., New York, 1941).

TRUMPY, B. Z., Phys. 66, 720 (1930).

UNSÖLD, A., A. Phys., 43, 563 (1927).

VINTI, J. P., Phys. Rev., 41, 813 (1932).

YOUNG, H. D., Statistical Treatment of Experimental Data, (McGraw Hill Book Company, 1962).

ZORN, J. C., G. E. Chamberlain, and V. W. Hughes, Phys. Rev., 129, 2566 (1963).